A 14,000-YEAR RECORD OF WILDFIRE AND ALLUVIAL FAN DEPOSITION REVEALS RELATIONSHIPS AMONG FIRE, CLIMATE, VEGETATION, AND SEDIMENT YIELDS IN THE MIDDLE FORK SALMON RIVER, IDAHO

by

Kerry Elizabeth Riley

A thesis

submitted in partial fulfillment

of the requirements for the degree of

Master of Science in Hydrologic Sciences

Boise State University

May 2012

BOISE STATE UNIVERSITY GRADUATE COLLEGE

DEFENSE COMMITTEE AND FINAL READING APPROVALS

of the thesis submitted by

Kerry Elizabeth Riley

Thesis Title: A 14,000-Year Record of Wildfire and Alluvial Fan Deposition Reveals Relationships Among Fire, Climate, Vegetation, and Sediment Yields in the Middle Fork Salmon River, Idaho

Date of Final Oral Examination: 28 February 2012

The following individuals read and discussed the thesis submitted by student Kerry Elizabeth Riley, and they evaluated her presentation and response to questions during the final oral examination. They found that the student passed the final oral examination.

Jennifer Pierce, Ph.D.	Chair, Supervisory Committee
David Wilkins, Ph.D.	Member, Supervisory Committee
Elowyn Yager, Ph.D.	Member, Supervisory Committee
Benjamin T. Crosby, Ph.D.	Member, Supervisory Committee

The final reading approval of the thesis was granted by Jennifer Pierce, Ph.D., Chair of the Supervisory Committee. The thesis was approved for the Graduate College by John R. Pelton, Ph.D., Dean of the Graduate College.

DEDICATION

This thesis is dedicated to my best friend, Matthew Feicht, for his continuous love and support throughout this process. Although not a scientist, his curiosity and enthusiasm in the world around him motivated and inspired me to see the world with similar eyes. Matt contributed significantly to this thesis by driving 100's of miles to and from the river, spending hours washing and pre-treating charcoal in the lab, and backpacking to study debris flow fans in the wilderness.

This thesis is also sincerely dedicated to my advisor Dr. Jen Pierce. This project was 'a dream come true' for me. Jen's research vision enabled me to spend the last three years investigating one of the most amazing rivers on the planet. I could not have asked for a more exciting project and I am forever grateful.

AKNOWLEDGEMENTS

My thanks and appreciation go out to my field assistants-Austin Hopkins, Pat Hass, Nick Sutfin, Rebecca Morris, Jason Compton, Jenny Morris, and Anna Rebelino for spending weeks on the river. Thanks go out to Lar Svenson, Mike Polous, and Randy Walters for hiking into the wilderness to do field work. I would like to acknowledge my thesis committee including Dr. David Wilkins, Dr. Elowyn Yager, Dr. Ben Crosby, and Dr. Jen Pierce. This group of amazing geomorphologists continues to inspire, encourage, and support this reasearch and my academic progress. I would like to thank Jenny Rylee, Carolyn Volk, and Kristin Lundstrom at the Foothills Learning Center and Dr. Emily Hinz, Dr. Karen Viskupic, Dr. Dave Wilkins, and Dr. Jim Belthoff for their help with the GK-12 fellowship. I would like to thank the Middle Fork Ranger District and the National Forest Service for providing the permit to study in the wilderness and on the river. The Idaho EPSCoR program and the National Science Foundation, award number EPS-0814387, funded this project. The Geological Society of America Student Research Grant (#014L101150), the National Science Foundation GK-12 Program, Boise State Geosciences Department, and Boise State STEM Station provided additional funding and support.

AUTOBIOGRAPHICAL SKETCH OF THE AUTHOR

I was born in Morgantown, West Virginia where I became fascinated with moving water. After graduating high school, I travelled west to study at the University of Colorado, where I received my Bachelor's degree in physical geography and environmental studies. I started guiding rivers in Colorado during college, spending my summers in the Arkansas River Valley. After receiving my undergraduate degree, I moved to Oregon, where I taught outdoor and science education to K-12 in the winter and guided whitewater in Arizona and Idaho during the spring and summer. My curiosity in rivers has driven me to understand how moving water shapes the landscape across the world. Rivers brought me to Boise State University and gratefully to my Master's thesis work.

ABSTRACT

Changes in climate influence vegetation distributions and the frequency and severity of fire and post-fire erosion. While the frequency of large fires has increased on all vegetated continents over the last decade, it remains unclear whether recent large fires are extraordinary over millennial timescales. In the Middle Fork Salmon River of central Idaho, over 40% of the watershed has burned in the last 30 years and the subsequent increase in erosion from severely burned hillslopes has produced many large fire-related debris flows. Fires have burned throughout the steep topographic gradient of the watershed that encompasses high elevation sub-alpine and mixed conifer forests and lower elevation rangeland ecosystems.

This study uses ^{14}C-dating of charcoal fragments from discrete alluvial fan deposits to reconstruct a 14,000 yr record of fire and fire-related sedimentation along an ecological gradient of the Middle Fork Salmon River. We investigate the role of climate on spatial and temporal variations in the timing, frequency, and severity of fire and the associated erosional response. We combine recent (1997-2008) fire-related debris flow sediment yields and reconstructed fire-related debris flow frequencies over the last 6 ka to quantify long-term (10^3 yr) sediment yields.

Overall, fire-related deposits compose 74 ± 25% of total alluvial fan thickness in upper, wetter ecosystems versus 41 ± 33% recorded in lower, drier basins. Synchronous

fires (multi-basin fires) burned 110 ±150, 450 ±120, 860 ±75, 1120 ±75, 1560 ±50, 1790 ± 70, 2070 ±70, 2240 ±100, 2780 ±60, 3730 ±100, and 6440 ±120 cal. yr BP. Fires burning during the early (14-8.5 ka) and late Holocene (4 ka – present) primarily produced debris flow deposits while fires burning during the mid-Holocene (8-5.5 ka) primarily produced sheetflood deposits. We hypothesize the shift in sediment delivery process was a consequence of decreased vegetation density and therefore fire severity driven by a stable, warm, dry mid-Holocene climate that resulted in more frequent and smaller magnitude depositional events (i.e., sheetfloods).

Recent (1997-2008) debris flow events occurred following moderate to high severity fires that burned ecosystems containing soils composed of easily erodible Idaho Batholith granites and produced a range in sediment yields from ~1,450-34,550 $Mgkm^{-2}yr^{-1}$. Lower, drier basins produced significantly smaller single event debris flow yields than upper, wetter basins. Fire frequency, severity, and synchronicity have been high during the last 2 ka and fire-related debris flows have supplied 83-262 $Mgkm^{-2}yr^{-1}$ of sediment to the main-stem river. Increased fire and debris flow activity during the last 2 ka corresponds with the arrival of dense lodgepole pine (pinus contorta) forests at high elevations during the cool and effectively wetter late Holocene. Over the last 6 ka, we estimate fire-related debris flows have contributed ~30-101 $Mg\ km^{-2}\ yr^{-1}$ of sediment to the Middle Fork Salmon River, which is lower than the last 2 ka because of decreased debris flow activity during the mid-Holocene.

Our results demonstrate fire is a primary contol of millennial sediment yields in the Middle Fork Salmon River. We hypothesize that centennial scale intervals of

increased fire frequency and severity occur during long-term intervals of relatively cool and (or) wet climate conditions and associated increased fuel production. Increased fuel loads, coupled with annual to decadal-scale droughts, produce widespread severe fire and debris flows, which contribute significantly to long-term sediment yields in the Middle Fork Salmon River.

TABLE OF CONTENTS

LIST OF TABLES

LIST OF FIGURES

LIST of EQUATIONS

Equation 1 $\ln V = 7.2 + .6 (\ln A) + .7 (B)^{1/2} + .2 (T)^{1/2} + .3$

A = area with slope ≥ 30% (km^2)
B = area moderately to severely burned (km^2)
T = storm precipitation depth (mm)
V = volume

Equation 2 radius of curvature (r_c) = C2 / 8M + M/2

C = chord
M = middle ordinate distance

Equation 3 velocity (v) = $(g * r_c (\cos\acute{\alpha}) * (\tan\beta))^{1/2}$

g = gravity
ά = banking angle
β = longitudinal slope

Equation 4 $Q_{max} = A_{max} * \nu$

A_{max} = maximum cross sectional area of debris flow snout
Q_{max} = maximum discharge

Equation 5 volume = $794.6 * Q_{max}^{0.849}$

LIST OF ABBREVIATIONS

DEM – Digital Elevation Model

NBR – Differenced normalized burn ratio

FR – Deposits contain abundant charcoal and/or underlain by burn surface

LIA – Little Ice Age

MFSR – Middle Fork Salmon River

MCA – Medieval Climatic Anomaly

NAIP – National Agriculture Imagery Program

PDSI – Palmer Drought Severity Index

SFP – South Fork Payette River

YSNP – Yellowstone National Park

CHAPTER 1: FIRE AND HOLOCENE VEGETATION CHANGE PROVIDE PRIMARY CONTROLS ON GEOMORPHIC RESPONSE IN THE MIDDLE FORK SALMON RIVER, IDAHO BATHOLITH

Abstract

Climate-driven changes in vegetation structure and species distributions influence the size and severity of wildfire throughout the world. During the 1980s, the frequency, severity, and duration of large fires increased in the western United States. It remains unclear, however, if recent fires are extraordinary over millennial timescales. In the Middle Fork Salmon River (MFSR) of central Idaho, US, over 40% of the watershed has burned in the last 30 years, and increased erosion from severely burned hillslopes has produced many large fire-related debris flows. This study radiocarbon dates charcoal fragments from recently incised alluvial fan deposits to reconstruct fire and fire-related depostion (i.e., geomorphic response) over centennial and millennial timescales. We investigate the role of climate and vegetation change on spatial and temporal variations in the timing, frequency, and inferred severity of fire. In addition, we investigate fire-related deposition on alluvial fans across a modern ecosystem gradient, which spans high elevation, mixed conifer forests and lower elevation, rangeland ecosystems.

Over Holocene timescales, fire-related deposits compose significantly greater alluvial fan thicknesses in upper, wetter basins versus lower, drier basins. Eight periods of widespread fire were recorded during the last 14 ka, inferred from fires that burned multiple basins throughout a large area. Six periods of widespread fire burned during the last 4 ka. Over Holocene timescales, sheetflood deposits were significantly more abundant in lower, drier basins compared to upper, wetter basins. Fires burning during the early (14 - 8.5 ka) and late Holocene (4 ka – present) primarily produced debris flow deposits while fires burning during the warm, dry mid-Holocene (8 - 5.5 ka) primarily produced sheetflood deposits. Severe fires are inferred from thick fire-related debris flow deposits, while less severe fires are inferred from fire-related sheetflood deposits. Starting ~4 ka, the frequency of inferred severe fires increased and fires burned at similar times in both upper and lower basins. Importantly, over the past ~2 ka, generally cooler but variable climate conditions, (as well as a shift to dense lodgepole pine (*pinus contorta*) forests in the upper MFSR basin) were accompanied by an increase in fire activity.

We hypothesize that centennial-scale intervals of increased fire frequency and severity result from increased fuel loads produced during long-term intervals of relatively cool and (or) wet climate conditions, coupled with annual to decadal-scale drought. In contrast, during millennial scale warm and dry conditions, vegetation density decreases, the abundance of fire resistant species such as Douglas fir increases, fires are less severe and more frequent, and large fire-related sedimentation events are reduced.

Introduction

Climate-driven changes in vegetation structure and species distributions influence the size and severity of wildfire throughout the world (Power et al., 2008); conversely, wildfires also drive global changes in vegetation and ecosystem composition (Bowman et al., 2009; Swetnam, 1993; Whitlock et al., 2003). The frequency of large wildfires has increased on all vegetated continents over the last decade (Bowman et al., 2009; Cochrane et al., 2002; Forsyth and Wilgen, 2008; Lohman et al., 2007; Page et al., 2002; Westerling et al., 2006). And predicted increases in extreme fire events (IPPC, 2007) could greatly influence global climate, vegetation distributions, and landscape erosion rates.

In order to understand, predict, and manage for future effects of fire on the landscape, it is important to understand how relationships among fire, climate, and vegetation have affected the landscape in the past. Future fire regimes may reflect climate-driven vegetation changes and vegetation communities that have no modern analog. Since climate is a primary driver of wildfire, then understanding fire regimes over Holocene centennial to millennial climate cycles may provide the historic context needed to understand recent increases in wildfire activity.

Fire reconstructions have been created using mapped fire perimeters, tree rings, and fire scars, providing annual, decadal, and centennial records of fire. Longer fire reconstructions have been made using charcoal found in lakes (e.g., Brunelle et al., 2005; Power et al., 2008; Whitlock et al., 2010); however, lakes are absent in many geographic areas and ecosystem types. Alternatively, alluvial charcoal sourced from burned

vegetation in contributing basins and deposited in alluvial sediments can be used to reconstruct longer fire histories where lakes are not present (e.g., Meyer et al., 1995). In addition, the type and magnitude of the erosional response to fire reflects burn severity and vegetation type within the burned basin; therefore, characteristics of fire-related deposits provide insight into the extent and severity of fire (e.g. Meyer et al., 1995; Pierce et al., 2004; Cannon et al., 2010). Alluvial fans act as long-term sediment traps that can span Holocene timescales and this long-term perspective is important to understand how millennial-scale changes in climate have affected fire and fire-related erosion in the past.

During the 1980s, large wildfires increased in severity and frequency throughout the western United States across a range of ecosystems (Westerling et al., 2006); however, mid-elevation (1680-2590 m) Northern Rocky Mountain forests have experienced the greatest increases (Westerling et al., 2006). Synchronicity in fire activity has increased across broad regional scales (e.g., Northern Rocky Mountains; Morgan et al., 2008) and climate, not prior management, is shown to be the primary control on wildfire activity (Westerling et al., 2006). In particular, severe droughts and associated early snowmelt years have resulted in fires burning vast areas of both rangeland and forest ecosystems. For example, in 2007, ~8100 km^2 (2 million acres) burned in Idaho (NIFC, 2010) during an extreme drought year (NOAA, 2012); in contrast, only ~60 km^2 (13,981 acres) burned in Idaho in 2004 (NIFC, 2010) under non-drought conditions (NOAA, 2012). It is well established that severe summer drought is a primary driver of widespread fire (e.g. Heyerdahl et al., 2008; Westerling et al., 2006) on annual timescales. However, over annual to millennial timescales, fire regimes are also a

function of fuel characteristics (e.g., forest density and type of vegetation burning). Therefore, it is important to understand the role wildfire plays among different ecosystems and across timescales that encompass millennial-scale climate change.

While some literature (e.g., Barrett, 1988), policy decisions, and subsequent land management attribute recent large severe fires to the unnatural accumulation of fuels caused by fire suppression, recent research attributes recent large fires to climate extremes, specifically extreme drought years (Meyer et al., 1995; Schoennagel et al., 2004; Westerling et al., 2006). More studies are needed that examine both modern and historic fire regimes in the absence of anthropogenic disturbance; however, few forests in the western USA have been unaffected by logging, roads, and fire suppression. The Middle Fork Salmon River (MFSR) flows through the 9,580 km^2 Frank Church-River of No Return Wilderness in central Idaho (Figure 1-1), which provides a unique location for examining natural processes functioning in the absence of confounding management and land use.

This study examines changes in the timing, frequency, and inferred severity of wildfire with changes in Holocene climate along the MFSR in central Idaho. The MFSR contains a rich history of both modern and Holocene fire-related erosion events preserved in alluvial sediments, and the river corridor provides a natural ecological gradient over which spatial and temporal changes in fire activity and vegetation can be investigated. This study seeks to answer the following questions: 1) how does fire frequency and severity vary over ecological gradients spanning subalpine to sagebrush steppe ecosystems; 2) how have fire-related erosion events changed spatially and temporally

along the Middle Fork Salmon River over Holocene timescales; and 3) how does the type of depositional process relate to fire severity, vegetation, and climate conditions.

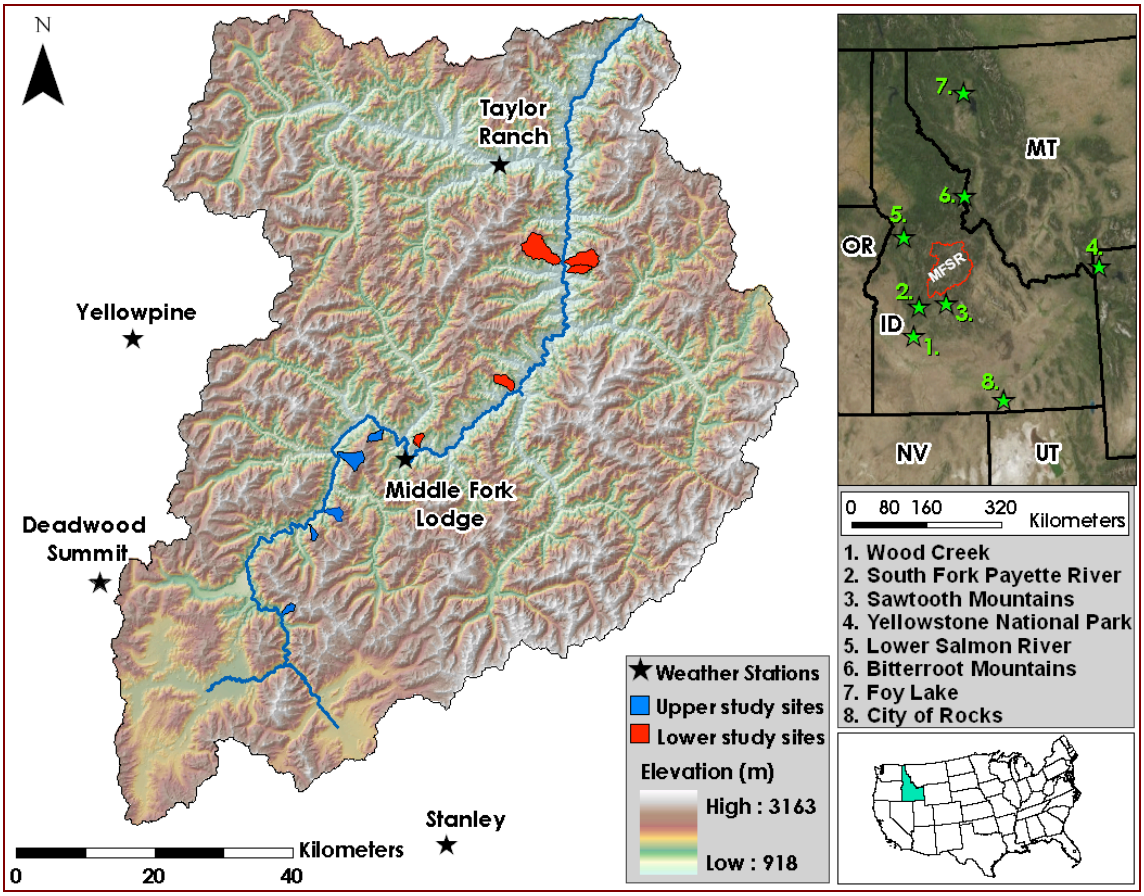

Figure 1-1: Map of the Middle Fork Salmon River (MFSR) watershed. Red polygons show five lower, drier sub-basins (red) and five upper, wetter sub-basins (blue) used in this study. The numbered green stars on the regional map represent the locations of climate proxy data discussed in this study.

Background

Fires and Geomorphic Response

Wildfire reduces vegetation and ground cover (e.g., litter, duff, organic material) which decreases surface roughness (Lavee et al., 1995). Fires produce fine-grained ash and can create or intensify soil hydrophobicity, which act to reduce infiltration rates (e.g., Meyer and Wells, 1997; Shakesby and Doerr, 2006), increase surface runoff, and increase surface erosion (Doerr et al., 2006; Shakesby and Doerr, 2006; Wondzell and King, 2003). Over longer time periods (months to years), if vegetation is completely killed, root cohesion decreases, which also increases hillslope erosion (e.g., Malmon et al., 2007; Roering and Gerber, 2005; Schmidt, 2001). Types of fire-related erosion processes include debris flows, sheetfloods, and sediment charged floods. The ratio of sediment to water greatly influences the type of erosional process transporting sediment, where debris flows have higher ratios of sediment to water compared to sheetfloods and floods. Fire-related debris flows are primarily generated by progressive sediment bulking of runoff by sediment eroded from both the hillslope and within the channel (Cannon et al., 2003; Parise and Cannon, 2012). Cannon et al. (2010) demonstrated that there is a positive correlation between the magnitude of a debris flow event and the area of a basin moderately to severely burned, area of the basin with slopes greater than or equal to 30%, and the total storm rainfall initiating the event. Large fire-related debris flows found in the stratigraphic record have been inferred to have followed high severity, stand-replacing fires in the South Fork Payette River, Idaho (Pierce et al., 2004). Low severity

fires result in a patchy vegetated landscape, where runoff is discontinuous, limiting sediment yields during post-fire storm events (Lavee et al., 1995).

Modern Relationships between Vegetation and Fire

Modern fire regimes in Northern Rocky Mountain high elevation and(or) moist ecosystems are generally not limited by fuel availability, but instead are limited by the frequency of extreme drought conditions needed to dry fuels. In mid-to-high elevation forests, trees generally lack resistance to fire, canopies are dense, and forests contain abundant ladder fuels; subsequently, these forests typically burn infrequently (200-400 yrs) but exhibit high severity (Agee, 1993), stand replacing fires (e.g., Despain, 1990; Schoennagel et al., 2003).

Fire spread in drier and (or) lower elevation ecosystems is limited by vegetation density (i.e., fuel accumulation). Xeric conifer forests (e.g., ponderosa pine forests) need drought during the year of the fire preceded by wet years to accumulate ladder fuels to produce widespread fire (Swetnam and Betancourt, 1998; Veblen et al., 2000). Ponderosa pine and Douglas fir have fire adaptations (e.g., thick bark, deep roots, and less flammable foliage) that allow trees to survive fire. Ponderosa pine fire studies in central and northern Rocky Mountains forests suggest a mixed severity fire regime, with frequent surface fires (20-30 yr) and infrequent (150-400 yr) high severity fires (Arno et al., 1995; Barrett, 1988; Brown et al., 1999; Shinneman and Baker, 1997) during times of drought (Pierce et al., 2004; Veblen et al., 2000). Sagebrush steppe-dominated ecosystems also need antecedent high moisture conditions to increase vegetation

production and accumulate fuel (Miller and Tausch, 2001) followed by dry conditions to ignite and carry fire. While fire return intervals have been estimated to range from 35-200 yr (Baker, 2006; Nelson and Pierce, 2010) for sagebrush-steppe communities, the invasion of cheatgrass has dramatically increased fine-fuel loads and increased fire frequency regimes in many sagebrush ecosystems (Baker, 2006).

Regional Holocene Climate and Vegetation Records

Holocene records of climate and vegetation change in the Northern Rocky Mountain region are derived from paleo-ecological records including fossil pollen, plant macrofossils, and charcoal collected in lake sediment cores (Brunelle et al., 2005, Whitlock et al, 2008, Whitlock et al., 2010), stable isotopes $\delta^{18}O$ and $\delta^{13}C$ in soil carbonates (Davis et al., 2002), lake level reconstructions (Shuman et al., 2009), and fire histories derived from alluvial charcoal (e.g., Meyer et al., 1995, Pierce et al., 2004) and fire scars (Svenson, 2010). Though none of these reconstructions are located in the MFSR, several (Davis et al., 2002, Whitlock et al., 2010, Biondi et al., 1999; Svenson, 2010) are in the greater Salmon watershed, and the rest of the reconstructions are in the Northern Rocky Mountain region (Figure 1-1). Vegetation and fire reconstructions from lake sediments, fire-scars, and alluvial sediments in the Sawtooth Mountains (Whitlock et al., 2010; Svenson, 2010), located in the headwaters of the Salmon River, provide a valuable source of information about vegetation change and fire history within the upper watershed.

The amplification of seasonal insolation variations in the Northern Hemisphere between 12,000 and 6000 cal. yr BP, resulted in generally increased summer temperatures, increased evapo-transpiration, and suppressed summer precipitation (Bartlein et al., 1998). Regional records suggest that late Pleistocene-early Holocene climate (11-8.5 ka) was generally cool (Whitlock et al., 2010) and variable (unstable) (Davis et al., 2002, Brunelle et al., 2005, Whitlock et al., 2010). During this time, forests in the Bitterroot Mountains, north of the MFSR, transitioned from open forests composed of spruce and alpine meadows to dense pine and Douglas fir forests (Brunelle et al., 2005). Inferred forest composition in the Sawtooth Mountains, south of the MFSR, prior to 8420 cal. yr BP was *Pinus contorta* (lodgepole pine) and *Pseudotsuga* (Douglas fir) (Whitlock et al., 2010).

During the mid-Holocene (~7 - 4 ka), low lake levels throughout Rocky Mountains (Shuman et al., 2009), warmer taxa in the pollen record (Whitlock et al., 2010, Brunelle et al., 2005), and low variability in the stable isotope record (Davis et al., 2002) suggest climate was generally drier, warmer, and more stable. In the Sawtooth Mountains, the open Douglas fir forests that covered the landscape 8.4-6 ka transitioned to closed Douglas fir forests from 6-2.6 ka (Whitlock et al., 2010), suggesting this mid-Holocene interval of warmth and stability was followed by cooler effectively wetter conditions.

Other regional studies suggest late-Holocene (4 ka-present) climate was generally cooler, wetter, and more variable when compared to the mid-Holocene (Davis et al., 2002, Brunelle et al., 2005, Whitlock et al., 2010). Mesic vegetation increased in the

lower Salmon River during the late Holocene (Davis et al., 2002), pine expanded throughout the Northern Rocky Mountains ~3.5 ka (Whitlock et al., 2008), and modern forests were established ~3 ka, in the nearby Bitterroot Mountains (Brunelle et al., 2005). Modern conifer forests including lodgepole pine were established ~ 2.6 ka, in the Sawtooth Mountains (Whitlock et al., 2010).

Two well-documented periods of climate change occurred during the last millennia. The Medieval Climatic Anomaly (MCA) ~1050-650 cal. yr BP stands out in many climate records as a period of multi-decadal severe drought (Cook et al., 2004; Stine, 1994) and high climate variability (Cook et al., 2004; Stine, 1994). During the Little Ice Age (LIA) ~650-100 cal yr. BP glaciers advanced in Northern Rocky Mountains (Carrara, 1989; Grove, 1988; Luckman, 2000) and cold climate conditions were recorded throughout the Northern Hemisphere (Esper et al., 2002; Grove, 1988; Pollack et al., 1998). Climate in the Sawtooth-Salmon Mountains has been characterized by generally high levels of climate variability with prolonged warm periods (550-600 and 400-450 cal. yr BP) and multi-decadal periods of cool climate conditions (350, 560, 610, and 650 cal. yr BP) (Biondi et al., 1999). However, over broader spatial scales (e.g., western USA), prolonged drought decreased following the MCA and climate variability was lower during the LIA compared to the MCA (Cook et al., 2004).

Study Area

The MFSR begins at the confluence of Marsh Creek and Bear Valley Creek and flows through the Frank Church-River of No Return Wilderness (FC-RNR) in central Idaho (Figure 1-1). The large (~7,400 km^2) watershed has steep rugged topography with a mean hillslope gradient of ~54 % (~28.5°) and encompasses elevations ranging from 900-3160 m. The Sawtooth Mountains border the watershed to the south, and the MFSR flows northeast through the Salmon Mountains. The underlying geology within the watershed includes Precambrian meta-sediments, Cretaceous calc-alkaline intrusive rocks from the Idaho Batholith, and Eocene silicic and basaltic rock from Challis volcanism (Herron and Freeman, 2008; Figure 1-2). Soils mantling hillslopes directly adjacent to the main-stem river are derived primarily from weathered Idaho Batholith granite (Figure 1-2); this, grus is generally coarse textured, provides little cohesion, and is easily eroded (Clayton and Megahan, 1997). Soils composed of these well-weathered granites are suggested to be the highest producers of sediment in the area (Steele et al., 1981).

Pacific-driven precipitation falling primarily as snow during winter months accounts for 55-60% of total annual precipitation (Steele et al., 1981). Moisture generally moves from the west to east, and the high relief north-south trending Salmon River Mountains create an orographic decrease in precipitation to the eastern (leeward) side of the watershed. The main-stem river is steep with a river elevation that drops from ~2050 m at the headwaters to ~920 m at the confluence of the main Salmon River. Annual precipitation ranges from ~360 mm measured at Taylor Ranch, located in the drier eastern part of the watershed and situated at a lower elevation, to ~840 mm

measured at Deadwood Dam located along the wetter, western edge of the watershed and at a higher elevation (Figure 1-2). Precipitation regimes include rain-dominated elevations (500-1500 m), mixed rain and snow (1500-2500 m), and snow-dominated (2250-3250 m) elevations (Tennant, 2011). The distribution of precipitation type affects surface hydrology. Rain-dominated basins experience surface runoff throughout winter and spring months with lower peak, median, and base flows (Tennant, 2011). In contrast, snow-dominated basins produce higher peak, median, and base flows during early spring to summer months (Tennant, 2011). While occasional summer convective thunderstorms do not contribute significantly to annual precipitation, they can initiate large fire-related debris flows. In the Northern Rocky Mountains of central Idaho and especially in the FC-RNR wilderness, lightening-started fires are generally restricted to late April-October and are the primary control on the distribution of total fires during the summer (Hostetler et al., 2006).

Ten small (0.2-14 km^2), steeply sloping sub-basins (40-70% mean gradient), with recently incised alluvial fans at the tributary-trunk stream junctions, were selected as study sites (Table 1-1). Contributing areas of study sites are composed primarily of easily erodible Idaho Batholith Cretaceous intrusive rocks (Figure 1-2). Study sites span ~100 km of the ~170 km long main-stem river. Sub-basin elevations range from 1100-2750 m, encompassing the "Northern Rocky Mountain middle elevations" (1680-2590 m), recognized by Westerling et al., (2006) as highly vulnerable to increases in fire frequency due to warmer temperatures. Vulnerability was determined by the spatial

distribution of forest area and the sensitivity of the local moisture-deficit for October through September (Westerling et al., 2006).

The large range of elevations and precipitation regimes throughout the watershed manifests as a mosaic of vegetation types. The MFSR flows through densely forested headwaters to dry sagebrush and cheatgrass dominated basins at the confluence of the MFSR and the main Salmon River (Figure 1-3). Sub-basins also show aspect-influenced vegetation distributions, with increased vegetation density and greater forest cover on north-facing slopes. Dense forest-cover at higher elevations and on north-facing slopes increases fuel loads and the potential for increased burn severity.

Upper Basins

Five upper elevation, wetter sub-basins (Figure 1-3 a-c) are characterized by subalpine to mixed conifer forests. Subalpine ecosystems are located at higher elevations (~3,000-1,700 m) and major tree species include subalpine fir (*Abies lasiocarpa*), lodgepole pine (*Pinus contorta*), Engelmann spruce (*Picea englemannii*), whitebark pine (*Pinus albieaulis*), Douglas fir (*Pseudotsuga menziesii*), and subalpine larch (*Larix lyallii*); (Steele et al., 1981). Lodgepole pine is the dominant species in upper basins, however Douglas fir are more common on south-facing warmer hillslopes (Steele et al., 1981). Understory species include dwarf huckleberry (*Vaccinium caespitosum*), thimbleberry (*Rubus parviflorus*), fireweed (*Epilobium angustifolium)*, lupine (*Lupinus sericeus)*, stinging nettle (*Urtica dioica)*, and yarrow (*Achillea millefolium*). At mid-elevations (1700-1380 m) within upper basin study sites, Douglas fir and ponderosa pine

(Pinus ponderosa) co-dominate the warmer south-facing slopes and lodgepole pine dominates on cooler sites (Steele et al., 1981).

Lower Basins

Five lower elevation, drier basins (Figure 1-3 d-f) contain abundant shrub and grassland communities with sparse Douglas fir and ponderosa pine open forest communities. The density of conifers increases toward ridge tops and on north-facing hillslopes with cooler, moister aspects. Lower basin vegetation include sagebrush, curl-leaf mountain-mahogany (*Cercocarpus ledifolius)*, bitterbrush *(Purshia tridentate)*, rabbit brush *(Chrysothamnus viscidiflorus),* bear grass *(Xerophyllum tenax*), and cheatgrass (*Bromus tectorum).*

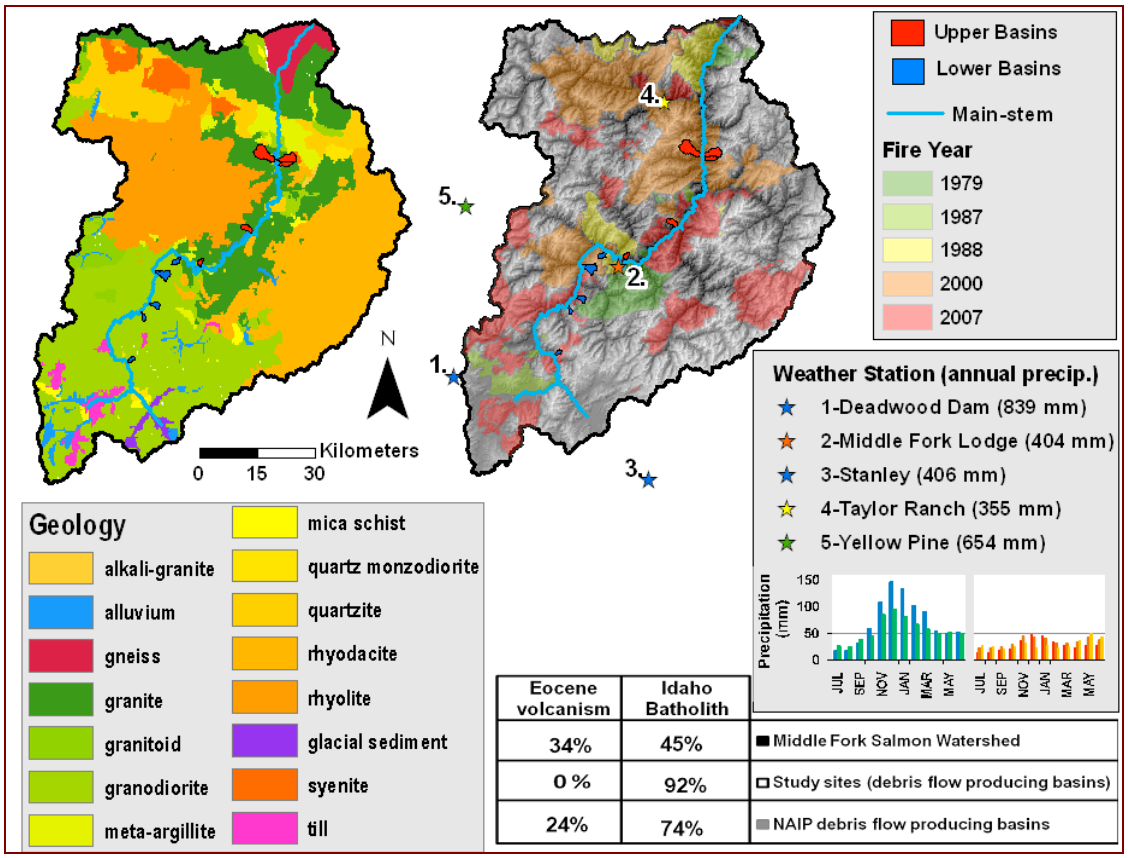

Figure 1-2: Geologic map of MFSR (Ludington et al., 2006) show major rock types within the watershed. Polygons show the five largest fire years in the MFSR. Numbered stars represent locations of weather stations (Gibson and Morgan, 2009) and the bar graph shows annual precipitation distribution with the total annual precipitation labeled in the legend. Percentages represent lithology derived from the two major lithologic groups for the ten study study sites, ten debris flow producing basins located away from the main-stem river identified using NAIP imagery, and the distibution within the larger MFSR watershed.

Table 1-1: Summary of ten contributing areas of recently incised tributary alluvial fan study sites

Study site (tributary basin of alluvial fan)	Latitude	Longitude	Area (km^2)	Elevation (m)		Mean Slope (%)	Vegetation	Rock type	Recent fire year and name	Total / moderate-to-severely burned area (%)
				Max.	Min.					
Kotch	N 44° 30.695'	W 115° 14.254'	1.7	2750	1788	70	Engelmann spruce, Douglas fir, subalpine fir, lodgepole pine,	granodiorite	2006 Boundary Complex	100 / 82
Sheepeater[1]	N 44° 37.792'	W 115° 11.792'	1.6	2600	1550	68	Douglas fir, lodgepole pine	granodiorite	2007 Cascade Complex	100 / 88
Greyhound	N 44° 38.886'	W 115° 10.050'	3.0	2600	1560	54	Douglas fir, lodgepole pine, ponderosa pine	granodiorite	2007 Cascade Complex	95 / 72
Lake	N 44° 43.287'	W 115° 08.443'	6.1	2660	1450	35	lodgepole pine, Douglas fir, ponderosa pine	granodiorite	2000 Little Pistol	100 / 68
Orelano	N 44° 45.355'	W 115° 03.605'	2.5	2430	1380	62	Douglas fir, ponderosa pine	granodiorite	2000 Little Pistol	60 / 2
Upper basins mean			**3.0**	**2608**	**1546**	**58**				**91 / 64**
Sunflower	N 44' 73.088	W 114' 99.425	2.4	2115	1323	53	sagebrush Douglas fir	granodiorite granite	1988 Battle Axe	No data
Jack	N 44' 80.577	W 114' 82.188	4.2	2384	1231	62	sagebrush Douglas fir ponderosa pine	granite	1996 and 2000	69 / 9
Reservoir	N 44° 57.779'	W 115° 43.918'	3.6	2370	1110	48	sagebrush, Douglas fir ponderosa pine	granodiorite granite	1988	89 / 31
Pole	N 44° 58.329'	W 115° 44.018'	7.8	2650	1105	40	sagebrush Douglas fir ponderosa pine	granodiorite granite meta-argillite syenite	1988	69 / 23
Bernard	N 44° 58.532'	W 115° 44.178'	13.3	2550	1102	67	sagebrush Douglas fir ponderosa pine	granodiorite granite	2000	95 / 68
Lower basins mean			**4.5**	**2302**	**1218**	**54**				**84 / 33**

[1] Sheepeater is the site name used for an un-named tributary across (river right) from Sheepeater Hot Springs (river left). It does not refer to the official Sheepeater Creek.

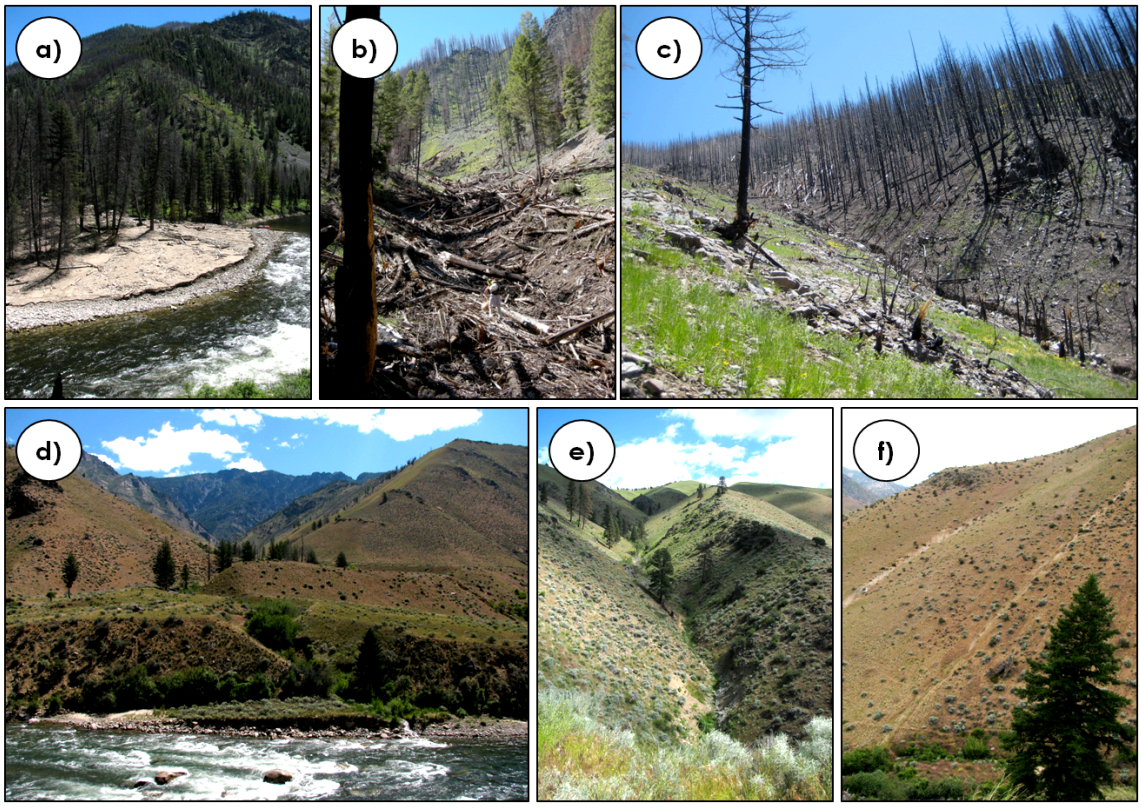

Figure 1-3: a) Upper basin (Sheepeater) alluvial fan formed by fire-related debris flow event in the summer of 2008. b) Half-mile long log jam located within the channel high in the contributing basin of Sheepeater. c) During the summer of 2000, the Little Pistol fire severely burned the north-facing slope of contributing basin of Lake Creek. d) Two fan surfaces located at tributary (Pole Creek) junction. The recent (1997) debris flow deposit incised through the older Holocene fan surface. e) Lower less-forested sub-basin (Sunflower Ck) f) hillslopes are characterized by sagebrush steppe with sparse ponderosa pine and Douglas fir.

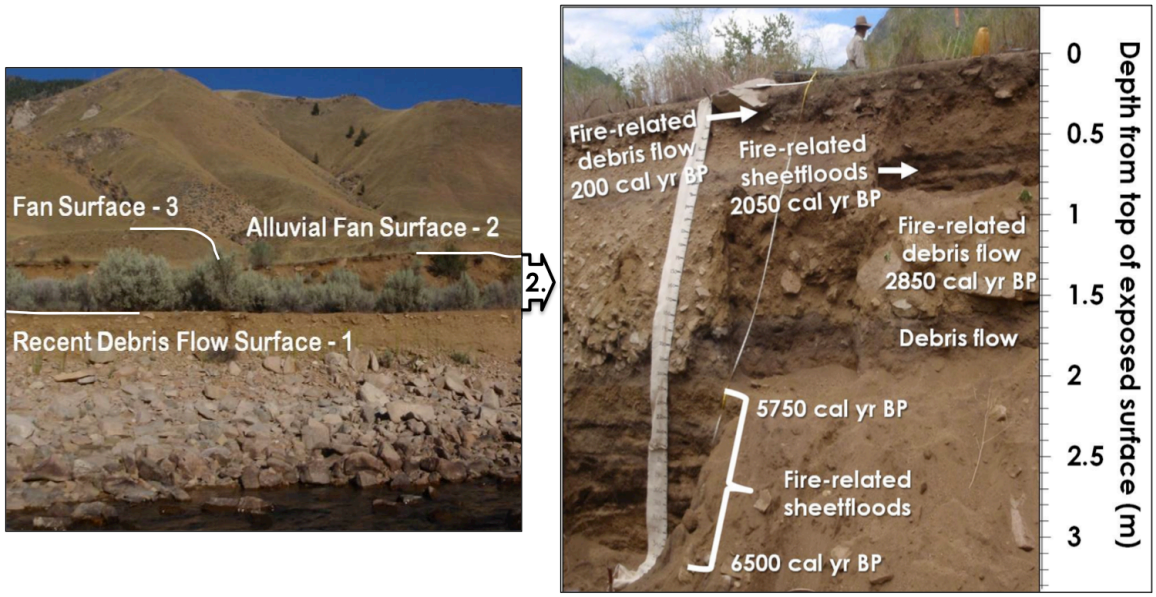

Figure 1-4: (Left) Photograph of Reservoir Creek sub-basin with three fan surfaces annotated. (Right) Incision of alluvial fan surface two reveals a snapshot of the depositional history of the contributing sub-basin.

Methods

Field Methods

We compared millennial-scale fire-related deposition on alluvial fans in lower elevation, drier ecosystems with deposition from higher elevation, wetter ecosystems. One stratigraphic profile exposes a sequence of depositional events of many older deposits within the larger fan complex (Figure 1-4). Deposition and facies type can vary across a fan complex during a single depositional event as a function of catchment geomorphology, lithology, sediment supply, and precipitation (e.g., Wells and Harvey, 1987). Therefore, multiple profiles (two to six) within each fan complex (five upper and five lower basins) were selected based on exposure of vertical sections within fans

containing clear fan stratigraphy. Exposures were targeted near the fan apex, where deposition from the steep contributing area is likely and where erosion by the main-stem river is less probable. In total, 35 stratigraphic profiles were investigated and 23 profiles dated within ten alluvial fan complexes. Obviously, not all fires were recorded in the stratigraphic record, and not all fires are exposed and dated. However, dating and describing fire records from multiple basins provides a statistical random sample of fire events that have burned the watershed.

Within each profile, discrete depositional layers were described by color, field texture (< 2 mm size fraction), depth, continuity, thickness, degree of sorting, angularity, charcoal abundance (Meyer et al., 1995), and percent gravel (> 2 mm size fraction). Discrete deposits were classified as fire-related based on a qualitative estimate of charcoal abundance. Fire-related deposits contained abundant charcoal and/or were underlain by a burned soil surface (Meyer et al., 1995). Charcoal fragments for ^{14}C-dating were carefully chosen within discrete deposits, based on their in-situ presence within the layer (e.g., lack of any bioturbation associated with burrows), angularity of charcoal fragment (indicating that charcoal had not been reworked by multiple events), and charcoal type. Needles, twigs, and other annually produced material was targeted in order to reduce inbuilt age errors (Gavin, 2001).

Depositional process was inferred based on deposit characteristics. In general, debris flow deposits were poorly sorted, matrix supported, and contained large angular clasts. Recent (2008) debris flow deposit characteristics were used as analogs to help identify past fire-related deposit characteristics in stratigraph ic profiles. Hyper-

concentrated flow deposits contained slight imbrication, less matrix material than debris flow deposits, and looked like dilute debris flows. Overbank flood deposits contained well-sorted fine-grained (fine sand-clay) sediment. Flood deposits often contained hydro-dynamically separated charcoal lying on top of the fine-grained sediment. Sheetflood deposits contained couplets of moderately well sorted, fine and coarse sand-sized sediment of varying thicknesses. Overbank flood deposits and sheetfloods with abundant charcoal were considered fire related (Meyer et al., 1995).

Analytical Methods

Individual charcoal fragments (n = 64) were ^{14}C-dated from 23 stratigraphic profiles to reconstruct fire histories in ten small steep sub-basins. We specifically targeted burnt twigs and needles in order to reduce inbuilt age errors associated with dating parts of a tree that are older than the year of the fire. Twigs were identified in the lab using a microscope to locate curved rings with small radius of curvatures. Individual charcoal samples werepretreated and ^{14}-C dated at the NSF-Arizona Accelerator Mass Spectrometry Laboratory and Lawrence Livermore National Laboratoy. Radiocarbon dates were calibrated using CALIB 6.0 (Reimer et al., 2004) and reported median calibrated ages were rounded to the nearest decade.

Ten pairs (20 samples) of field duplicates (two different charcoal fragments from the same discrete depositional layer) were radiocarbon dated. Individual calibrated age distributions of the duplicate sample pairs were statistically compared using a two sample paired t-test. The statistical test was used to test the assumption that charcoal fragments

found within one discrete deposit represent the same fire that caused the fire-related erosion and deposition event. A range in charcoal ages within one discrete deposit can result from charcoal being reworked by subsequent erosional events within the sub-basin, or from inbuilt age produced from burning of old parts of the vegetation. The magnitude of the difference in radiocarbon ages between duplicate samples helps to determine the cause of age discrepancies. If duplicate samples contained statistically indistinguishable ages, one sample was eliminated from the final analyzed data set to avoid exaggeration of fire peaks in the record because the same fire likely produced the two charcoal fragments. In addition, if statistically indistinguishable fires were recorded in multiple stratigraphic profiles within one fan complex, one of the duplicate samples was eliminated from final data set. Samples that resulted in a modern age (post-1950) and were located low in the stratigraphic profile were assumed to be from inset deposits within the incised channel and post-1950 ages from deposits at the top of stratigraphic profiles were considered to represent recent events.

We reconstructed the MFSR fire history using 64 radiocarbon-dated alluvial charcoal fragments from ten sub-basins adjacent to the main-stem. Although 64 charcoal fragments were dated (Table 1-2), seven pairs of field duplicates showed statistically indistinguishable ages, three samples recorded statistically indistinguishable ages from deposits within different profiles within the same fan complex, and five samples that were modern (i.e., post-1950) deposits. The final data set used for analysis contained 49 age distributions representing discrete fires across the landscape. The filtered data (n = 49) are presented in three ways: 1) upper basins fires, 2) lower basins fires, and 3) all

samples. The cumulative probability curves were smoothed with a 100-year running mean and were not normalized.

We measured 398 discrete deposits within 35 stratigraphic profiles from ten alluvial fans. While deposit thickness and deposit characteristics are highly variable spatially on a fan, deposit thickness values from multiple profiles within the same fan complex provide a more complete fire and depositional history for the fan complex. Discrete deposit thicknesses associated with debris flow, sheetflood, and fire-related deposits were summed throughout individual sub-basin alluvial fan sites, averaged among upper and lower basins, and then statistically compared between upper and lower basins. If the thickness distribution for the deposit type was normal and homoscedastic, then a t-test was performed. If distributions failed either assumption, then the non-parametric Kruskal-Wallis statistical test was performed.

Modern relationships between burn severity and debris flows were used to make inferences about past drivers of fire-related debris flow deposition. Classified burn severity data (MTBS, 2010) was derived from the differenced Normalized Burn Ratio (Key and Benson, 1999), an index formulated from Landsat TM band 7 and band 4 pre- and post-fire reflectance, and used to classify burn severity. Classes are assumed to represent the degree of canopy removal, which intercepts precipitation and the removal of understory, ground cover, litter, and duff, which creates roughness on hillslopes. We collected fire severity data for the six fires that burned (1988-2007) across nine of the ten study sub-basins prior to recent debris flow initiation and deposition (Table-1-1). Data was extracted for nine sub-basin contributing areas (Appendix C) defined as the upstream

contributing area of the recent debris flow deposit at the tributary junction alluvial fan. Fire severity data were statistically compared between upper and lower basins using a t-test. Fire severity data was also compared among aspects.

Results

Method Validation

An important assumption of this study is that the age of charcoal in the deposit is similar to the timing of deposition. To test this hypothesis, ten pairs of field duplicates (charcoal samples within the same discrete deposit) were dated to determine if the charcoal represented the same fire event. Seven duplicate pairs showed statistical indistinguishable ($\alpha = .05$) calibrated ages, suggesting that seven out of ten times deposition of alluvial charcoal on alluvial fan surfaces was likely related to the timing of a single fire event (Figure 1-5). Three field duplicate charcoal samples had a statistically significant ($\alpha = .05$) difference in ages, suggesting the older of the two duplicates was either from the encorportation of older reworked sediment containing older charcoal or the sample was derived from the inner heartwood of an older part of the tree. The magnitude of difference between median ages of duplicate pair charcoal samples was 310, 1010, and 1090 cal. yr BP. The two larger age discrepancies (1010 and 1090 cal. yr BP) are likely a result of the incorporation of older charcoal on the landscape into a younger fire-related deposit. Meyer et al. (1995) also examined the range of charcoal ages from discrete fire-related debris flow deposits and found that four out of five

charcoal fragments within one deposit represented statistically indistinguishable age distributions. Regardless, if charcoal has been reworked, charcoal found in an alluvial fan burned during a fire in the contributing basin. However, ~30% of the time, the charcoal fragment chosen to date could represent a fire that burned prior to the most recent depositional event.

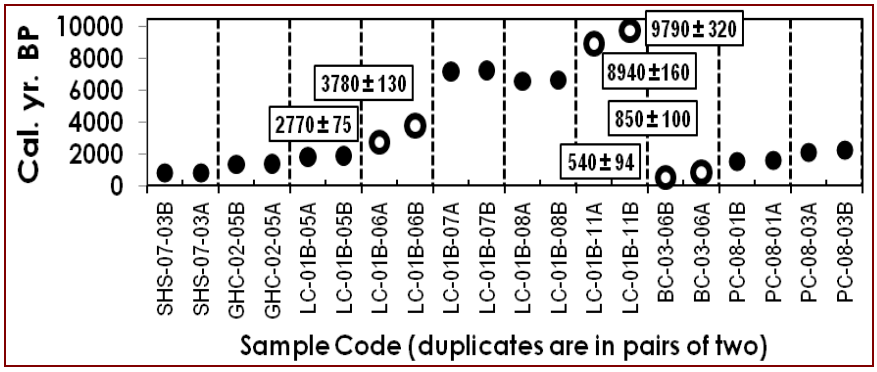

Figure 1-5: Calibrated radiocarbon age distributions of field duplicate (two pieces of charcoal from discrete deposit) are statistically compared using a paired t-test. Black dots represent samples with statistically (α=.05) indistinguishable calibrated age distributions. White dots represent field duplicates with statistically different calibrated age distributions and their median age with two-sigma error is labeled.

Recent Fire and Debris Flow Relationships

Despite a diversity of lithologies present in the MFSR watershed, all alluvial fan study sites along the main-stem MFSR were located within the Idaho Batholith. Approximately 90% of the total contributing basin area from ten study sites was underlain by granite or granodiorite (Figure 1-2). Incision along the main-stem MFSR has primarily occurred in Idaho Batholith granite and therefore the likelihood of alluvial fan sites in this lithology is high. However, ten additional recent debris flows were

located using 1 meter resolution photographs (NAIP, 2009). These additional ten debris flow sites were away from the main-stem river and 75% of their contributing basin areas were also underlain by Idaho Batholith granite and granodiorite (Figure 1-2).

Recent debris flows in the Middle Fork Salmon were associated with fire; modern observations indicate that ~80% of total study site contributing areas burned in the last 20 years. The timing between fire and debris flow production varied among sub-basins from one to nine years (Figure 1-6). The time lag between fire and debris flow generally decreased with increasing elevation. High severity fires occurred primarily on north and east-facing aspects, and fires were generally more severe in upper basins compared with lower basins (Figure 1-6). However, the difference in burn severity with aspect and with elevation was not statistically significant.

Recent debris flows in the MFSR appear to initiate primarily from sediment bulking mechanisms (Cannon et al., 2001; Meyer and Wells, 1997) inferred from the presence of rill formation close to watershed divides and pervasive rills on burned hillslopes (Figure 1-7). Rills converged downslope, where incision increased and sediment was added to the debris flow. While debris flow initiation has often been associated with a slope failure identified by a discrete landslide-scar (e.g., Iverson, 1997), the absence of these scars and the presence of pervasive rilling suggests the dominant mechanism causing debris flow initiation was sediment bulking, not slope failure.

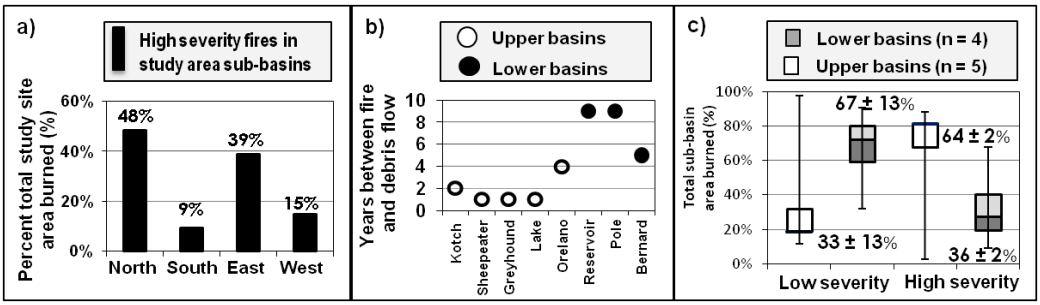

Figure 1-6: a) Plot shows relationship between modern classified burn severity data (MTBS) and aspect for nine study site areas combined, b) Plot shows lag between the timing of fire and erosion response, and c) Box plots show relationship between burn severity (MTBS) in upper versus lower basins. Labels show the mean ± standard error of the mean. The difference in burn severity between upper and lower basin is not significant.

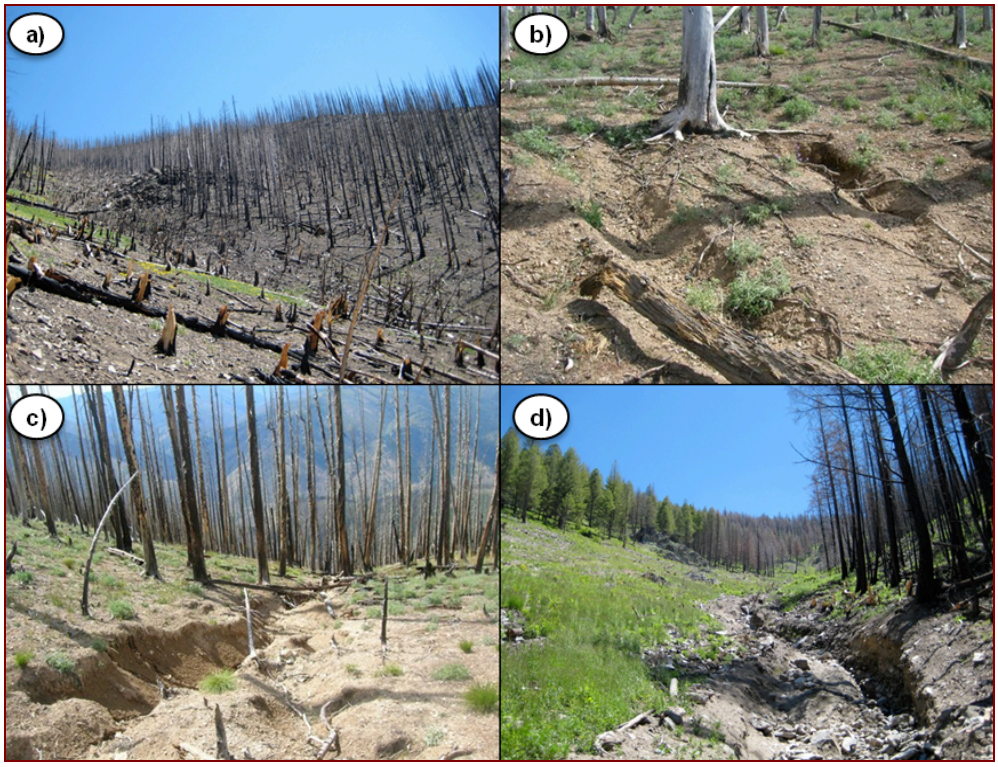

Figure 1-7: a) Photograph of a severely burned lodgepole pine forest on the northwest facing hillslope of Sheepeater basin. b) Photograph of rill formation on hillslopes high in the contributing basin of Lake Creek. c) A photograph of the incising rills downslope of formation in Lake Creek sub-basin. d) High in Sheepeater's contributing sub-basin where recent debris flow activity both incised the channel and deposited material along the channel's lateral margin.

Table 1-2: Summary of all radiocarbon dated deposits.

Sample #	Lab Code	Sample Code	Basin	Depositional Process	Fire Related (FR)	Thickness (cm)	% total depth	^{14}C age ± 1 sigma	Calibrated (Median) ± 2 sigma
1 †	AA88192	SHS-04-04	Sheepeater	Debris flow	FR	25	0.05	modern	modern
2 †	AA88198	LC-01-08	Lake	Overbank	FR	Unknown	NA	modern	modern
3 †	AA88208	PC-02-06	Pole	Sheetflood	FR	10	0.017	modern	modern
4 †	AA88209	NNC -01-01	No name	Debris flow	FR	158	0.88	modern	modern
5 ‡	149568	OC-04B-02 B‡‡	Orelano	Debris flow	FR	11	5	modern	modern
6 ‡ §	149560	OC-04B-02 A‡‡	Orelano	Debris flow	FR	11	5	90 ± 30	0 (107) 265
7 ‡ § **	149558	BC-03-03	Bernard	Burn surface	FR	5	2	95 ± 30	0 (109) 267
8 † §	AA88207	HR-01-02	Pole	Sheetflood	FR	26	7	135 ± 39	0 (137) 283
9 † § **	AA88202	BC-01-01	Bernard	Debris flow	FR	22	8	147 ± 38	0 (148) 283
10 †	AA88205	RC-03-09	Reservoir	Debris flow	FR	27	8	243 ± 38	0 (289) 429
11 ‡ §	153900	KC02-01	Kotch	Debris flow	FR	15	9	335 ± 60	309 (390) 477
12 ‡ §	153909	BC05-03	Bernard	Debris flow	Scarce	22	10	365 ± 60	316 (429) 501
13 † § **	AA88199	LC-02-05	Lake	Debris flow	FR	140	27	380 ± 36	316 (442) 508
14 † § **	AA88196	LC-01-01	Lake	Overbank	FR	2	< 1	385 ± 34	318 (450) 509
15 † §	AA88206	HR-01-01	Pole	Debris flow	FR	67	19	419 ± 82	299 (449) 557
16 ‡	149572	BC-03-06B‡‡	Bernard	Debris flow	Scarce	35	14	520 ± 35	505 (536) 630
17 †	AA88193	SHS-06-03	Sheepeater	Debris flow	FR	53	48	675 ± 35	558 (642) 681
18 ‡ § **	149567	OC-03-06	Orelano	debris flow	FR	80	16	875 ± 25	729 (777) 904
19 ‡ § ††	149557	SHS-07-03A‡‡	Sheepeater	Burn surface	FR	57	32	900 ± 35	738 (826) 911
20 ‡ § ††	149571	SHS-07-03B‡‡	Sheepeater	Burn surface	FR	57	32	870 ± 35	696 (778) 906
21 ‡ § **	149574	BC-03-06A‡‡	Bernard	Reworked	FR	35	14	925 ± 35	745 (849) 925
22 † § **	AA88203	OC-03-03	Orelano	Debris flow	FR	75	15	955 ± 35	790 (856) 931
23 † § **	AA88210	BC-02-04	Bernard	Burn surface	FR	2	2	1008 ± 40	795 (928) 1035
24 † §	AA88200	NNC-01-02	No name	Overbank	FR	12	7	1060 ± 240	555 (993) 1408
25 ‡	153901	KC02-04	Kotch	Sheetflood	FR	14	9	1070 ± 60	929 (975) 1055
26 ‡ §	153902	KC02-05	Kotch	Debris Flow	FR	26	16	1190 ± 60	1053 (1116) 1180
27 † §	AA88195	0C-04-01	Orelano	Sheetflood	FR	10	2	1195 ± 41	988 (1122) 1201
28 ‡ ††	149556	GHC-02-05B‡‡	Greyhound	Overbank	FR	4	2	1485 ± 35	1302 (1368) 1507
29 ‡	149559	GHC-02-03	Greyhound	Overbank	FR	4	2	1462 ± 36	1300 (1350) 1405
30 ‡ ††	149569	GHC-02-05A‡‡	Greyhound	Overbank	FR	4	2	1525 ± 35	1345 (1409) 1518
31 † § ††	AA88194	PC-08-01B‡‡	Pole	Debris flow	Scarce	224	79	1620 ± 30	1412 (1505) 1592

† Lab codes with prefix AA are from NSF-AMS Facility at the University of Arizona

‡ Charcoal processed at Lawrence Livermore National Laboratory

§ Grey boxes indicate samples with the statistically same age distribution (α=.05) (Separate adjacent groups include 31-33, 34-35, 37-38, 39-40, and 41-42)

** Sample represents fire that was sampled twice (two samples with statistically same age distribution) within the same small basin

†† Sample is a field duplicate with the statistically same age distribution as paired sample

‡‡ Duplicate sample indicated with A or B at the end of the sample code

Table 1-2: (continued)

Sample #	Lab Code	Sample Code	Basin	Depositional Process	Fire Related (FR)	Thickness (cm)	% total depth	^{14}C age ± 1 sigma	Calibrated (Median) ± 2 sigma
32 ‡ §	149561	GHC-01-05	Greyhound	Sheetflood	FR	14	4	1637 ± 36	1414 (1534) 1615
33 ‡ § ††	149550	PC-08-01A ‡‡	Pole	Debris flow	Scarce	2	1	1710 ± 30	1546 (1616) 1697
34 ‡ §	153910	BC05-04	Bernard	Debris flow	FR	23	11	1830 ± 70	1696 (1769) 1866
35 ‡ § ††	153904	LC01B-05 A ‡‡	Lake	Sheetflood	FR	37	7	1880 ± 60	1728 (1828) 1884
36 ‡ ††	153897	LC01B-05 B ‡‡	Lake	Sheetflood	FR	37	7	1955 ± 60	1827 (1906) 1987
37 ‡ §	149576	RC-03B-03	Reservoir	Sheetflood	FR	5 – 27 §§	2 - 8	2095 ± 30	1994 (2067) 2144
38 ‡ § ††	149555	PC-08-03A ‡‡	Pole	Debris flow	FR	31	11	2100 ± 30	1995 (2072) 2146
39 ‡ §	153903	KC02-06	Kotch	Debris flow	FR	40	25	2170 ± 60	2152 (2232) 2336
40 ‡ § ††	149563	PC-08-03B ‡‡	Pole	Debris flow	FR	31	11	2230 ± 35	2152 (2232) 2336
41 ‡ §	149551	LC-01B-06A ‡‡	Lake	Debris flow	FR	23	4	2660 ± 30	2742 (2769) 2844
42 ‡ §	153911	BC05-08	Bernard	Sheetflood	FR	12 – 55 §§	5-25	2735 ± 90	2756 (2830) 2928
43 †	AA88191	RC-01B-08	Reservoir	Debris flow	Scarce	82	25	2770 ± 45	2767 (2867) 2964
44 ‡	153912	BC05-09	Bernard	Overbank	FR	42	19	2975 ± 90	3000 (3158) 3268
45 ‡ §	153913	BC05-10	Bernard	Debris flow	FR	23	11	3405 ± 80	3558 (3656) 3826
46 ‡ §	149564	SHS-03-03	Sheepeater	Debris flow	Scarce	19	13	3481 ± 68	3576 (3756) 3922
47 † §	AA88201	LC-01B-06B ‡‡	Lake	Debris flow	FR	23	4	3510 ± 45	3644 (3781) 3899
48 ‡	153914	SH508-02	Sheepeater	Debris flow	Scarce	60	14	4520 ± 90	5039 (5163) 5314
49 ‡	149575	0C-04-04	Orelano	Debris flow	FR	120	36	4693 ± 48	5316 (5415) 5526
50 ‡	149545	RC-03-04	Reservoir	Sheetflood	FR	3	1	5005 ± 30	5653 (5733) 5889
51 ‡	149546	SC-01-02	Sunflower	Sheetflood	FR	10 – 197 §§	2 - 39	5110 ± 40	5746 (5823) 5929
52 ‡	149548	RC-01B-18	Reservoir	Sheetflood	FR	2 – 121 §§	1 - 36	5585 ± 50	6290 (6366) 6453
53 † §	AA88204	SC-01-04	Sunflower	Sheetflood	FR	21	4	5650 ± 35	6318 (6432) 6498
54 ‡ §	149565	RC-03-01	Reservoir	Sheetflood	FR	14 – 90 §§	4 - 26	5689 ± 64	6318 (6480) 6638
55 ‡ ††	149566	LC-01B-08A ‡‡	Lake	Burn surface	FR	5	1	5785 ± 35	6495 (6587) 6665
56 † ††	AA88197	LC-01B-08B ‡‡	Lake	Burn surface	FR	5	1	5850 ± 30	6566 (6672) 6741
57 ‡ ††	153898	LC01B-07 B ‡‡	Lake	Debris flow	FR	26	5	6280 ± 90	7067 (7212) 7311
58 ‡ ††	153905	LC01B-07 A ‡‡	Lake	Debris flow	FR	26	5	6325 ± 90	7163 (7256) 7330
59 ‡	149552	LC-01-07	Lake	Overbank	FR	19	4	7347 ± 47	8025 (8154) 8310
60 ‡	149562	HR-01-06	Hood	Debris flow	FR	36	24	7720 ± 50	8417 (8499) 8589
61 ‡	149570	LC-01B-11A ‡‡	Lake	Debris flow	Scarce	47	9	8040 ± 30	8778 (8942) 9021
62 ‡	149549	LC-01B-11B ‡‡	Lake	Debris flow	Scarce	47	9	8780 ± 35	9626 (9792) 10113
63 ‡	149547	SHS-08-05	Sheepeater	Debris flow	FR	30	7	9960 ± 45	11248 (11383) 11611
64 ‡	149547	JC-01-02	Jack	Debris flow	Scarce	178	48	11730 ± 130	13315 (13581) 13834

§§ Sheetflood deposit contains a thickness range because couplets could be derived from single or multiple events

Holocene Fire Reconstruction

The MFSR fire record spans the last 14,000 cal. yr BP (Table 1-2; Figure 1-8). The number of dated deposits decreases with time likely in part because of the fading record, where older deposits are less likely to be preserved and exposed (e.g., Ballenger and Mabry, 2011; Meyer et al., 1995; Surovell et al., 2009). MFSR fire records show both spatial and temporal synchronicity, defined as periods in time when multiple (≥ 2) sub-basins contain deposits with statistically indistinguishable ages. Periods of inferred spatially widespread fire include 110 ±150, 450 ±120, 860 ±75, 1120 ±75, 1560 ±50, 1790 ±70, 2070 ±70, 2240 ±100, 2780 ±60, 3730 ±100, and 6440 ±120 cal. yr BP (mean pooled ages rounded to the nearest decade). These times are represented as the highest peaks in the smoothed cumulative age distribution curves (Figure 1-8). Eight out of the 11 periods of inferred widespread fire burned both upper and lower ecosystems. Five of these eight periods (110 ±150, 450 ±120, 2240 ±100, 2780 ±60, and 3730 ±100 cal. yr BP) produced large fire-related debris flows in upper and lower basins. Only three periods (1120 ±75, 2070 ±70, and 6440 ±120 cal. yr BP) resulted in fires burning in only upper or lower ecosystems.

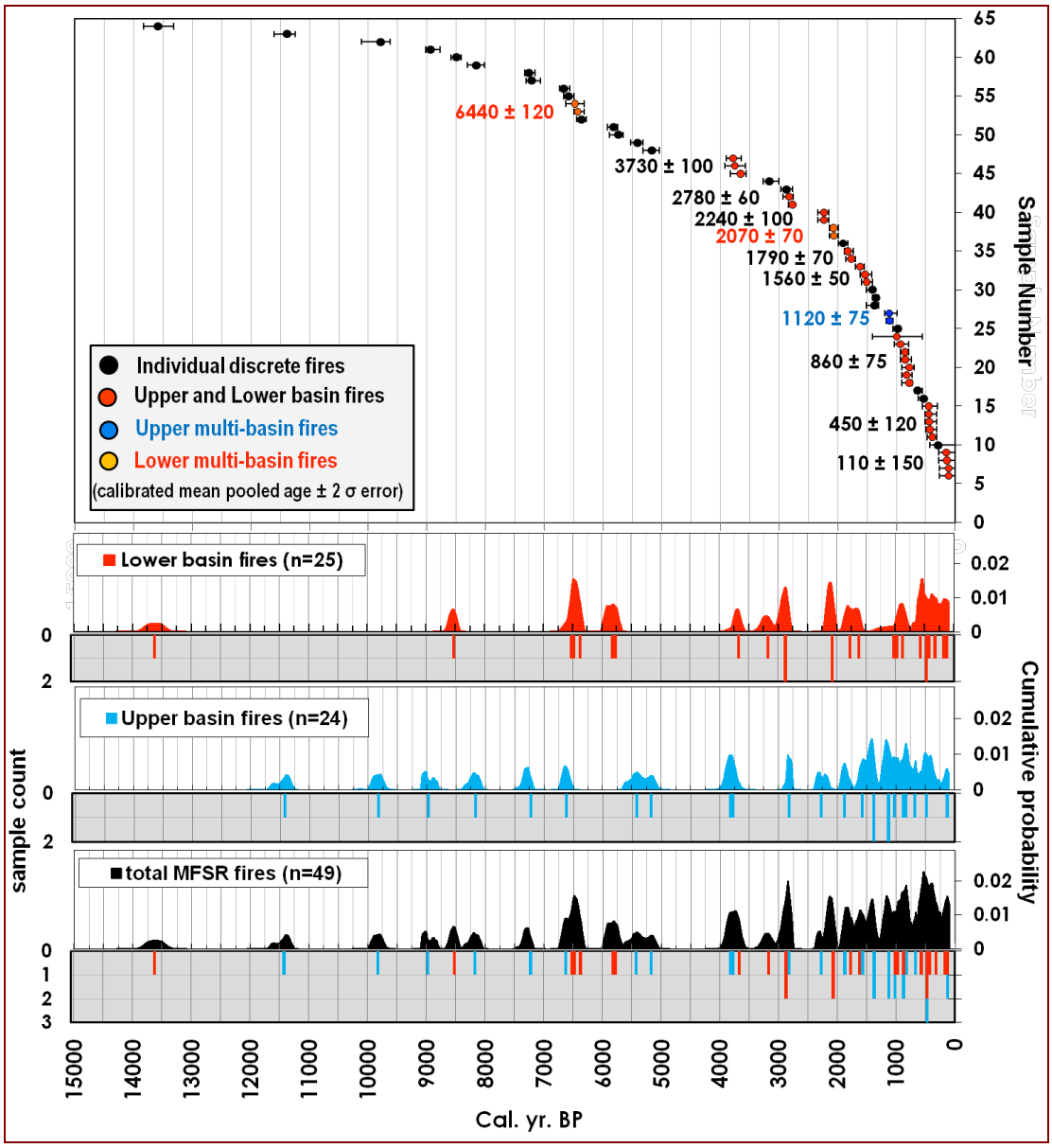

Figure 1-8: Top graph shows all calibrated ^{14}C-dates (n=64) with 2-sigma error. Labels show 11 mean pooled ages that represent times when charcoal fragments from different sub-basins contain the statistically (α = .05) indistinguishable age distributions. Black labels represent fires burning in upper and lower basins, red labels represent lower and blue upper multi-basin fires. Bottom graphs show three cumulative fire probability distributions representing only discrete fires. The upper basin fires (blue curve) represent wetter basins, lower basin fires (red curve) represent drier basins, and the total MFSR fires (black curve) include fires from all basins. Bar graphs represent the number of samples for a given time interval. Red bars are samples from lower basins and blue bars are from upper basins.

Alluvial charcoal records indicate the frequency and synchronicity of fires in the MFSR have changed throughout the Holocene. Here, "fire frequency" is defined as the number of fires recorded in the alluvial charcoal record from ten contributing sub-basins per time interval (yr/fire). While the actual fire frequency is much higher than this, this "fire frequency" allows for comparison of relative frequency changes over the Holocene. Four fires were recorded between 14–9 ka (1250 yr/fire), then fire frequency increased between 9–8 ka to three fires in 1000 years (330 yr/fire). Fire frequency continued to increase between 7.5-5 ka to eight fires in a 2500-year interval (310 yr/fire). During the 500 yr period between 6.25-6.75 ka, four fires burned in both upper and lower basin ecosystems (125 yr/fire). A gap in the fire record between 5–4 ka represents the longest fire-free period over the last 10 ka. This hiatus was followed by increased fire frequency from 4–3 ka, when seven fires were recorded in approximately 1000 years (140 yr/fire). Fires became synchronous in space and time starting ~3.8 ka, burning both upper and lower basins. Ten out of the 11 periods of synchronous fires (3730, 2780, 2240, 2070, 1790, 1560, 1120, 860, 450, and 110 cal. yr BP) burned during the last 4 ka.

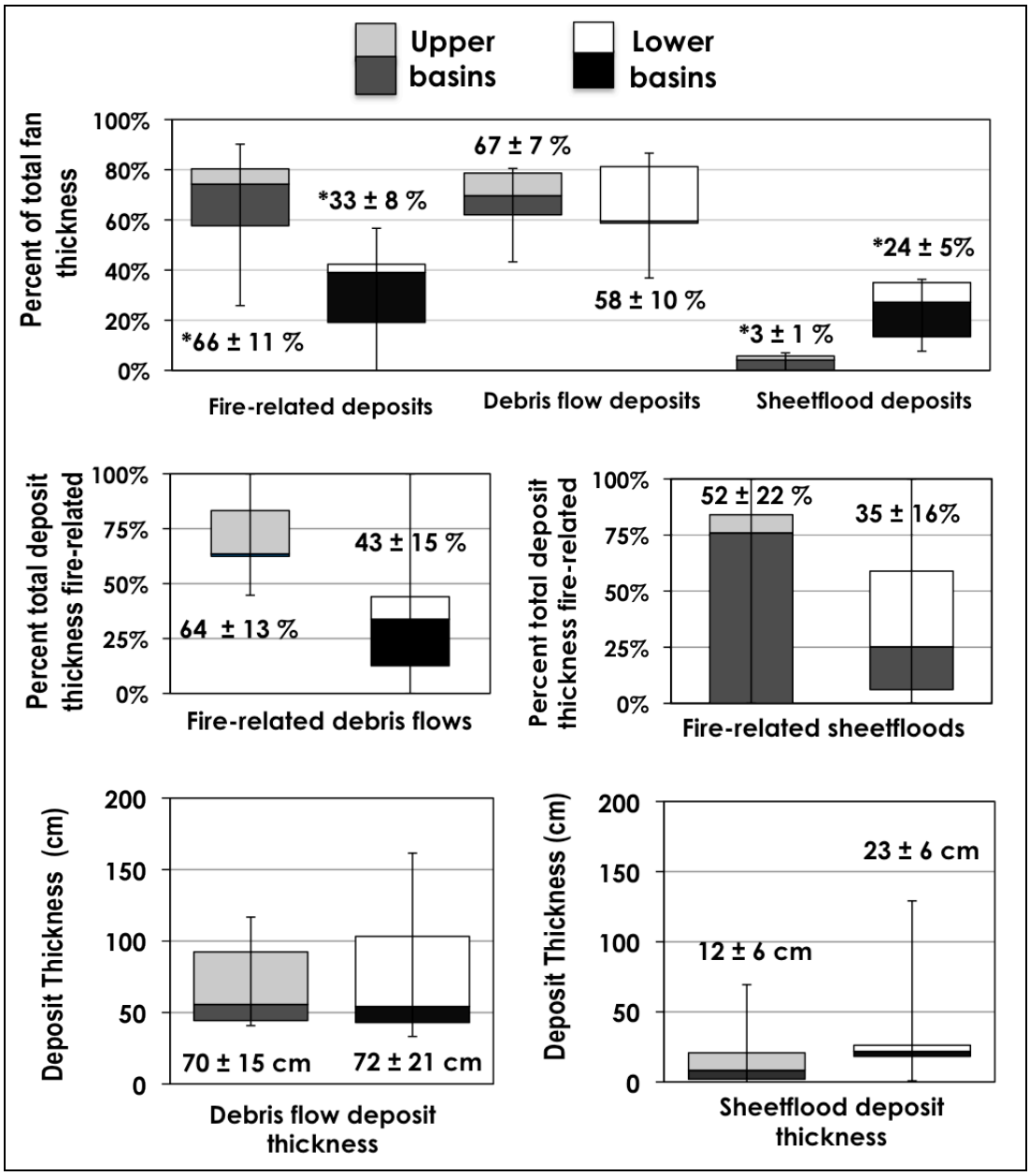

Figure 1-9: Upper basin (n=5) and lower basin (n=6) box plots show the interquartile data range and error bars represent minimum and maximum data values. Labels report the mean and standard error of the mean. The top set of box plots shows deposit-type thickness as a percent of the total measured fan thickness. The middle box plots represent the percent of deposits that were classified as fire-related. Bottom box plots show thickness of debris flow deposits and sheetflood deposits. (Sunflower sub-basin was divided into two basins increasing the lower basin population size to 6). Statistically significant differences (α=.05) are represented with an asterisk.

Fire-related Depositional Process

We compared upper vs. lower basin alluvial fan deposit thicknesses in order to 1) examine the role of fire-related vs. non-fire related sediment transport to alluvial fans, 2) investigate the difference between fire-related deposition in upper and lower basins, and 3) infer the severity of past fires based on the thickness and type of fire-related deposit **(**Figure 1-9**)**. The two primary deposit types are debris flows and sheetfloods, where thick fire-related debris flows are inferred to be generated from extensive and severe fires (e.g., Pierce et al., 2004; Cannon et al., 2001). All deposit thickness results are reported as a mean with the standard error of the mean. Fire-related deposits comprised significantly greater total fan thicknesses in upper basin fans (66 ± 11%) compared to lower basin fans (33 ± 8%). Debris flow deposits comprised 67 ± 7% of upper basin fan deposits vs. 58 ± 10% for lower basin fans, and ~64 ± 13% of all debris flow deposits in the upper basin vs. 43 ± 15% of all debris flow deposits in the lower basin were fire-related**.** Sheetflood deposits comprised significantly less of the total upper basin fan deposits (3 ± 1%) than lower basin fan deposits (24 ± 5%). Approximately 52 ± 22% of all sheetflood deposits in the upper basin and 35 ± 16 % in the lower basin were fire-related. Debris flow deposits were significantly thicker than sheetflood deposits. The thickness of sheetflood packages ranged from two centimeters to two meters, with thinner median sheetflood deposit thickness (12 ± 6 cm) recorded in upper basins than in lower basins (23 ± 6 cm). The mean debris flow deposit thickness was 70 ± 15 cm in upper basins and 72 ± 21 cm in lower basins.

Thick fire-related debris flows were produced in upper basins throughout the Holocene while debris flow deposits in lower basins are only preserved during the early and late Holocene (Figure 1-10). Lower basin debris flow activity peaked between 2-4 ka and 100-600 cal. yr BP. Sheetfloods were the dominant erosional process depositing sediment onto lower basin alluvial fans between 7-5 ka.

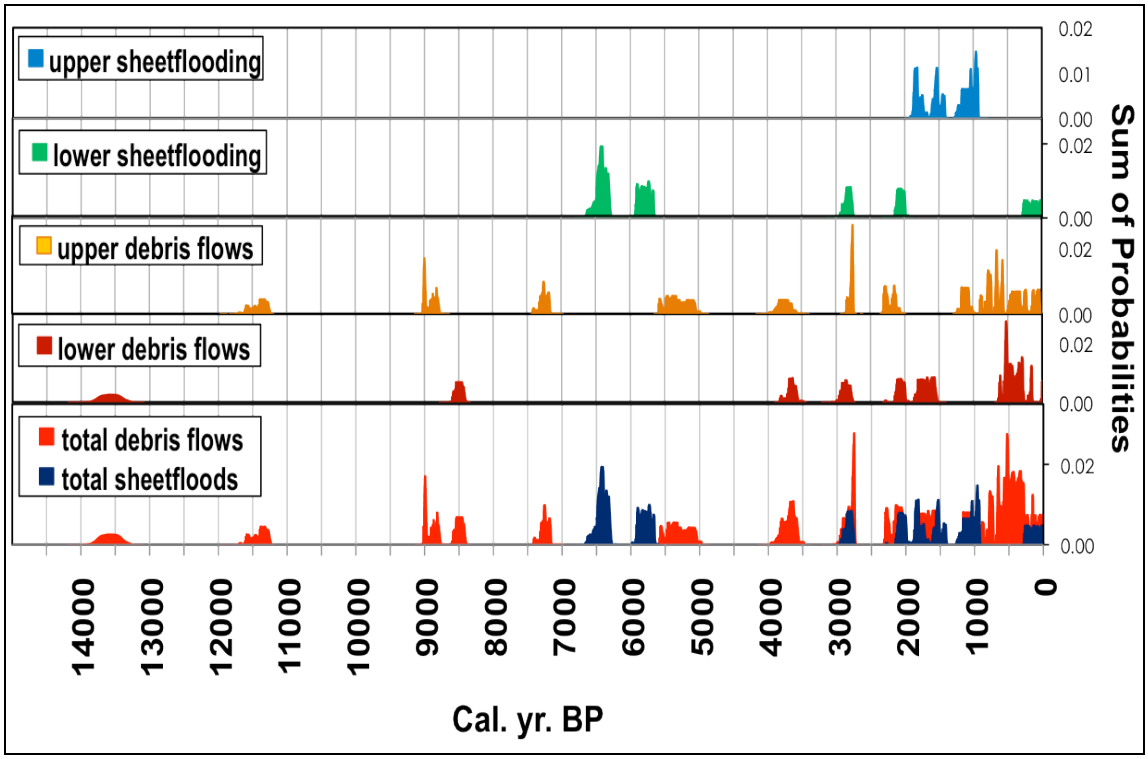

Figure 1-10: Summary of dated sheetflood and debris flow deposits. Cumulative fire probability curves are deconstructed by upper and lower basins and by primary depositional process.

Discussion

Holocene records of wildfire and fire-related sedimentation span the last 14 ka and reveal fire has played a dominant role in alluvial fan deposition and therefore

hillslope erosion, main-stem aquatic habitat, river geometry, and sediment supplied to the fluvial Middle Fork Salmon River. The timing and severity of wildfire and the magnitude, frequency, and type of fire-related deposition have varied spatially and temporally during the Holocene. Fire-related deposition on alluvial fans was greater in upper wetter basins compared to lower drier basins. We attribute this finding to two primary mechanisms. First, burning rangeland fuels composed of small shrubs and grasses produce charcoal fragments that are likely to be removed by wind, surface runoff events, and through soil development resulting in poor preservation of charcoal over time and therefore a weaker fire signal. For example, in lake sediment studies, a stronger fire signal has been found to be associated with greater biomass within contributing basins (Marlon et al., 2006; Whitlock et al., 2004). Secondly, rangelands are generally fuel-poor (compared to denser forested ecosystems) and contain patchy vegetation distributions. Modern burn severity data suggests that recent severe fires burned less total area in lower drier basins (Figure 1-6). In these xeric naturally patchy ecosystems, the landscape promotes continuous surface runoff events that are limited in sediment transport capacity (Lavee et al., 1995) without the needed influence of severe fire as a catalyst. Naturally lower vegetation cover on lower basin hillslopes may make these basins more susceptible to non-fire-related erosional events. Meyer et al., 2001 found that large sheetfloods were produced from an unburned rangeland watershed and produced similar sediment yields to a nearby burned previously forested watershed. Therefore moderate to severe fires are not necessarily needed to initiate a large geomorphic response in drier, less-vegetated lower basins.

Widespread severe fires, inferred from multi-basin statistically indistinguishable fire distributions that correlate to large fire-related debris flows, are recorded frequently during the last 4 ka in the stratigraphic record. Widespread severe fires require both high fuel loads combined with severe or prolonged drought. Modern analogs from severe fire years in 2000 and 2007 indicate that fires burn throughout a range of ecosystems during severe drought years that follow longer intervals of fuel accumulation (e.g., Morgan et al., 2008; Pierce and Meyer, 2008; Westerling et al., 2003). In addition, these recent severe fires produced large fire-related debris flows in the MFSR. We infer, then, that conditions similar to modern analogs promoted widespread fires during the Holocene. Severe droughts following wet conditions build up fuels and drive synchronous fires. Fires burned in both upper and lower basins of the MFSR and produced large fire-related debris flows ~110, 450, 860, 2240, 2780, and 3730 cal. yr BP (Figure 1-10). Pollen records from the Sawtooth Mountains (Whitlock et al., 2010) suggest modern differences in vegetation between upper and lower basins likely existed for the last 2.6 ka. In addition, pollen and charcoal records from the Bitterroot Mountains (Brunelle et al., 2005) suggest fire regimes across ecological gradients are currently more similar than at any other time during the Holocene. Therefore, it is reasonable to assume that the modern vegetation differences (wetter, more densely vegetated upper basins vs. more xeric lower elevation basins) and associated differences in fire regimes have persisted across ecological boundaries over Holocene timescales. Vegetation types and densities at a given site, however, have varied with both millennial-scale changes in climate and with

post-glacial migrations of tree species (Figure 1-11; Whitlock et al., 2010; Marlon et al., 2006).

The oldest fires recorded (~13.5, 11.5, and between 9-8 ka) are from charcoal fragments found in thick fire-related debris flow deposits (1-11). Since few alluvial charcoal fire records extend this far back in time, the preservation of these late Pleistocene-early Holocene fire-related deposits suggests these events were likely large and associated with high severity fires. A pollen study in the Sawtooth Mountains pine forest expanded in the headwaters of the MFSR during the early Holocene (Whitlock et al., 2010). An increase in fuel loads, coupled with periodic drought, would have resulted in severe fires and large fire-related debris flows. Frequent flood events were recorded in the small headwater lake in the Sawtooths (Whitlock et al., 2010), which suggest increased storminess and thus a high likelihood of lightening caused fire ignition. During the late Pleistocene-early Holocene (12-9 ka) precipitation was highly variable in the lower Salmon River (Davis et al. 2002) suggesting regional increases in precipitation variability and unstable climate conditions. If older inferred severe fires in the MFSR are significant regionally, then ~13.5, 11.5, and between 9-8 ka were potentially times of regional droughts (Figure 1-9). These oldest fire peaks in the MFSR record roughly correspond with peaks in fire activity over the broad scale of North America ~13.9, 13.2, and 11.7 (Marlon et al., 2009) which also suggest regionally extensive droughts. Two MFSR fire peaks (~10 and 8 ka) correlate to inferred droughts in the Sawtooth Mountains (Whitlock et al., 2010).

The frequency of recorded fires in the MFSR increased between 9-8 ka, corresponding to both peak fire frequency and a vegetation transition from closed pine and Douglas fir forests to open Douglas fir forests and sagebrush steppe in the Sawtooth Mountains (Whitlock et al., 2010) persisted in the pollen record to ~ 6 ka (Whitlock et al., 2010). Fires burned in Yellowstone National Park (Huerta et al., 2009; Meyer et al., 1995) and at Cygnet and Burnt Knob Lake, Idaho (Brunelle et al., 2005) at ~8 ka. Fire frequency throughout the Northern Rocky Mountain forests increased ~9 ka (Whitlock et al., 2008) and is suggested to have peaked 7-6 ka (Power et al., 2011). Fire frequency peaked between 7-5.5 ka in the MFSR record, evident by high synchronicity of fires among basins and short intervals between fires.

Changes in depositional process during the mid-Holocene (8-5.5 ka) support widespread xeric vegetation communities throughout the MFSR watershed. While fire-related debris flows dominate the stratigraphic record from 14 until 8 ka in the MFSR (where debris flows represent 4 of 6 dated deposits), sheetfloods are the primary depositional processes between 8-5.5 ka in lower basins (where sheetfloods represent 5 of 8 dated deposits; Figure 1-10). Sheetflood deposits are associated with warm dry conditions evident spatially along the ecosystem gradient of the MFSR composing greater percentages of alluvial fan thickness in lower basins compared to upper basins (Figure 1-9) are observed in modern lower basin channels but are not seen in upper basins. Packages of sheetfloods cluster around the mid-Holocene and consist of sequences of thin (8-22 cm) deposit couplets. These packages represent multiple frequent (< 140 yr/fire), small erosional events. A similar landscape response was

observed in the South Fork Payette River, Idaho between 6600-7400 cal. yr BP with stratigraphic profiles containing frequent (33-80 yr/fire) small fire-related sheetflood deposits (Meyer et al., 2001). Spatial and temporal patterns in the MFSR and regional support the association between sheetflood deposits and warm dry climate conditions. Xeric sparsely forested ecosystems burn in frequent, less severe fires. Less severe fires create a patchy landscape, discontinuous flow paths, decreased hydrophobicity in soils, and surface runoff entrains less sediment (Lavee et al., 1995), which all act to decrease the likelihood of producing a debris flow under similar storm conditions.

Fire-related debris flows, inferred to be associated with severe fires, became more frequent and synchronous in space and time ~4 ka. The marked increase in fire activity during the last 4 ka corresponds to pine expansion throughout the Northern Rocky Mountains (Whitlock et al., 2008) and the establishment of modern forests in the nearby Bitterroot Mountains (Brunelle et al., 2005). The emergence of closed, dense lodgepole pine forests in the Sawtooth Mountains at ~2650 cal. yr BP (Whitlock et al., 2010) corresponds to the highest frequency of severe fires and large fire-related debris flows in the MFSR record (27 discrete fires over 2500 yrs; Figure 1-11). Increased forest density increases the abundance of fuel and the severity of fires during warm dry spring and summer seasons.

Climate has been found to apply strong chemical and physical controls on landscape evolution (e.g. Dixon et al., 2009). A generally cooler, wetter climate would drive forest expansion, increasing cohesion needed to maintain steep hillslopes (Collins et al., 2004), and increase sediment storage on hillslopes. Wetter climates also increase

weathering rates (Riebe et al., 2004; White and Blum, 1995). When these overall cooler, wetter climate conditions are punctuated by severe drought and fire, the large amounts of sediment stored on destabilized slopes produce large debris flows during storm events.

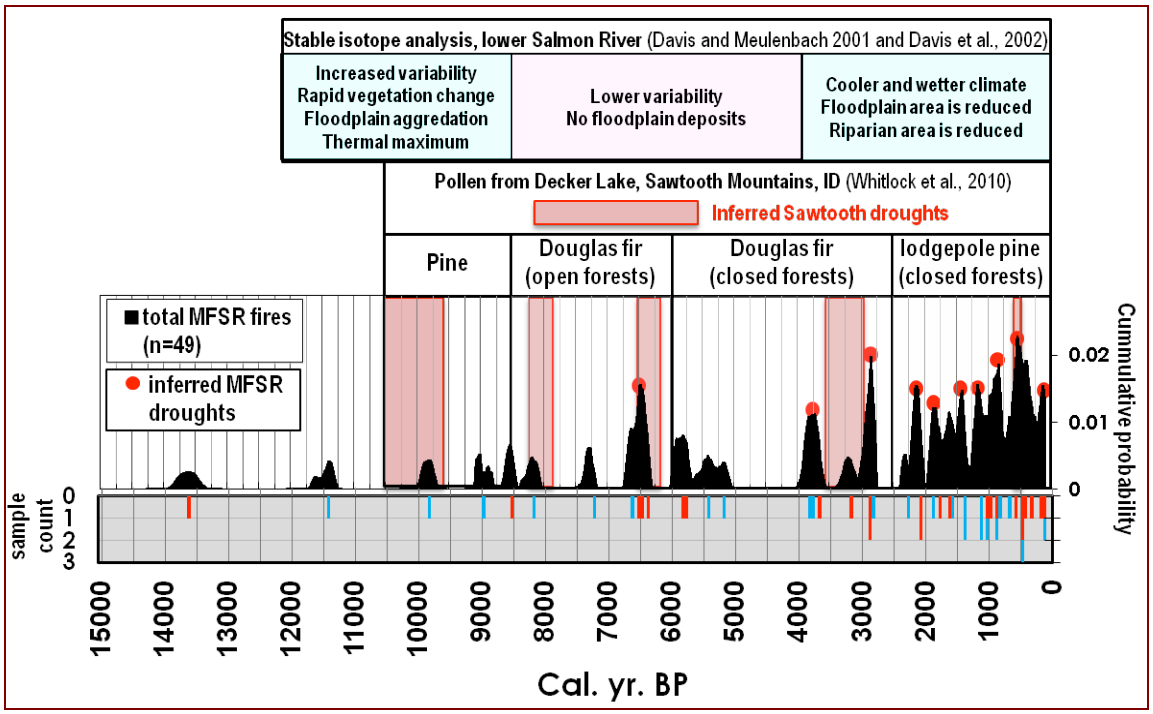

Figure 1-11: The fire record from the MFSR is in black with upper (blue) and lower (red) basin fire count displayed in the inverted bar graph. MFSR inferred droughts are identified with red circles, representing times when fires were burning multiple basins. The fire record is compared to two regional climate proxies.

Alluvial charcoal records in the MFSR demonstrate that the Medieval Climatic Anomaly (MCA; ~1050-650 cal. yr BP) was a period when fires burned regionally throughout Idaho recorded alluvial sediments in the South Fork Payette (Pierce et al., 2004), Sawtooth Mountains (Svenson, 2010), City of Rocks (Weppner, 2012), and Wood Creek (Nelson and Pierce, 2010). Large fire-related sedimentation events were produced

during the MCA in both the South Fork Payette, Idaho (Pierce et al., 2004) and in Yellowstone National Park (Meyer et al., 1995). Lower basin alluvial fans in the MFSR did not record large fire-related debris flows during the MCA while upper basins in the MFSR and regionally mesic ecosystems fire peaks were derived from charcoal within fire-related debris flow deposition during this time (Figure 1-13). The smaller fire peaks in the lower elevation basins of the MFSR and in xeric ecosystems during the MCA suggests that perhaps the warm and dry climate conditions in these basins limited accumulation of fuels and therefore fires during this time. This contrasts with the nearby South Fork Payette record, which shows fires burning throughout a range of ecosystems during this time (Pierce et al., 2004).

The highest peak in fire and fire-related debris flows is recorded in the MFSR between 200-600 cal. yr BP (Figure 1-13), which corresponds with the Little Ice Age (LIA; 100-650 cal yr. BP). This is also the highest peak in fire activity in the South Fork Payette, Idaho, when frequent but perhaps lower severity fires burn throughout a range of ecosystems (Pierce et al., 2004). Although many records have characterized this period as generally cooler, periodic drought conditions were inferred from punctuated declines in pine from 600-500 cal. yr BP, in the Sawtooth Mountains, (Whitlock et al., 2010) and drought conditions recorded at ~450 and 550 cal. yr BP from tree rings in the Sawtooth-Salmon River (Biondi et al., 1999). A large multi-basin fire is recorded in both tree rings and alluvial charcoal ~320 cal. yr BP in the Sawtooth Mountains (Svenson, 2010). A clear fire peak is seen regionally ~ 500 cal. Yr BP across drier ecosystems in lower elevation south-facing slopes of the South Fork Payette River, ID (Pierce et al., 2004),

Wood Creek, ID (Nelson and Pierce, 2010), and in the City of Rocks, ID (Weppner, 2012; Figure 1-12; Figure 1-13). While overall cool climate conditions of the LIA would suppress fire spread in mesic ecosystems, it would promote vegetation growth in moisture-limited xeric ecosystems, increasing fuel abundance needed to increase burn severity and promote debris flow generation during periodic drought.

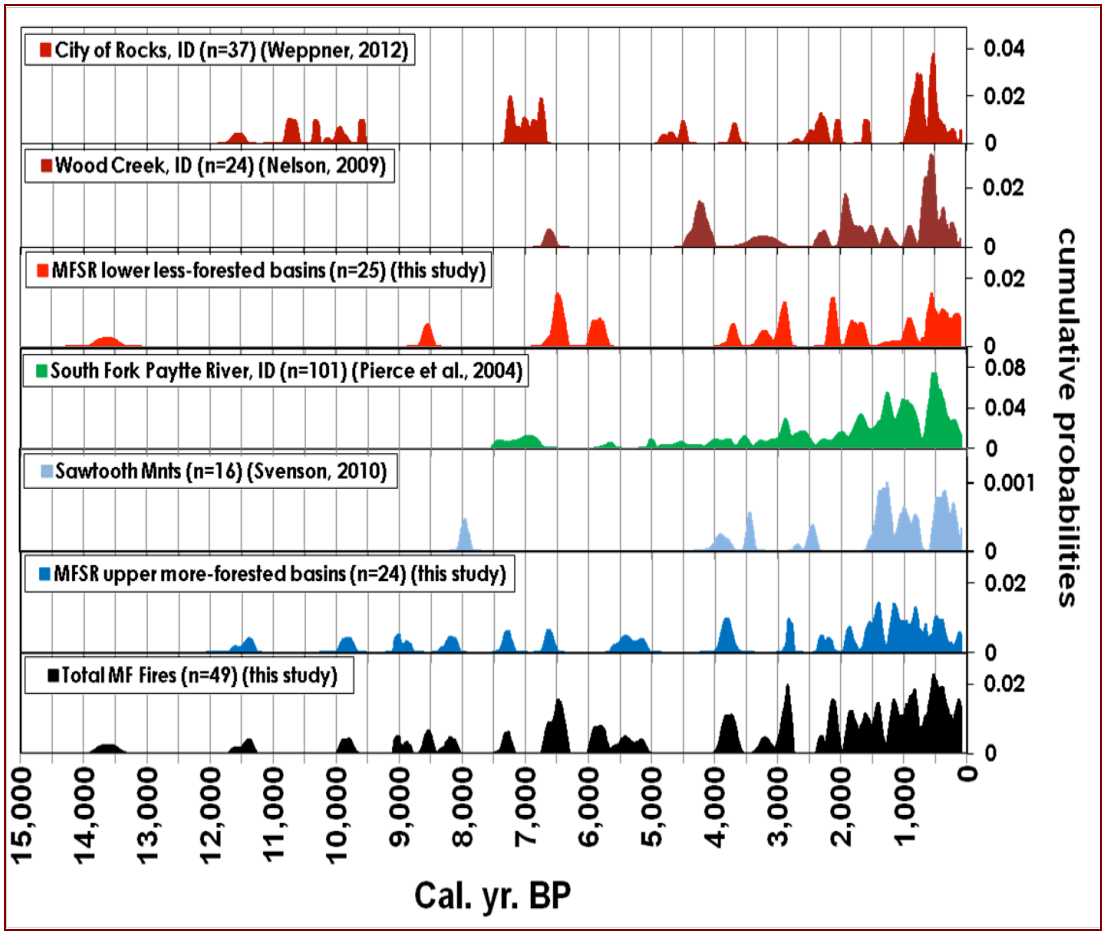

Figure 1-12: Comparison of regional Holocene fire records from throughout Idaho. Drier study sites include City of Rocks, ID (Weppner, 2012), South Fork Payette, ID low elevation and south-facing slopes, Wood Creek, ID (Nelson and Pierce, 2010), and lower basins in the MFSR (this study). Wetter study sites include South Fork Payette, ID high elevation and north-facing slopes, Sawtooth Mountains (Svenson, 2010) and upper basins in the MFSR (this study).

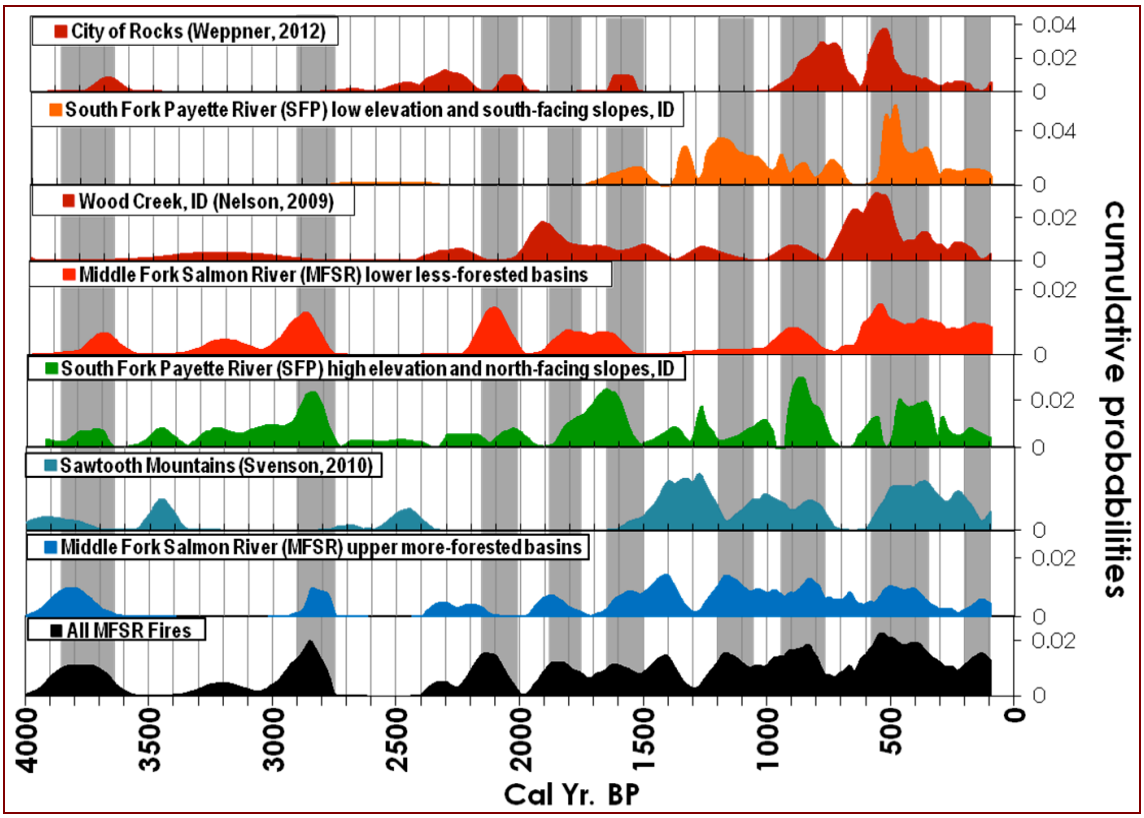

Figure 1-13: Comparison of regional fire records during last 4 ka. Drier study sites include City of Rocks, ID (Weppner, 2012), South Fork Payette, ID low elevation and south-facing slopes, Wood Creek, ID (Nelson and Pierce, 2010), and lower rangeland basins in the MFSR (this study). Wetter study sites include South Fork Payette, ID high elevation and north-facing slopes, Sawtooth Mountains (Svenson, 2010). Grey boxes are periods (mean calibrated pooled age with 2-sigma error) of synchronous widespread fire in MFSR, inferred as periods of drought.

Conclusion

The long-term fire record in the MFSR demonstrates that fires have been a significant geomorphic agent throughout the watershed despite changes in vegetation and climate conditions. The MFSR provides critical habitat for spawning Chinook salmon (*Oncorhynchus tshawytscha*). This species has been listed as threatened or endangered

since 1992, and the relationship among climate, sedimentation, and salmon habitat in the headwater ecosystems is a primary concern to their recovery. Fire has played a dominant role in alluvial fan deposition and therefore aquatic habitat and sediment supply characteristics of the main-stem Middle Fork Salmon River. Fire severity, vegetation type, and climate conditions influence the type of erosional response recorded in alluvial deposits. Large severe debris-flow-producing fires burned during the cooler and more variable early and late Holocene; however, large fire-related debris flow deposits are scarce during the warmer, more stable mid-Holocene. Instead, the mid-Holocene is characterized by fire-related sheetfloods, produced following low severity fires on sparsely vegetated hillslopes. Independent climate records support the hypothesis that less severe fires result from a climatically driven decrease in biomass (e.g., Marlon et al., 2006; Whitlock et al., 2004).

Fires have increased in frequency, severity, and synchronicity during the last 4 ka. Fire activity peaked during the last ~2.5 ka, subsequent to the introduction of lodgepole pine to high elevation forests. Centennial scale intervals of increased fire frequency and severity correspond to long-term intervals of relatively cool and wet conditions coupled with periods of annual to decadal drought that dried fuels and produced synchronous widespread severe fire across ecosystem boundaries. These climate conditions increased fuel loads in both low xeric ecosystems and high mesic ecosystems. In fuel-limited systems (e.g., sagebrush steppe), this increase in fuel load is probably necessary for widespread fires to occur. This suggests that the timing of fire is not random and fire

synchronicity and periodicity are driven by changes in climate and vegetation distributions.

This study demonstrates the overriding role of climate, not 20th century fire suppression, as a primary driver of recent large severe fires. We argue that the recent effects of fire suppression are minimal in comparison to the role climate has played on vegetation distribution and fire activity over the Holocene. This is especially true given the MFSR is located within a rugged wilderness, where the influence of fire suppression and other land-use activities have always been minimal. Current climate models predict increased summer temperatures in Idaho over the next century (Mote and Salathe, 2009), and central Idaho is predicted to be highly vulnerable to increased fire activity due to its extensive forested area and sensitivity to changes in water balance and the timing of spring (Westerling et al., 2006). Ecosystems throughout central Idaho will likely continue to burn in frequent severe fires that will drive small, steep basins to produce fire-related debris flows. Fire may act as a catalyst for vegetation restructuring adapted to future climate change scenarios.

CHAPTER 2: CLIMATE, FIRES, AND DEBRIS FLOWS CONTROL LONG-TERM SEDIMENT YIELDS IN THE MIDDLE FORK SALMON RIVER, IDAHO

Abstract

Wildfires can have profound influences on erosion rates, particularly in steep mountain basins where fire-related debris flows liberate hillslope material and contribute large episodic pulses of sediment to streams. However, the contribution of fire-related erosional events to millennial-scale erosion rates has received little attention. This study quantifies fire-related sedimentation from small, steep tributaries of the Middle Fork Salmon River in central Idaho to evaluate the timing, frequency, and magnitude of debris flows during the Holocene. We combine sediment yields from recent (1997-2008) single-event fire-related debris flows with debris flow frequencies reconstructed from ^{14}C-dated charcoal in alluvial stratigraphic sections to quantify long-term (10^3-10^4) sediment yields. Recent large debris flows emanate from basins underlain by weathered granite, where vegetation burned in moderate to high severity fires, producing single-event fire-related sediment yields from ~1,450-34,550 Mg km^{-2} yr^{-1}. By applying modern single event fire-related sediment yields to the Holocene record of fire and fire-related sedimentation, we reconstruct a minimum average annual sediment yield for the last 2 ka of 83-262 Mg km^{-2} yr^{-1}. Over the last 6 ka, when overall reconstructed fire frequency was lower, fire-related debris flows contributed a minimum of ~30-101 Mg km^{-2} yr^{-1} of

sediment to the Middle Fork Salmon River. We hypothesize generally cool, wet climate conditions and the expansion of lodgepole pine during the last ~2 ka have increased both fuel loads for fire and sediment storage on hillslopes; severe multi-decadal droughts and large fires punctuate this overall wetter interval and produce fire-related debris flows.

Introduction

Many studies (e.g., Burbank, 1992; Molnar, 2001; Montgomery et al., 2001) have focused on deciphering the roles of climatic and tectonic drivers of hillslope erosion and subsequent sediment inputs to stream channels. In tectonically active landscapes, the rate of erosion exceeds the ability of the system to weathering that material (Hren et al., 2007), and therefore erosion rates are associated with uplift rates (e.g., Snyder et al., 2000), seismicity (Dadson et al., 2004; Dadson et al., 2003), and uplift-induced landsliding (Montgomery and Brandon, 2002). In tectonically inactive regions, erosion rates have been found to limit the rate of chemical weathering (Hren et al., 2007). Large-scale climate patterns have also been associated with topographic evolution in many locations (e.g., Molnar, 2004; Montgomery et al., 2001; Reiners et al., 2003). However, despite numerous studies that show wildfire dramatically increases erosion on recently burned slopes (e.g. Cannon et al., 2001, Meyer et al., 2001, Meyer and Pierce, 2003; Roering and Gerber, 2005), the role of forest fires in driving erosion rates on longer (millennial) timescales has received little attention (Istanbulluoglu et al., 2004; Meyer et al., 2001).

Wildfires have increased in size, duration, and severity during the last 30 years (Westerling et al., 2006) and have profound influences on short-term (1-10 yrs) erosion rates, particularly in steep mountain basins. Fire-related erosion varies in both magnitude and impact as a function of burn severity, basin characteristics, and timing and intensity of local climate conditions (Cannon et al., 2001, Meyer and Pierce, 2003). Fires reduce ground-cover (e.g., vegetation, litter, and organic material), therefore decreasing surface roughness (Lavee et al., 1995), and change soil and sediment properties that can decrease soil cohesion, increase soil hydrophobicity (Shakesby and Doerr, 2006; Wondzell and King, 2003), and reduce infiltration rates (e.g., Robichaud, 2000). This, in turn, increases surface runoff and erosion of surface sediments (e.g., Doerr et al., 2006; Shakesby and Doerr, 2006) via rilling and progressive sediment bulking debris flows formed in small steep drainages (Cannon, 2001; Cannon et al., 2003; Cannon et al., 2001; Meyer and Wells, 1997; Parise and Cannon, 2012). While debris flows can be initiated by infiltration-triggered landsliding caused by reduced cohesion in colluvium from root decay (Clayton and Megahan, 1986; Roering and Gerber, 2005), only 12% of total documented fire-related debris flow cases demonstrate this initiation mechanism (Parise and Cannon, 2012).

Debris flows occur in small, steep sub-basins and can follow average (i.e., < 2 yr return interval) storm event durations and intensities on severely burned slopes (Cannon et al., 2008). Fire accelerates erosion by increasing the frequency and magnitude of debris flows in small, high relief basins contributing large pulses of sediment to streams. Single event fire-related debris flow yields are orders of magnitude larger than both long

and short-term sediment yields in Idaho (Meyer et al., 2001), and Istanbulluoglu et al. (2004) suggest that wildfires control the timing of sediment delivery in Idaho Batholith granitic terrain. If fires and fire-related sedimentation are primary controls on sediment delivered to the fluvial system in the Idaho Batholith, then large-fire-related debris flows should contribute significantly to long-term sediment yields in central Idaho; however, millennial-scale records of fire-related erosional events and measurements of sediment yields from fire-related erosion have hitherto not been available.

Fire-related deposits, as observed from exposed alluvial fan deposits located at small steep tributary junctions, allow evaluation of the timing, frequency, and thickness of fire-related debris flows during the Holocene. This study estimates longer-term (millennial) sediment yields by combining frequencies of past fire-related debris flow events reconstructed using ^{14}C dating of fire-related deposits, with measured modern sediment yields from single fire-related debris flows. With this information, we quantify the influence of fire and episodic debris flows on long-term sediment yields, and evaluate the temporal and spatial variability of fire-related deposition along the ~170 km Middle Fork Salmon River (MFSR), located in central Idaho.

Study Area

We investigated alluvial fan deposition in ten small steep basins within the Middle Fork Salmon River (MFSR) watershed. The Frank Church-River of No Return Wilderness surrounds the watershed and buffers the landscape from anthropogenic

disturbances (e.g., effective fire suppression, logging, and roads). Recent fires, then, are attributed to drought and other climatic drivers, not the influence of prior management (e.g., Westerling et al., 2006; Pierce et al., 2004). During the last 30 years, fires burning over 40% of the watershed (Gibson and Morgan, 2009) have initiated many debris flows in steep basins that are primarily composed of weathered Idaho Batholith granite. The affects of fire on the MFSR landscape are clearly evident. Scorched lodgepole pine and ponderosa pine forests create a mosaic of vegetation disturbance and observed erosion on burned hillslopes includes tree throws, rills, gullies and incised channels. Large debris flows have deposited sediment and burned wood on alluvial fans, which extend into the main-stem river; recent debris flows have also incised through and exposed older deposits in Holocene alluvial fans.

The large (7,500 km^2)**,** deeply incised Middle Fork Salmon is located in the Northern Rocky Mountains of central Idaho (Figure 2-1). Elevations range from 900-3160 m, creating a steep topographic gradient with a mean basin slope of 54%. While no major faults have been identified within the MFSR, incision rates have been estimated at 100-200 m/My (Meyer and Leidecker, 2007). Pacific maritime and continental air masses influence precipitation, which primarily falls as snow during winter months with occasional summer convective thunderstorms, which initiate fire-related debris flows. The high relief north-south trending mountains cause an orographic decrease in precipitation along the eastern (leeward) side of the watershed. Annual precipitation ranges from 350 mm at Taylor Ranch to 850 mm at Deadwood Reservoir. The large range in elevations and thus precipitation regimes (Tennant, 2011) produce a mosaic of

vegetation distributions from sub-alpine and mixed conifer forests to rangeland ecosystems.

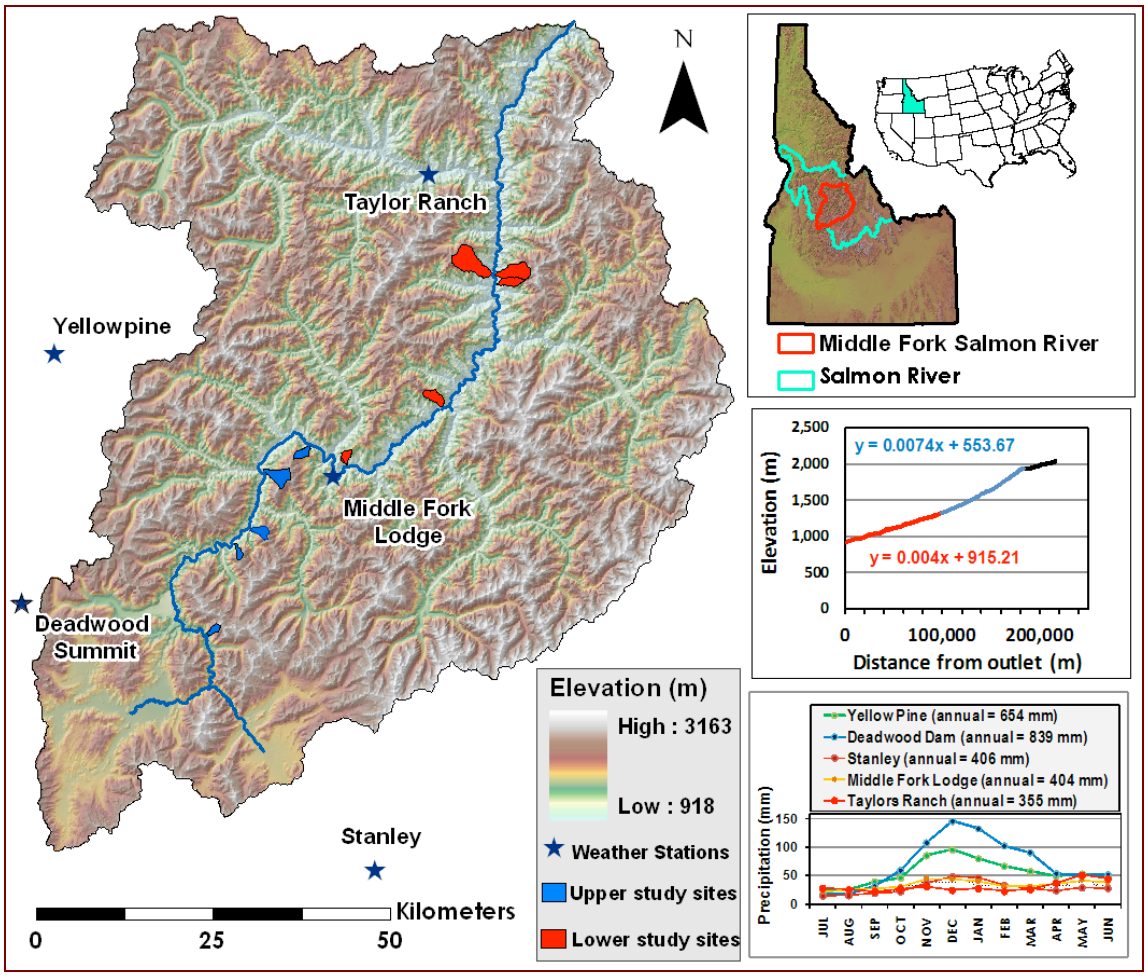

Figure 2-1: (left) Map of Middle Fork Salmon River watershed. Blue and red polygons show the contributing areas of ten debris-flow producing basins. The blue line is the main-stem Middle Fork Salmon River that flows southwest to northeast. The stars represent the locations of five nearby weather stations. (Top right) The location of the larger (~35,079 km^2) Salmon River watershed is outlined with a blue polygon and MFSR is outlined in red. (Middle right) MFSR longitudinal profile with linear equations displayed for upper and lower reaches. (Bottom right) Annual precipitation distributions are shown for the five weather stations.

Methods

Ten small (1-13 km^2), steep (35-70% gradient) sub-basins, composed of easily erodible Idaho Batholith granites with recently incised tributary junction alluvial fans, were selected as study sites. Tectonics, lithology, and basin morphology were similar among the ten sub-basins, isolating climate and vegetation as the primary independent variables controlling alluvial fan deposition. Five upper (2750-1380 m), wetter basins characterized by subalpine and mixed conifer forests were compared to five lower (2650-1100 m), drier basins characterized by abundant grass and shrubs with scarce Douglas fir and ponderosa pine (Table 1-1; Figure 1-3). Five modern debris flow deposits were surveyed and 35 alluvial fan stratigraphic profiles investigated within the ten study sites.

We surveyed recent (1997–2008) fire-related debris flow deposits (2 upper basins and 3 lower basins) using a real-time kinematic GPS (sub-meter accuracy) during the summer of 2010 (Figure 2-2). Recent debris flows incised into pre-existing Holocene fan sediments, and extended into the active channel. Depositional boundaries between fresh and older deposits were easily identified based on vegetation cover and sediment characteristics. Sediment volumes from marginal levee deposits and recent deposition within the tributary channel were negligible when compared to the total deposit volume (< 5 % of total volume) and were not included in the calculation. NAIP (2004 and 2009) and historic pre- and post-event images were used to establish whether or not new fan deposits drape existing fan deposits, or form new deposits in the active channel. There was little visible evidence of debris flow fan deposits (i.e., large boulders or visible roughness) observed in three out of five tributary junction main-stem channel reaches

prior to the most recent debris flow deposition (Figure 2-3). New fan deposits were deposited directly in the active channel; therefore, a flat base of the new deposit was assumed.

Debris-flow deposit surfaces were digitized using radial basis functions to interpolate across surveyed data points. We calculated the volume of material under the digitized surface area using two different assumed flat bottoms to the deposit. We first set the base elevation equal to the minimum fan elevation surveyed. We also set the base elevation equal to average surface water elevation for the reach of the main-stem spanning the tributary junction post debris flow event. Only recent debris flow deposits within the active main-stem channel were included in the volume calculation. Volumes were converted to sediment yields using an assumed average sediment bulk density for granite-derived regolith of 1500 kg/m^3 (Istanbulluoglu et al., 2004; Kirchner et al., 2001; Meyer et al., 2001) and the upslope contributing area of the debris flow fan apex measured using 30 m digital elevation models from the National Elevation Dataset (Gesch, 2007; Gesch et al., 2002).

Streamflow in the main-stem MFSR truncated modern debris flow deposits between the time of the event and the time of the survey (1-13 yrs). To quantify the eroded sediment, multiple radial fan slopes were projected into the modern channel (Appendix E). Large angular boulders within the modern channel or debris flow deposit on the opposite bank were used to estimate the farthest extent of the debris flow event. We used projected data points to extrapolate the measured surface into the river, reconstructing the original fan surface area and volme. The difference between the

deposit surveyed in 2010 and the projected original deposit fan surface represented the amount of sediment transported downstream since the time of the debris flow event. To validate the survey and extrapolation method, volumes were compared to two independent empirical debris flow volume prediction models (Cannon et al., 2010, Iverson et al., 1994); (Appendix F-H).

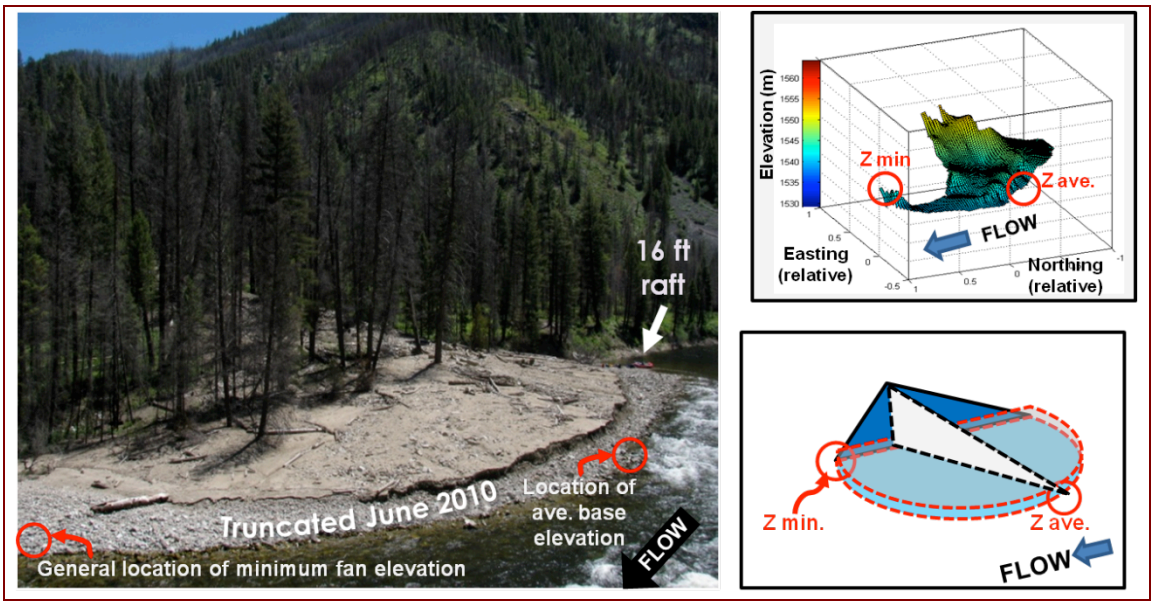

Figure 2-2: (Left) Photograph of Sheepeater debris flow fan, an example of one of the five debris flow fans used to measure single event sediment yields. (Top right) Image of the digitized surface topography of the 2010 truncated Sheepeater debris flow fan. (Bottom right) Drawing of a simple half cone illustrates the constant base elevation assumption used in calculation. In all three images, the approximate locations of the two assumed horizontal base elevations of the deposit are shown (z min. equals minimum assumed elevation and z ave. equals the average of the upstream water surface elevation and the downstream water surface elevation).

Figure 2-3: (Top) Photograph of Kotch Creek tributary junction with main-stem MFSR looking upstream at the recent debris flow fan emanating from the older incised perched fan. Dotted line represents the pre-event main-stem bank. (Left) Image is from NAIP 2004 and shows the Holocene alluvial fan at the tributary junction of Kotch Creek. (Right) Imagery from NAIP 2009 is of the same location as image on the left following debris flow deposition in the summer of 2007. The recent debris flow deposited material on top of the Holocene fan as marginal levee deposits and deposited material into the currently active MFSR channel.

We estimated millennial-scale debris flow frequencies using ^{14}C-dated charcoal fragments preserved in discrete fire-related deposits exposed in recently incised alluvial fans. Multiple profiles (2-6) within ten fan complexes (five upper and five lower basins) were selected based on exposure of vertical sections within fans containing clear fan stratigraphy. We targeted exposures near the fan apex because depositional events from the steep contributing area are most likely to reach this location and are also least likely to be eroded by the main-stem river, therefore recording the greatest number of depositional events over millennia. We dated 64 charcoal fragments from ten alluvial fans to produce 21 age-constrained stratigraphic profiles (Appendix A). Within each stratigraphic profile, we described discrete depositional layers by color, texture, depth, continuity, thickness, degree of sorting, clast size, clast angularity, charcoal abundance, and percent gravel to identify the primary depositional process. Discrete deposits were classified as fire-related based on high charcoal abundance, and/or deposits with abundant charcoal that overlie discrete burn surfaces, identified by high organic components, roots, and soil development (Meyer et al., 1995; Pierce et al., 2004). The two primary deposit types resulting from fire were debris flow deposits and sheetflood deposits. Debris flows deposits were very poorly sorted, matrix-supported, and contained large angular clasts. Sheetfloods result from unconfined fluvial sediment transport and deposits were characterized by couplets of moderately sorted, fine and course-grained sediment, of varying thicknesses.

Importantly, the estimated frequency of debris flow events is a minimum because not all deposits were preserved, older deposits were less likely to be exposed, and we

only dated a discrete number of deposits from a few locations in ten alluvial fans. We used the maximum number of discrete debris flow deposits per sub-basin and per time to calculate long-term yields. We also estimated debris flow frequency using age anomalies associated with ^{14}C-dating two charcoal fragments from the same discrete deposit. Statistically different age distributions are a result of either inbuilt age (difference between the age of charcoal and time-since-fire; (Gavin, 2001) or reworking of a previous fire-related event that deposited charcoal higher in the contributing basin. The latter provided insight into the frequency of events within individual basins. We calculated long-term (10^3 yr) sediment yields by combining normalized sediment yields from recent individual fire-related debris flow events with reconstructed Holocene fire-related debris flow frequencies, over a 2000 yr moving windows, throughout the last 6000 yr.

To compare long-term sediment yield estimates from fire-related debris flows with basin-wide sediment yields from cosmogenic radionuclides, we limited individual event yields to sediment deposited within the active main-stem channel (Figure 2-3) that is likely to be fluvially transported over millennial timescales. We estimated single event fire-related debris flow maximum sediment yields using the extrapolated original deposit yield, not including perched levee deposits that are likely to be stored over millennia. Minimum yield estimates were made using the amount of material eroded by the main-stem MFSR since the time of the event (i.e., missing deposit).

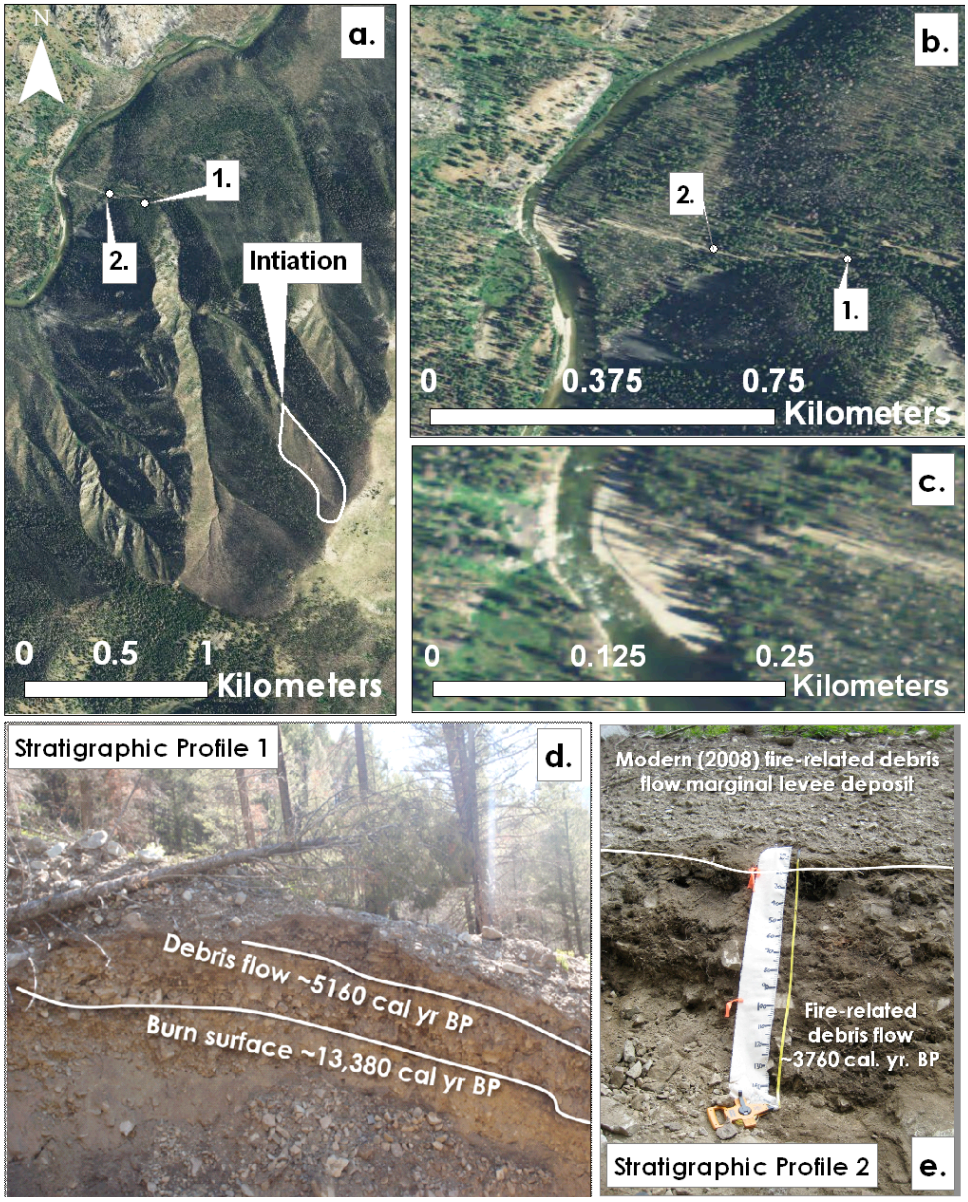

Figure 2-4: a) NAIP 2011 images of the contributing basin of Sheepeater debris flow fan. b) NAIP 2011 image of the Holocene alluvial fan. c) Modern 2008 debris flow deposit incizing the perched truncated fan and depositing fresh material into the active channel of the main-stem MFSR. Only debris flow material reaching the active main-stem channel was included in long-term sediment yield estimates. Marginal levee deposits adjacent to the incised paleo-fan were not included in long-term estimates. d) Stratigraphic profile 1 was located at the paleo-fan apex where the narrow tributary opens up to the main-stem corridor. The 2008 debris flow deposited material onto of profile 1 and 2. e) Stratigraphic profile 2 was located closer to the main-stem MFSR.

Table 2-1: Measured and extrapolated single event fire-related debris flow sediment yields.

Debris Flow Site	Area (km^2)	Year of event	Min. z_{base} / Ave. z_{base} (m)	Measured fan deposit (min. z_{base} / ave. z_{base}) (Mg km^{-2} $event^{-1}$)	Extrapolated original fan deposit (min. z_{base} / ave. z_{base}) (Mg km^{-2} $event^{-1}$)	Deposit removed downstream (min. z_{base} / ave. z_{base}) (Mg km^{-2} $event^{-1}$)	Percent fan eroded (%)
Kotch (upper)	1.6	2008	1776 / 1779	7,190 / 770	22,950 / 5,330	15,760 / 4,560	70 / 86
Sheepeater (upper)	1.5	2008	1539 / 1541	17,780 / 12,470	34,550 / 22,730	11,820 / 5,310	34 / 30
[2]Reservoir (lower)	3.4	2003	1097 / 1097	1,950	5,600	3,650	65
[3]Pole (lower)	7.4	1997	1086 / 1086	400	1,840	1,450	79
Sub-basin of Bernard (lower)	4.3	1997	1091 / 1092.5	2,960 / 1,680	4,480 / 3,970	1,500 / 2290	34 / 58

Results

Single-event fire-related debris flow sediment yields ranged from ~1,840-34,550 Mg km^{-2} $event^{-1}$ accounting for all material that reached the active main-stem MFSR corridor emanating out of the Holocene alluvial fan sediment trap (Table 2-1). Two of

[2] Reservoir Creek tributary junction intersects the MFSR at a low gradient reach of the main-stem. Change in elevation between the farthest upstream and downstream fan extent is less than 1 meter.

[3] Pole Creek tributary junction intersects the MFSR at a low gradient reach of the main-stem. Change in elevation between the farthest upstream and downstream fan extent is less than 1 meter.

the five modern debris flows surveyed, deposited marginal levees on top of the older, incised fan surface. The approximate volume of material in levee deposits at Kotch Creek (~975 m^3) accounts for only ~4% of the total volume of material deposited. Extrapolated single event yields were within an order of magnitude of yields estimated using empirical models (Cannon et al., 2010; Iverson et al., 1994; (Figure 2-5)), which suggests the method used in this study to calculate single-event yields is reasonable. Lower, drier basins produced lower fire-related debris flow sediment yields (~1,840-5,600 Mg km^{-2} yr^{-1}) than upper, wetter basins (~22,950-34,550 Mg km^{-2} yr^{-1}; Figure 2-6). Comparison of preserved vs. eroded deposit volumes indicates large percentages (~30-80%) of debris flow deposits are quickly (2-13 yrs) transported downstream during peak flows following the depositional event (Table 2-1; Figure 2-6).

Although the record of alluvial fan deposition extends back 14.5 ka, we constrained our long-term sediment yield reconstruction to the last 6 ka because of potential issues with preservation and exposure of debris flow deposits though time. Fire-related sheetflood deposits, not debris flows, are the primary deposit type preserved in lower basin site between 8.5-4 ka (Figure 2-7). Between 4-2 ka, debris flows were infrequent, (~500 years between events entering the main-stem from ten sub-basins), but synchronous (inferred from statistically indistinguishable calibrated age distributions) in upper and lower basins ~3730 ± 100, 2780 ± 60, and 2240 ± 100 cal. yr BP. Fire-related debris flow frequency increased ca. 1200 cal. yr BP in upper basins and ca.700 cal. yr BP in lower basins (Figure 2-7). The largest peak in lower elevation fire-related debris flows was between 700-200 cal. yr BP (Figure 2-7). During the last 2 ka, at least 28 discrete

debris flows were deposited, resulting in a frequency ~70 yr/event for the entire study area and a mean frequency per sub-basin of ~335 yr/event. One pair of field duplicates also revealed a difference in age between charcoal fragments from the same depositional event of ~310 yrs. Since this older charcoal fragment was likely burned in a fire ~300 yrs prior to the next fire and depositional event, this may also provide information about the fire return interval for individual basins or the residence time of sediment in the contributing basin.

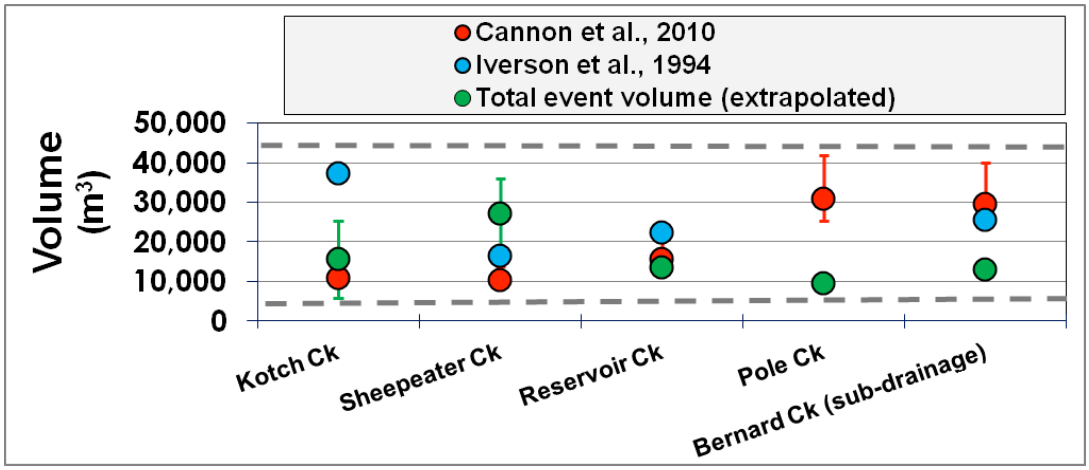

Figure 2-5: Comparison of three methods used to estimate single-event fire-related debris flow deposit volumes. The green dots represent mean volumes calculated in this study, where positive error bars represent volumes calculated using the minimum deposit elevation as base elevation of debris flow deposit and negative error bars represent volumes calculated using the mean water surface elevation for the tributary junction reach as the base elevation of debris flow deposit. The red dots are mean volumes derived from Cannon et al., (2010) fire-related debris flow volume prediction model (Appendix F). Error bars (red dots) show variability associated with the total storm precipitation used in the equation and represent the maximum storm depth and the mean storm depth for the period of record measured at three weather stations (Middle Fork Lodge, Yellow Pine, and Deadwood Reservoir) in and surrounding MFSR. The blue dots represent debris flow volume calculations made using super-elevation principles applied to debris flows around bends or obstacles by Iverson et al., (1994); (Appendix G). Grey dotted lines bound all method volumes and errors addressed.

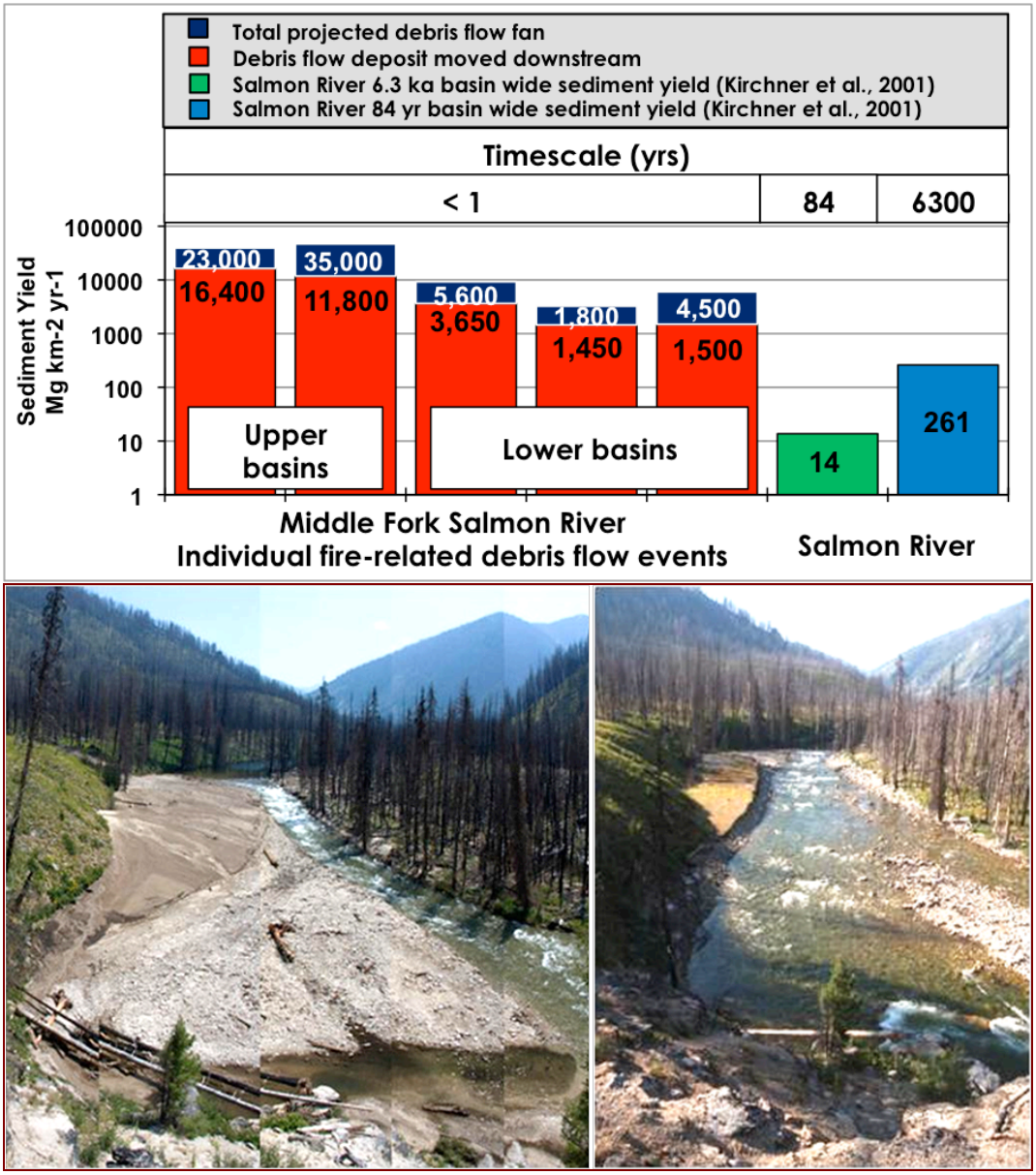

Figure 2-6: The stacked bar graph represents the maximum yield (blue bars) associated with the total fan deposit and the minimum yield (red bar) associated with the amount of deposit moved downstream since the time of the event. Yields displayed were derived using the minimum deposit elevation as the base of the debris flow. The green bar is a long-term (6.3 ka) Salmon River basin-wide yield estimated using ^{10}Be and the blue bar is a short-term (84 yr) yield (Kirchner et al., 2001). Photographs are repeat photographs of Kotch Creek debris flow fan first taken the summer of 2008 soon after a fire-related debris flow (photo by Leidecker, 2008) and after substantial erosion of the deposit during summer, 2010.

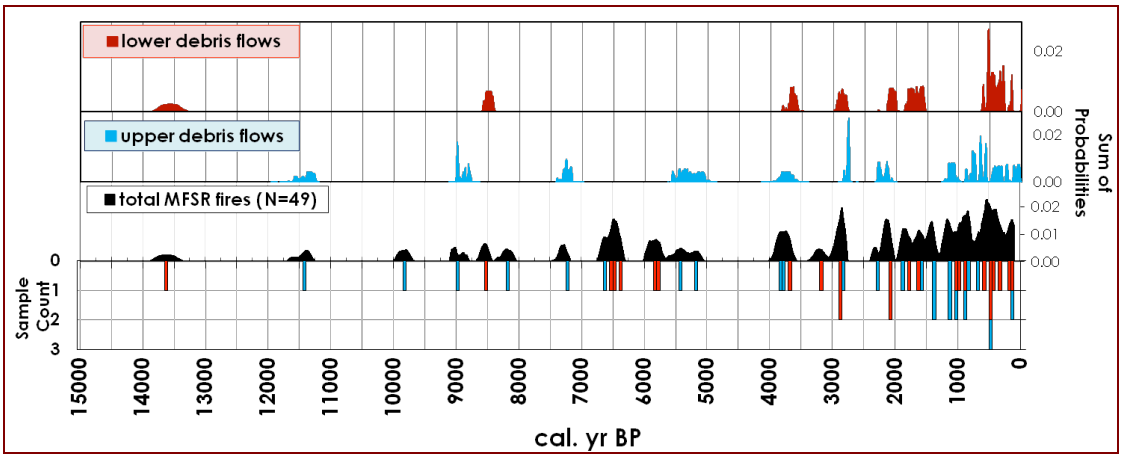

Figure 2-7: Smoothed curves represent radiocarbon-dated deposits in the Middle Fork Salmon River. The x-axis is calibrated years BP (Stuiver and Reimer, 1993) with 0 cal. yr BP equaling 1950 AD. The data in the inverted bar graph represents the sample count of the number of dated charcoal fragments creating the smoothed curves above. Red bars are lower basin samples and blue bars are upper basin samples. The black curve represents all dated fires (n=49) collected from within all deposits types (i.e., debris flows, burn surfaces, hyper-concentrated flows, sheetfloods, and over-bank deposits). The blue curve (not smoothed) represents dated upper basin and red curve (not smoothed) dated lower basin debris flow deposits.

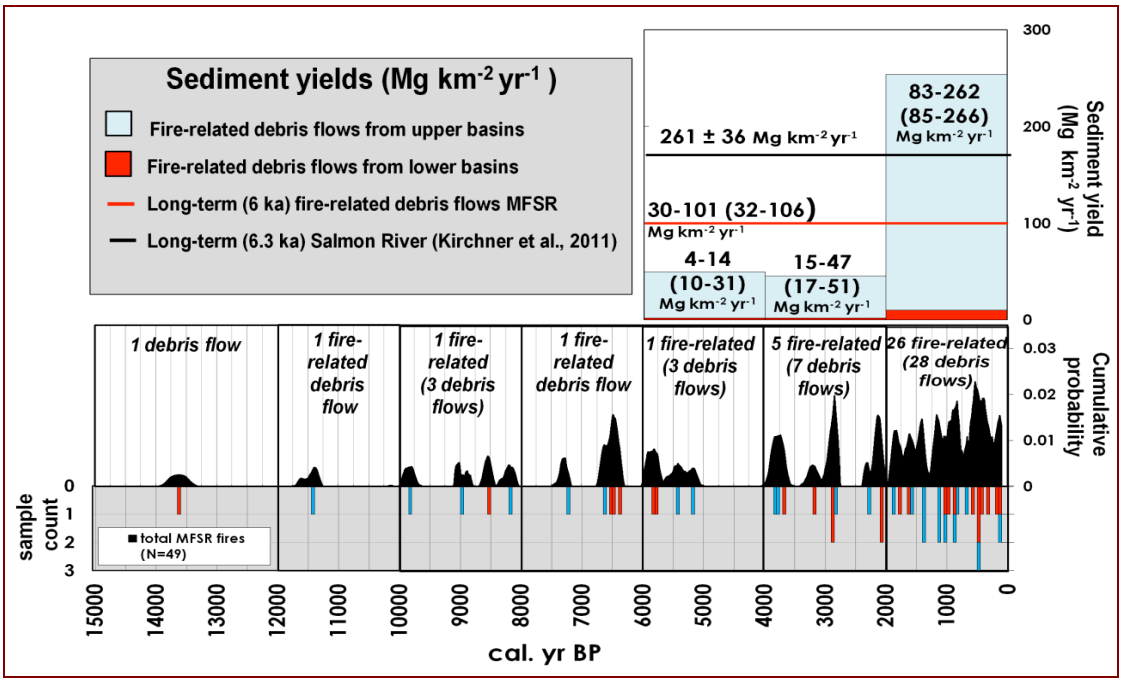

Figure 2-8: Long-term sediment yields for the MFSR are presented above the smoothed fire history and sample count. The contribution from lower (red) vs. upper (blue) sub-basins is represented in the stacked bar graph. The black labels in the bar graph represent the total contribution from upper and lower basin sites. This first number represents only fire-related debris flow yields followed by all debris flow yields in parenthesis. The number of age constrained discrete debris flow deposits are labeled in 2000 yr increments above the smoothed fire history.

We estimated long-term yields in 2000 yr time increments over the last 6 ka (Figure 2-8). We quantified sediment yields in two ways including: 1) all discrete debris flow deposits, and 2) only fire-related debris flow deposits. Minimum yields were derived from the eroded deposit and maximum yields derived from the extrapolated yields. Given the difference in single-event magnitude between upper and lower basins, we averaged upper basin maximum and minimum yields independently from lower basin maximum and minimum yields and used these two single-event averages to reconstruct

long-term yields in both upper and lower basins. Independent upper and lower basin long-term yields were combined to estimate the yield from all ten sub-basins. With this method, we aimed to include the variability associated with differences in debris flow magnitudes among sub-basins and differences in transport capacity of main-stem discharge over time. Since pre-event photos show little preserved deposition in the active channel corridor, it is likely that this new material will be removed over 10-100 yr timescales. Single-event yields extrapolated over the last 2 ka (17 debris flows in upper basins and 11 debris flows in lower basins), results in a long-term (2 ka) yield of ~73-244 Mg km^{-2} yr^{-1} in upper basins, of which all debris flows are related to wildfire. Lower basins contributed ~10-22 Mg km^{-2} yr^{-1} of sediment to the main-stem, of which ~4-10 Mg km^{-2} yr^{-1} of sediment is related to wildfire. Combined upper and lower basin debris flow sediment yields contributed 85-266 (83-262 fire-related) Mg km^{-2} yr^{-1} of material to the Middle Fork Salmon River over the last 2 ka, 17-51 (15-47 fire-related) Mg km^{-2} yr^{-1} of sediment between 2-4 ka, and 10-31 (4-14 fire-related) Mg km^{-2} yr^{-1} of sediment between 4-6 ka. The cumulative yield for all study basins averaged over the last 6 ka was 32-106 (30-101 fire-related) Mg km^{-2} yr^{-1} of sediment transported from small steep sub-basins to the main-stem MFSR. Of the 38 total debris flows indentified and dated over the last 6 ka, 32 were fire-related (84%) and five out of the six debris flows not identified as fire-related were located in lower basin fans.

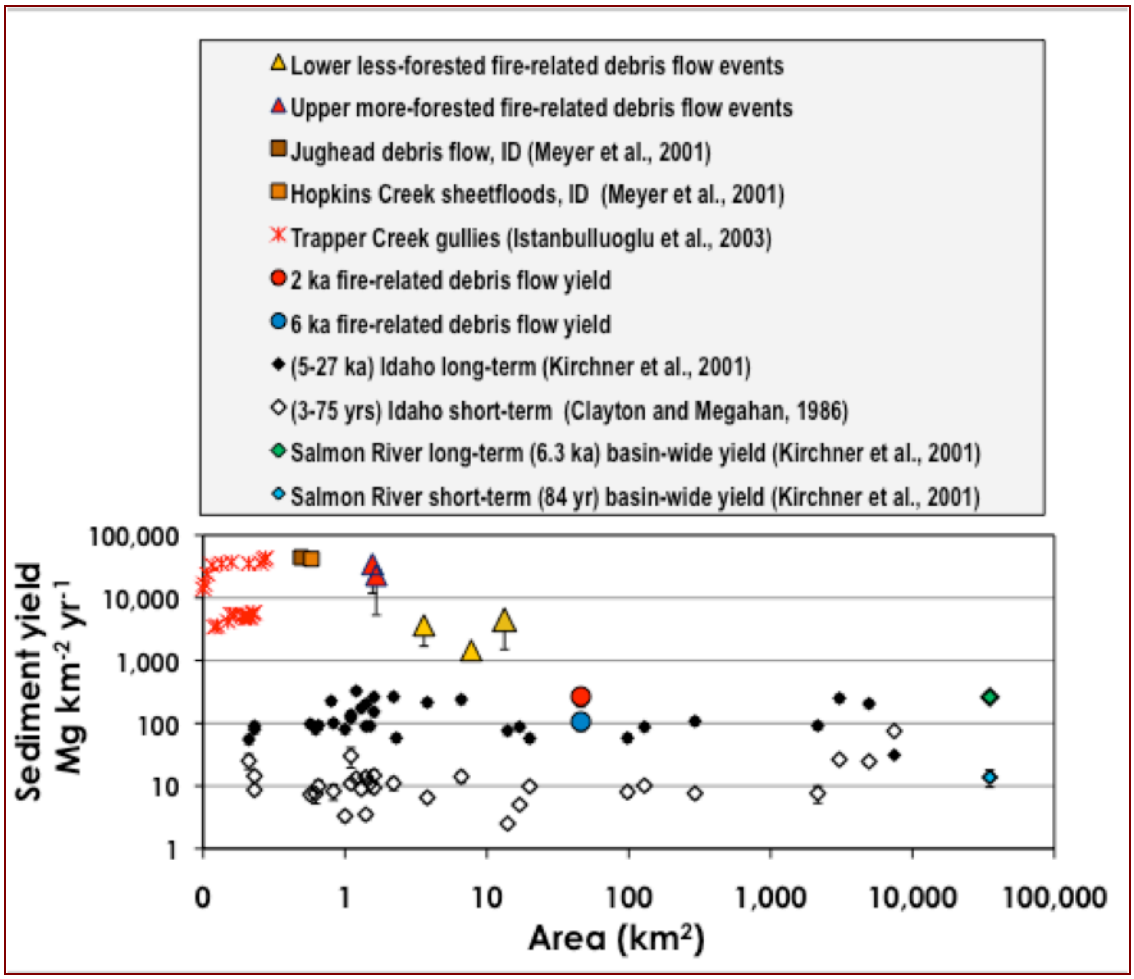

Figure 2-9: Single debris flow event sediment yields are presented from the MFSR (this study), South Fork Payette River, Idaho (Meyer et al., 2001), and Trapper Creek, Idaho (Istanbulluoglu et al., 2003). MFSR long-term (2 ka and 6 ka) sediment yield area includes the contributing area of the ten debris flow alluvial fans used in the study. Error bars for MFSR data represent the amount of material eroded since the time of the event and are minimum estimates of long-term fire-related debris flow yields. Background basin-wide long-term sediment yields from the Idaho Batholith, derived from cosmogenic radio-nuclides, are presented as black diamond's, except for the green diamond which is the Salmon River long-term yield (Kirchner et al., 2001). Short-term sediment yields, derived from traditional traps, gauges, and sediment rating curves from the Idaho Batholith, are presented as white diamonds, except for the blue square, which represents the Salmon River short-term yield (Clayton and Megahan, 1986; Kirchner et al., 2001).

Discussion

The frequency of fires and fire-related debris flows are primary controls on long-term sediment delivery in the Idaho Batholith. Climate drives vegetation distributions that influence fire frequency and severity (Power et al., 2008) and therefore the frequency and magnitude of fire-related erosion and deposition (e.g., Cannon et al., 2010). In the MFSR, debris flow deposits are the dominant deposit type and compose the greatest thickness of tributary junction alluvial fans and over 50% of total measured alluvial fan thickness was related to fire. We suggest fire-related debris flows are the primary erosional process delivering the greatest quantity of sediment from hillslopes to the main-stem MFSR.

Modern debris flows in the MFSR follow high severity wildfire and deliver large magnitudes of sediment from steep hillslopes to the main-stem river at tributary junctions, where sediment is readily available to be fluvially transported. Single-event fire-related debris flow yields are orders of magnitude larger than previously published short and long-term yield measurements throughout the Idaho Batholith (Figure 2-10). This relationship was previously demonstrated in the Idaho Batholith by field observations in the South Fork Payette, Idaho (Meyer and Pierce, 2003; Meyer et al., 2001) and field observations and numerical modeling in the north fork of the Boise River (Istanbulluoglu et al., 2004). We have demonstrated that modern fire-related debris flow deposits in the MFSR are both large and quickly remobilized and transported downstream.

In 2009, ~68% of total suspended sediment delivered to the reservoir behind lower Granite Dam, on the downstream Snake River, was derived from the Salmon Basin above White Bird (Teasdale, 2010). We converted the volume of sediment to a yield using an assumed bulk density (1500 kg/m^3) and the contributing area of the larger Salmon watershed (~ 35,000 km^2), resulting in an average 2009 sediment yield of ~500 Mg km^2 yr. This yield is within an order of magnitude of long-term estimates made for a range of basin areas throughout the Idaho Batholith using cosmogenic radionuclides (Kirchner et al., 2001; Figure 2-10). However, this yield is much higher than short-term yields made using traditional sediment traps and gauges (Clayton and Megahan, 1986). The high annual sediment yield measured in 2009 potentially reflects the influence of recent increases in fire frequency and severity in Northern Rocky Mountain forests (Westerling et al., 2006) and increased fire-related debris flow producion.

Climate and vegetation have played major roles in the type and magnitude of geomorphic response in the MFSR during the Holocene. Fire-related deposits composed greater total fan thicknesses in upper basins compared to lower basins, the magnitude of modern fire-related debris flows was greater in upper, wetter basins compared to lower, drier basins, while thinner sheetflood deposits comprise greater proportions of fan thicknesses in lower, drier basins vs. upper, wetter basins. Wildfire lowers erosional thresholds on a hillslope; however, the accumulation of sediment on a hillslope prior to fire also influences the geomorphic response initiated by the fire. Through numerical modeling, Istanbulluoglu et al. (2004) demonstrated that sediment yield probability distributions increase in magnitude as root cohesion increases. Vegetation has been

shown to increase regolith transport and mixing via tree throw, bioturbation, root activity (Heimsath et al., 2001), increase soil porosity, bulk density, and infiltration (Brimhall et al., 1992), and increase roughness on the hillslope and cohesion within the mobile regolith needed to maintain steep slopes (Collins et al., 2004). Furthermore, weathering rates have been shown to be faster in wetter climates (e.g., Riebe et al., 2004; White and Blum, 1995). In tectonically inactive regions, the rate of supply (erosion transporting sediment off of the hillslope) has been found to limit the rate of chemical weathering on the hillslope (Hren et al., 2007). Debris flow production appears to be strongly related to the timing of wildfire (84% of all debris flow deposits are fire-related over the last 6 ka). If erosion rates in the MFSR control weathering rates and therefore the production of mobile sediment, then the timing of fire is a significant control on landscape evolution in the MFSR.

Temporal changes in climate and vegetation during the Holocene have influenced the type, frequency, and magnitude of fire-related sedimentation on alluvial fans. The frequency of debris flow deposition was greater 10-8 ka compared to 8-6 ka suggesting that decreases in fire-related debris flow sediment yields in the mid-Holocene (6-4 ka) is not just a consequence of the fading record. Between 8.5-4 ka, the primary inferred depositional process on alluvial fans was fire-related sheetflooding. Small fire-related events (i.e., sheetfloods) also dominate the interval between 7.4–6.6 ka in the South Fork Payette River, Idaho producing a mid-Holocene fire-related sediment yield of only ~16 Mg km^{-2} yr^{-1} (Meyer et al., 2001). Importantly, the mid-Holocene yield by Meyer et al. (2001) does not include large fire-related deposits. Regional synchronicity in the timing,

type, and relative magnitude of erosional response suggests climate as a primary control on geomorphic response. During the regionally warm, dry, stable climate conditions of the mid-Holocene (Brunelle et al., 2005; Davis et al., 2002; Shuman et al., 2009; Whitlock et al., 2010) fire-related debris flows were potentially limited by vegetation scaricity (fuel) needed to both produce severe fires and to accumulate sediment on the hillslope. We infer decreased widespread fire-related sedimentation during warm, arid, and more stable climate conditions.

While small frequent fire-related depositional events characterize the mid-Holocene, large fire-related debris flows and high sediment yields characterize the late Holocene. Late Holocene (4 ka - present) climate was generally cooler, wetter, and more variable in central Idaho (Davis et al., 2002; Whitlock et al., 2010). Fire-related debris flow frequency began to increase ~4 ka and was greatest during the last 2 ka. Upper basin fire-related debris flow frequency has remained high since ~1200 cal. yr BP contrasting to lower, drier basins in the MFSR, where no evidence of debris flows were observed between 1500-700 cal. yr BP (Figure 2-7). The Medieval Climatic Anomaly (MCA) was a period of warming between 1250-600 cal. yr BP (e.g., Esper et al., 2002; Stine, 1994). MCA climate conditions resulted in fire-related debris flow deposits preserved in upper basins but not in lower basins, emphasizing the importance of both fuel and drought conditions needed to produce severe fires and initiate large fire-related debris flows. Fire-related debris flow frequency peaked in lower basins between 700-200 cal. yr BP, corresponding to the Little Ice Age (LIA; 450-100 cal. yr BP). Glaciers advanced in Northern Rocky Mountains during the LIA (Carrara, 1989; Grove, 1988;

Luckman, 2000), cold climate conditions were recorded throughout the Northern Hemisphere (Esper et al., 2002; Grove, 1988; Pollack et al., 1998), and climate in the Sawtooth-Salmon Mountains, Idaho has been characterized by generally high levels of climate variability (Biondi et al., 1999). Cooler, wetter, and more variable climate conditions would increase forest cover and vegetation abundance throughout the area, increasing fire severity during dry conditions, and increase the likelihood of fire-related debris flows.

If MFSR erosion rates over the last 2000 yrs represent the longer-term eroding landscape, then erosion rates in the MFSR have been ~262 m Myr^{-1} (assuming minimum debris flow fan elevation is the base of the deposit and including all extrapolated sediment). Average erosion rates derived from fire-related debris flows over the last 6 ka are ~67 m Myr^{-1}, which is remarkably similar to long-term average erosion rates throughout the Idaho Batholith (73 ± 6 m Myr^{-1}) derived from cosmogenic radionuclides (Kirchner et al., 2001). While sediment yields may vary significantly through time, we suggest that periods of accelerated erosion (e.g., last 2 ka), caused by wildfire induced lower erosion thresholds, play a significant role on yields averaged over longer timescales.

Conclusion

Depositional patterns in alluvial fans provide a long-term (10^3-10^4 yr) perspective on relationships among climate, vegetation, fire, and geomorphic response (i.e., type, magnitude, and frequency of episodic hillslope erosion). This study quantified fire-

related sedimentation from small, steep tributaries of the Middle Fork Salmon River in central Idaho to evaluate the timing, frequency, and magnitude of debris flows during the Holocene. Recent large debris flows emanate from basins underlain by weathered granite that have burned in moderate to high severity fires, producing single-event sediment yields that were orders of magnitude greater than short and long-term estimates made throughout the Idaho Batholith. By applying modern single-event sediment yields to the Holocene record of fires, we reconstructed average minimum annual sediment yields for the last 6 ka, which are similar in magnitude to the average long-term basin-wide erosion rate in the Idaho Batholith.

Fire-related debris flows appear to be a primary contributor to long-term sediment delivery. Fires have lowered erosion thresholds and initiated large episodic pulses of sediment from hillslopes that have varied in size and frequency as a function of climate-driven vegetation distributions and drought. Fire is an important geomorphic agent in steep forested ecosystems in the Idaho Batholith, profoundly influencing erosion rates during the Holocene. We hypothesize generally cool, wet climate conditions and the expansion of lodgepole pine during the last ~2 ka have increased both fuel loads and sediment storage on hillslopes; severe multi-decadal droughts and large fires punctuate this overall wetter interval and produce fire-related debris flows.

LITERATURE CITED

Agee, J.K., 1993, Fire Ecology of Pacific Northwest Forests.

Arno, S.F., Scott, J.H., and Hartwell, M.G., 1995, Age-class structure of old-growth ponderosa pine douglas-fir stands and its relationship to fire history: Usda Forest Service Intermountain Research Station Research Paper, p. 1-25.

Baker, W.L., 2006, Fire and restoration of sagebrush ecosystems: Wildlife Society Bulletin, v. 34, p. 177-185.

Ballenger, J.A.M., and Mabry, J.B., 2011, Temporal frequency distributions of alluvium in the American Southwest: taphonomic, paleohydraulic, and demographic implications: Journal of Archaeological Science, v. 38, p. 1314-1325.

Barrett, S.W., 1988, Fire Suppression's Effects on Forest Succession within a Central Idaho Wilderness: Western Journal of Applied Forestry, v. 3, p. 76-80.

Bartlein, P.J., Anderson, K.H., Anderson, P.M., Edwards, M.E., Mock, C.J., Thompson, R.S., Webb, R.S., and Whitlock, C., 1998, Paleoclimate simulations for North America over the past 21,000 years: Features of the simulated climate and comparisons with paleoenvironmental data: Quaternary Science Reviews, v. 17, p. 549-585.

Biondi, F., Perkins, D.L., Cayan, D.R., and Hughes, M.K., 1999, July temperature during the second millennium reconstructed from Idaho tree rings: Geophysical Research Letters, v. 26, p. 1445-1448.

Bond, G., Kromer, B., Beer, J., Muscheler, R., Evans, M.N., Showers, W., Hoffmann, S., Lotti-Bond, R., Hajdas, I., and Bonani, G., 2001, Persistent solar influence on north Atlantic climate during the Holocene: Science, v. 294, p. 2130-2136.

Bowman, D.M.J.S., Balch, J.K., Artaxo, P., Bond, W.J., Carlson, J.M., Cochrane, M.A., D'Antonio, C.M., DeFries, R.S., Doyle, J.C., Harrison, S.P., Johnston, F.H., Keeley, J.E., Krawchuk, M.A., Kull, C.A., Marston, J.B., Moritz, M.A., Prentice, I.C., Roos, C.I., Scott, A.C., Swetnam, T.W., van der Werf, G.R., and Pyne, S.J., 2009, Fire in the Earth System: Science, v. 324, p. 481-484.

Brimhall, G.H., Chadwick, O.A., Lewis, C.J., Compston, W., Williams, I.S., Danti, K.J., Dietrich, W.E., Power, M.E., Hendricks, D., and Bratt, J., 1992, Deformational Mass-transport and Invasive Processes in Soil Evolution: Science, v. 255, p. 695-702.

Brown, P.M., Kaufmann, M.R., and Shepperd, W.D., 1999, Long-term, landscape patterns of past fire events in a montane ponderosa pine forest of central Colorado: Landscape Ecol., v. 14, p. 513-532.

Brunelle, A., Whitlock, C., Bartlein, P., and Kipfmueller, K., 2005, Holocene fire and vegetation along environmental gradients in the Northern Rocky Mountains: Quaternary Science Reviews, v. 24, p. 2281-2300.

Burbank, D.W., 1992, Causes of recent himalayan uplift deduced from deposited patterns in the Ganges Basin: Nature, v. 357, p. 680-683.

Cannon, S.H., 2001, Debris-flow generation from recently burned watersheds: Environmental & Engineering Geoscience, v. 7, p. 321-341.

Cannon, S.H., Gartner, J.E., Parrett, C., and Parise, M., 2003, Wildfire-related debris-flow generation through episodic progressive sediment-bulking processes, western USA, Volume 1: Conference Paper.

Cannon, S.H., Gartner, J.E., Rupert, M.G., Michael, J.A., Rea, A.H., and Parrett, C., 2010, Predicting the probability and volume of postwildfire debris flows in the intermountain western United States: Geological Society of America Bulletin, v. 122, p. 127-144.

Cannon, S.H., Gartner, J.E., Wilson, R.C., Bowers, J.C., and Laber, J.L., 2008, Storm rainfall conditions for floods and debris flows from recently burned areas in southwestern Colorado and southern California: Geomorphology, v. 96, p. 250-269.

Cannon, S.H., Kirkham, R.M., and Parise, M., 2001, Wildfire-related debris-flow initiation processes, Storm King Mountain, Colorado: Geomorphology, v. 39, p. 171-188.

Carrara, P.E., 1989, Late Quaternary glacial and vegetative history of the Glacier National Park region, Montana: US Geol. Surv. Bull., v. 1902, p. 1-64.

Clayton, J.L., and Megahan, W.F., 1986, Erosion and chemical denudation rates in the southwestern Idaho Batholith: Earth Surface Processes and Landforms, v. 11, p. 389-400.

—, 1997, Natural erosion rates and their prediction in the Idaho batholith: Journal of the American Water Resources Association, v. 33, p. 689-703.

Cochrane, M.A., United Nations Environment Programme. Division of Early, W., Assessment, and United Nations Environment Programme. Oficina Regional para América Latina y el, C., 2002, Spreading like wildfire : tropical forest fires in Latin America and the Caribbean : prevention, assessment and early warning: Mexico, D.F., DEWA.

Collins, D.B.G., Bras, R.L., and Tucker, G.E., 2004, Modeling the effects of vegetation-erosion coupling on landscape evolution: J. Geophys. Res., v. 109, p. F03004.

Cook, E., 2004, North American Summer PDSI Reconstructions, NOAA/NGDC Paleoclimatology Program: Boulder CO, World Data Center for Paleoclimatology

Cook, E.R., Woodhouse, C.A., Eakin, C.M., Meko, D.M., and Stahle, D.W., 2004, Long-term aridity changes in the western United States: Science, v. 306, p. 1015-1018.

Dadson, S.J., Hovius, N., Chen, H., Dade, W.B., Lin, J.C., Hsu, M.L., Lin, C.W., Horng, M.J., Chen, T.C., Milliman, J., and Stark, C.P., 2004, Earthquake-triggered increase in sediment delivery from an active mountain belt: Geology, v. 32, p. 733-736.

Dadson, S.J., Hovius, N., Chen, H.G., Dade, W.B., Hsieh, M.L., Willett, S.D., Hu, J.C., Horng, M.J., Chen, M.C., Stark, C.P., Lague, D., and Lin, J.C., 2003, Links between erosion, runoff variability and seismicity in the Taiwan orogen: Nature, v. 426, p. 648-651.

Davis, L.G., Muehlenbachs, K., Schweger, C.E., and Rutter, N.W., 2002, Differential response of vegetation to postglacial climate in the Lower Salmon River Canyon, Idaho: Palaeogeography Palaeoclimatology Palaeoecology, v. 185, p. 339-354.

Despain, D.G., 1990, Yellowstone's vegetation: the consequences of history and environment in a natural setting: New York.

Dixon, J.L., Heimsath, A.M., and Amundson, R., 2009, The critical role of climate and saprolite weathering in landscape evolution: Earth Surface Processes and Landforms, v. 34, p. 1507-1521.

Doerr, S.H., Shakesby, R.A., Blake, W.H., Chafer, C.J., Humphreys, G.S., and Wallbrink, P.J., 2006, Effects of differing wildfire severities on soil wettability and implications for hydrological response: Journal of Hydrology, v. 319, p. 295-311.

Esper, J., Cook, E.R., and Schweingruber, F.H., 2002, Low-frequency signals in long tree-ring chronologies for reconstructing past temperature variability: Science, v. 295, p. 2250-2253.

Forsyth, G.G., and Wilgen, B.W.v., 2008, The recent fire history of the Table Mountain National Park and implications for fire management: Koedoe : African Protected Area Conservation and Science, v. 50, p. 3-9.

Gavin, D.G., 2001, Estimation of inbuilt age in radiocarbon ages of soil charcoal for fire history studies: Radiocarbon, v. 43, p. 27-44.

Gibson, C.E., and Morgan, P., 2009, Atlas of digital polygon fire extents for Idaho and western Montana (1889-2003), USDA Forest Service, Rocky Mountain Research Station.

Grove, J.M., 1988, The Little Ice Age.

Heimsath, A.M., Dietrich, W.E., Nishiizumi, K., and Finkel, R.C., 2001, Stochastic processes of soil production and transport: Erosion rates, topographic variation and cosmogenic nuclides in the Oregon Coast Range: Earth Surface Processes and Landforms, v. 26, p. 531-552.

Herron, T., and Freeman, L., 2008, Middle Fork Salmon River Subbasin Assessment and Total Maximum Daily Loads, *in* Quality, D.o.E., ed.

Heyerdahl, E.K., Morgan, P., and Riser, J.P., 2008, Multi-season climate synchronized historical fires in dry forests (1650-1900), northern Rockies, USA: Ecology, v. 89, p. 705-716.

Hostetler, S.W., Bartlein, P.J., and Holman, J.O., 2006, Atlas of climatic controls of wildfire in the western United States, Scientific Investigations Report: USGS Numbered Series, p. iv, 69 p.

Hren, M.T., Hilley, G.E., and Chamberlain, G.P., 2007, The relationship between tectonic uplift and chemical weathering rates in the Washington cascades: Field measurements and model predictions: American Journal of Science, v. 307, p. 1041-1063.

Huerta, M.A., Whitlock, C., and Yale, J., 2009, Holocene vegetation-fire-climate linkages in northern Yellowstone National Park, USA: Palaeogeography Palaeoclimatology Palaeoecology, v. 271, p. 170-181.

IPPC, 2007, Climate Change 2007: The Physical Science Basis

in Change, W.G.I.t.t.F.A.R.o.t.I.P.o.C., ed.: Working Group I to the Fourth Assessment Report of the Intergovernmental Panel on Climate Change, Cambridge University Press.

Istanbulluoglu, E., Tarboton, D.G., Pack, R.T., and Luce, C., 2003, A sediment transport model for incision of gullies on steep topography: Water Resources Research, v. 39.

Istanbulluoglu, E., Tarboton, D.G., Pack, R.T., and Luce, C.H., 2004, Modeling of the interactions between forest vegetation, disturbances, and sediment yields: Journal of Geophysical Research-Earth Surface, v. 109.

Iverson, R.M., 1997, The physics of debris flows: Reviews of Geophysics, v. 35, p. 245-296.

Iverson, R.M., LaHusen, R.G., Major, J.J., Zimmerman, C.L., and Anonymous, 1994, Debris flow against obstacles and bends; dynamics and deposits: Eos, Transactions, American Geophysical Union, v. 75, p. 274.

Key, C.H., and Benson, N.C., 1999, Measuring and remote sensing of burn severity: the CBI and NBR, *in* Neuenschwander, L.F., and Ryan, K.C., eds., Proceedings Joint Fire Science Conference and Workshop, Volume Vol. II: Poster abstract: Boise, ID, University of Idaho and International Association of Wildland Fire, p. 284 pp.

Kirchner, J.W., Finkel, R.C., Riebe, C.S., Granger, D.E., Clayton, J.L., King, J.G., and Megahan, W.F., 2001, Mountain erosion over 10 yr, 10 k.y., and 10 m.y. time scales: Geology, v. 29, p. 591-594.

Lavee, H., Kutiel, P., Segev, M., and Benyamini, Y., 1995, Effect of surface roughness on runoff and erosion in a Mediterranean ecosystem: the role of fire: Geomorphology, v. 11, p. 227-234.

Leidecker, M., 2008, Matt Leidecker Photography, Volume 2012: Ketchum, ID.

Lohman, D.J., Bickford, D., and Sodhi, N.S., 2007, The Burning Issue: Science, v. 316, p. 376.

Luckman, B.H., 2000, The Little Ice Age in the Canadian Rockies: Geomorphology, v. 32, p. 357-394.

Ludington, S., Moring, B.C., Miller, R.J., Flynn, K.S., Evans, J.G., and Stone, P.A., 2006, Preliminary integrated geologic map databases for the United States - Western States - California, Nevada, Arizona, Washington, Oregon, Idaho, and Utah, Volume 2005-1305, U.S. Geological Survey.

Malmon, D.V., Reneau, S.L., Katzman, D., Lavine, A., and Lyman, J., 2007, Suspended sediment transport in an ephemeral stream following wildfire: Journal of Geophysical Research-Earth Surface, v. 112.

Marlon, J., Bartlein, P.J., and Whitlock, C., 2006, Fire-fuel-climate linkages in the northwestern USA during the Holocene: Holocene, v. 16, p. 1059-1071.

Marlon, J.R., Bartlein, P.J., Walsh, M.K., Harrison, S.P., Brown, K.J., Edwards, M.E., Higuera, P.E., Power, M.J., Anderson, R.S., Briles, C., Brunelle, A., Carcaillet, C., Daniels, M., Hu, F.S., Lavoie, M., Long, C., Minckley, T., Richard, P.J.H., Scott, A.C., Shafer, D.S., Tinner, W., Umbanhowar, C.E., and Whitlock, C., 2009, Wildfire responses to abrupt climate change in North America: Proceedings of the National Academy of Sciences of the United States of America, v. 106, p. 2519-2524.

Meyer, G.A., and Leidecker, M.E., 2007, Mass Movement effects on the Middle Fork Salmon RIver, Idaho, Geological Society of America Abstracts with Programs, Volume 39: Denver, p. 179.

Meyer, G.A., and Pierce, J.L., 2003, Climatic controls on fire-induced sediment pulses in Yellowstone National Park and central Idaho: a long-term perspective: Forest Ecology and Management, v. 178, p. 89-104.

Meyer, G.A., Pierce, J.L., Wood, S.H., and Jull, A.J.T., 2001, Fires, storms, and erosional events in the Idaho batholith: Hydrol. Process., v. 15, p. 3025-3038.

Meyer, G.A., and Wells, S.G., 1997, Fire-related sedimentation events on alluvial fans, Yellowstone National Park, USA: Journal of Sedimentary Research, v. 67, p. 776-791.

Meyer, G.A., Wells, S.G., and Jull, A.J.T., 1995, Fire and alluvial chronology in Yellowstone National Park: Climatic and intrinsic controls on Holocene geomorphic processes: Geol. Soc. Am. Bull., v. 107, p. 1211-1230.

Miller, R.F., and Tausch, R.J., 2001, The role of fire in pinyon and juniper woodlands: A descriptive analysis, *in* Galley, K.E.M.W., T.P., eds. , ed., Proceedings of the invasive species workshop: The role of fire in the control and spread of invasive species: Tallahassee, FL, Tall Timbers Research Station, p. 15-30.

Molnar, P., 2001, Climate change, flooding in arid environments, and erosion rates: Geology, v. 29, p. 1071-1074.

—, 2004, Late cenozoic increase in accumulation rates of terrestrial sediment: How might climate change have affected erosion rates?: Annual Review of Earth and Planetary Sciences, v. 32, p. 67-89.

Montgomery, D.R., Balco, G., and Willett, S.D., 2001, Climate, tectonics, and the morphology of the Andes: Geology, v. 29, p. 579-582.

Montgomery, D.R., and Brandon, M.T., 2002, Topographic controls on erosion rates in tectonically active mountain ranges: Earth and Planetary Science Letters, v. 201, p. 481-489.

Morgan, P., Heyerdahl, E.K., and Gibson, C.E., 2008, Multi-season climate synchronized forest fires throughout the 20th century, northern Rockies, USA: Ecology, v. 89, p. 717-728.

Mote, P.W., and Salathe, E.P., 2009, Future climate in the Pacific Northwest (in press), Washington Climate Change Impacts Assessment: Evaluating Washington's future in a changing climate.

MTBS, 2010, Monitoring Trends in Burn Severity Data Access, Fire Level Geospatial Data, Volume 2011, MTBS Project (USDA Forest Service/U.S. Geological Survey).

NAIP, 2009, Digital Orthoimagery Series of Idaho (2009, 1-meter, Natural Color and False Color), USDA-FSA-APFO Aerial Photography Field Office.

Nelson, N.A., and Pierce, J., 2010, Late-Holocene relationships among fire, climate and vegetation in a forest-sagebrush ecotone of southwestern Idaho, USA: Holocene, v. 20, p. 1179-1194.

NIFC, 2010, Wildland Fire Statistics, National Interagency Fire Center: Boise, ID.

NOAA, 2012, Historical Palmer Drought Indices National Climatic Data Center, Climate Services and Monitoring Division

Page, S.E., Siegert, F., Rieley, J.O., Boehm, H.-D.V., Jaya, A., and Limin, S., 2002, The amount of carbon released from peat and forest fires in Indonesia during 1997: Nature, v. 420, p. 61-65.

Parise, M., and Cannon, S.H., 2012, Wildfire impacts on the processes that generate debris flows in burned watersheds: Natural Hazards, v. 61, p. 217-227.

Pierce, J., and Meyer, G., 2008, Long-term fire history from alluvial fan sediments: the role of drought and climate variability, and implications for management of Rocky Mountain forests: International Journal of Wildland Fire, v. 17, p. 84-95.

Pierce, J.L., Meyer, G.A., and Jull, A.J.T., 2004, Fire-induced erosion and millennialscale climate change in northern ponderosa pine forests: Nature, v. 432, p. 87-90.

Pollack, H.N., Huang, S., and Shen, P., 1998, Climate change record in subsurface temperatures: a global perspective: Science, v. 282, p. 279-281.

Power, M.J., Marlon, J., Ortiz, N., Bartlein, P.J., Harrison, S.P., Mayle, F.E., Ballouche, A., Bradshaw, R.H.W., Carcaillet, C., Cordova, C., Mooney, S., Moreno, P.I., Prentice, I.C., Thonicke, K., Tinner, W., Whitlock, C., Zhang, Y., Zhao, Y., Ali, A.A., Anderson, R.S., Beer, R., Behling, H., Briles, C., Brown, K.J., Brunelle, A., Bush, M., Camill, P., Chu, G.Q., Clark, J., Colombaroli, D., Connor, S., Daniau, A.L., Daniels, M., Dodson, J., Doughty, E., Edwards, M.E., Finsinger, W., Foster, D., Frechette, J., Gaillard, M.J., Gavin, D.G., Gobet, E., Haberle, S., Hallett, D.J., Higuera, P., Hope, G., Horn, S., Inoue, J., Kaltenrieder, P., Kennedy, L., Kong, Z.C., Larsen, C., Long, C.J., Lynch, J., Lynch, E.A., McGlone, M., Meeks, S., Mensing, S., Meyer, G., Minckley, T., Mohr, J., Nelson, D.M., New, J., Newnham, R., Noti, R., Oswald, W., Pierce, J., Richard, P.J.H., Rowe, C., Goni, M.F.S., Shuman, B.N., Takahara, H., Toney, J., Turney, C., Urrego-Sanchez, D.H., Umbanhowar, C., Vandergoes, M., Vanniere, B., Vescovi, E., Walsh, M., Wang, X., Williams, N., Wilmshurst, J., and Zhang, J.H., 2008, Changes in fire regimes since the Last Glacial Maximum: an assessment based on a global synthesis and analysis of charcoal data: Climate Dynamics, v. 30, p. 887-907.

Power, M.J., Whitlock, C., and Bartlein, P.J., 2011, Postglacial fire, vegetation, and climate history across an elevational gradient in the Northern Rocky Mountains, USA and Canada: Quaternary Science Reviews, v. 30, p. 2520-2533.

Reimer, P.J., Baillie, M.G.L., Bard, E., Bayliss, A., Beck, J.W., Bertrand, C.J.H., Blackwell, P.G., Buck, C.E., Burr, G.S., Cutler, K.B., Damon, P.E., Edwards, R.L., Fairbanks, R.G., Friedrich, M., Guilderson, T.P., Hogg, A.G., Hughen, K.A., Kromer, B., McCormac, G., Manning, S., Ramsey, C.B., Reimer, R.W., Remmele, S., Southon, J.R., Stuiver, M., Talamo, S., Taylor, F.W., van der Plicht, J., and Weyhenmeyer, C.E., 2004, IntCal04 terrestrial radiocarbon age calibration, 0-26 cal kyr BP: Radiocarbon, v. 46, p. 1029-1058.

Reiners, P.W., Ehlers, T.A., Mitchell, S.G., and Montgomery, D.R., 2003, Coupled spatial variations in precipitation and long-term erosion rates across the Washington Cascades: Nature, v. 426, p. 645-647.

Riebe, C.S., Kirchner, J.W., and Finkel, R.C., 2004, Sharp decrease in long-term chemical weathering rates along an altitudinal transect: Earth and Planetary Science Letters, v. 218, p. 421-434.

Robichaud, P.R., 2000, Fire effects on infiltration rates after prescribed fire in Northern Rocky Mountain forests, USA: Journal of Hydrology, v. 231, p. 220-229.

Roering, J.J., and Gerber, M., 2005, Fire and the evolution of steep, soil-mantled landscapes: Geology, v. 33, p. 349-352.

Schmidt, K.M., 2001, The variability of root cohesion as an influence on shallow landslide susceptibility in the Oregon Coast Range: Can. Geotech. J., v. 38, p. 995-1024.

Schoennagel, T., Turner, M.G., and Romme, W.H., 2003, The influence of fire interval and serotiny on postfire lodgepole pine density in Yellowstone National Park: Ecology, v. 84, p. 2967-2978.

Schoennagel, T., Veblen, T.T., and Romme, W.H., 2004, The Interaction of Fire, Fuels, and Climate across Rocky Mountain Forests: BioScience, v. 54, p. 661-676.

Shakesby, R.A., and Doerr, S.H., 2006, Wildfire as a hydrological and geomorphological agent: Earth-Science Reviews, v. 74, p. 269-307.

Shinneman, D.J., and Baker, W.L., 1997, Nonequilibrium dynamics between catastrophic disturbances and old-growth forests in ponderosa pine landscapes of the Black Hills: Conserv. Biol., v. 11, p. 1276-1288.

Shuman, B., Henderson, A.K., Colman, S.M., Stone, J.R., Fritz, S.C., Stevens, L.R., Power, M.J., and Whitlock, C., 2009, Holocene lake-level trends in the Rocky Mountains, U.S.A: Quaternary Science Reviews, v. 28, p. 1861-1879.

Snyder, N.P., Whipple, K.X., Tucker, G.E., and Merritts, D.J., 2000, Landscape response to tectonic forcing: Digital elevation model analysis of stream profiles in the Mendocino triple junction region, northern California: Geological Society of America Bulletin, v. 112, p. 1250-1263.

Steele, R., Pfister, R.D., Ryker, R.A., and Kittams, J.A., 1981, Forest Habitat Tyes of Central Idaho, *in* Service, F., ed., Intermountain Forest and Range Experiment Station.

Stine, S., 1994, Extreme and persistent drought in California and Patagonia during medieval time: Nature, v. 369, p. 546-549.

Stuiver, M., and Reimer, P.J., 1993, Extended 14C data base and revised CALIB 3.0 14C age calibration program: Radiocarbon, v. 35, p. 215-230.

Surovell, T.A., Finley, J.B., Smith, G.M., Brantingham, P.J., and Kelly, R., 2009, Correcting temporal frequency distributions for taphonomic bias: Journal of Archaeological Science, v. 36, p. 1715-1724.

Svenson, L., 2010, Fire and Climate in a Lodgepole Forest of Central Idaho: Annula, Decadal, Centennial, and Millininial Persepectives: Boise, Boise State University.

Swetnam, T.W., 1993, Fire history and climate-change in giant sequoia groves: Science, v. 262, p. 885-889.

Swetnam, T.W., and Betancourt, J.L., 1998, Mesoscale disturbance and ecological response to decadal climatic variability in the American Southwest: J. Clim., v. 11, p. 3128-3147.

Teasdale, G.N., 2010, Sediment Load, Transport and Accumulation in Lower Granite Reservoir on the Snake River, 2nd Joint Federal Interagency Conference: Las Vegas, NV.

Tennant, C.J., 2011, The Influence of Precipitation Phase on Hydrograph Form: An Investigation of Twelve Tributaries to the Salmon River, Idaho: Pocatello, Idaho State university.

Veblen, T.T., Kitzberger, T., and Donnegan, J., 2000, Climatic and human influences on fire regimes in ponderosa pine forests in the Colorado Front Range: Ecol. Appl., v. 10, p. 1178-1195.

Wells, S.G., and Harvey, A.M., 1987, Sedimentologic and geomorphic variations in storm-generated alluvial fans, Howgill Fells, northwest England: Geological Society of America Bulletin, v. 98, p. 182-198.

Weppner, K., 2012, Climate drivers and landscape response: Holocene fire, vegetation and erosion, City of Rocks National Reserve, Idaho: Boise, Boise State University.

Westerling, A.L., Gershunov, A., Brown, T.J., Cayan, D.R., and Dettinger, M.D., 2003, Climate and wildfire in the western United States: Bull. Am. Meteorol. Soc., v. 84, p. 595-604.

Westerling, A.L., Hidalgo, H.G., Cayan, D.R., and Swetnam, T.W., 2006, Warming and earlier spring increase western US forest wildfire activity: Science, v. 313, p. 940-943.

White, A.F., and Blum, A.E., 1995, Effects of climate on chemical_ weathering in watersheds: Geochimica et Cosmochimica Acta, v. 59, p. 1729-1747.

Whitlock, C., Briles, C.E., Fernandez, M.C., and Gage, J., 2010, Holocene vegetation, fire and climate history of the Sawtooth Range, central Idaho, USA: Quaternary Research, v. 75, p. 114-124.

Whitlock, C., Dean, W., Rosenbaum, J., Stevens, L., Fritz, S., Bracht, B., and Power, M., 2008, A 2650-year-long record of environmental change from northern Yellowstone National Park based on a comparison of multiple proxy data: Quaternary International, v. 188, p. 126-138.

Whitlock, C., Shafer, S.L., and Marlon, J., 2003, The role of climate and vegetation change in shaping past and future fire regimes in the northwestern US and the implications for ecosystem management: Forest Ecology and Management, v. 178, p. 5-21.

Whitlock, C., Skinner, C.N., Bartlein, P.J., Minckley, T., and Mohr, J.A., 2004, Comparison of charcoal and tree-ring records of recent fires in the eastern Klamath Mountains, California, USA: Canadian Journal of Forest Research, v. 34, p. 2110-2121.

Wondzell, S.M., and King, J.G., 2003, Postfire erosional processes in the Pacific Northwest and Rocky Mountain regions: Forest Ecology and Management, v. 178, p. 75-87.

APPENDIX A

Stratigraphic profiles

Table A-1: Summary of stratigraphic profiles investigated containing 61 radiocarbon dated alluvial charcoal fragments. The summary excludes one profile from Big Creek containing two radiocarbon dates that was outside final set of study basins and one profile from Pole Creek where an inset debris flow deposit was dated post-bomb and contained probable Mazama ash deposit.

Tributary Profile	Incision depth (cm)	Average debris flow thickness (cm)	Average sheetflood thickness (cm)	% depth debris flow	% depth sheetflood	% depth fire-related	Number of deposits dated (number of field duplicates)
Kotch (KC) - 1	270	76	4	0.85	0.01	NA	
Kotch - 2	160	25	12	0.79	0.08	0.51	4 deposits dated
Kotch - 3	170	21	9	0.37	0.05	0.41	
Sheepeater (SHS) - 1	210	40	0	0.95	0.00	0.49	
Sheepeater - 2	210	58	2	0.82	0.01	0.54	
Sheepeater - 3	150	35	0	0.93	0.00	1.00	1 deposit dated
Sheepeater - 4	480	121	0	0.75	0.00	0.72	1 deposit dated
Sheepeater - 6	110	35	0	0.64	0.00	0.85	1 deposit dated
Sheepeater - 7	180	44	0	0.98	0.00	1.00	1 deposit dated (1 duplicate)
Sheepeater - 8	430	68	0	0.63	0.00	0.79	2 deposits dated
Greyhound (GHC) - 1	390	157	0	0.81	0.00	0.92	1 deposit dated
Greyhound - 2	190	77	0	0.81	0.00	0.86	2 deposits dated (1 duplicate)
Lake (LC) - 1	530	94	12	0.71	0.09	0.60	8 deposits dated (5 duplicates)
Lake - 2	510	57	19	0.45	0.07	0.74	1 deposit dated
Orelano (OC) - 3	495	78	0	0.47	0.00	0.68	2 deposits dated
Orelano - 4	201	37	49	0.73	0.24	1.00	3 deposit dated (1 duplicate)
Hood Ranch (HR) - 1	147	38	3	0.78	0.05	0.83	1 deposit dated
Hood Ranch - 3	214	19	62	0.09	0.57	0.09	
Sunflower (SC) - 1	509	91	77	0.54	0.45	0.60	2 deposits dated
Sunflower -2	151	40	0	0.79	0.00	0.46	
Jack (JC) - 1	373	162	50	0.87	0.13	0.00	1 deposit dated
Reservoir (RC) - 3	332	47	8.2	0.42	0.45	0.25	6 deposits dated
Reservoir - 5	255	40	11.2	0.63	0.22	0.30	
Reservoir - 6	308	50	11.25	0.32	0.44	0.13	
Pole (PC) - 1	360	70	29	0.58	0.24	0.26	2 deposits dated
Pole - 5	72	35	0	0.96	0.00	0.53	
Pole - 7	150	45	0	0.30	0.00	0.31	
Pole - 8	285	53	0	0.93	0.00	0.09	2 deposits dated (2 duplicates)
Bernard (BC) - 1	251	28	27	0.22	0.11	0.25	3 deposits dated (1 duplicate)
Bernard - 2	132	24	5	0.36	0.04	0.45	1 deposit dated
Bernard - 4	237	33	13	0.27	0.11	0.00	
Bernard - 5	219	24	11	0.43	0.25	0.66	5 deposits dated
Bernard - 6	320	12	12	0.04	0.78	0.70	

Table A-2: Summary of profiles and radiocarbon dates excluding two profiles and three ^{14}C-dates outside defined study areas.

Basin Classification	Investigated Stratigraphic Profiles	Dated Stratigraphic Profiles	Charcoal fragments dated
Upper	12	16	35
Lower	9	17	26
Total	**21**	**33**	**61**

Table A-3: Radiocarbon ages for all dated deposits grouped by sub-basin.

Lab Code	Sample Code	Basin / Classification	Depositional Process	Fire Related	Thickness (cm)	% total depth	^{14}C age ± 1 sigma	Calibrated (Median) ± 2 sigma
153900	KC-2-1	Kotch / Upper	Debris flow	FR	15	9	335 ± 60	309 (390) 477
153901	KC-2-4	Kotch / Upper	Burn surface below sheetflood	FR	14	9	1070 ± 60	929 (975) 1055
153902	KC-2-5	Kotch / Upper	Debris Flow	FR	26	16	1190 ± 60	1053 (1116) 1180
153903	KC-2-6	Kotch / Upper	Debris flow	FR	40	25	2170 ± 60	2152 (2232) 2336
AA88192	SHS-4-4	Sheepeater / Upper	Inset debris flow	FR	25	0.05	modern	modern
AA88193	SHS-6-3	Sheepeater / Upper	Debris flow	FR	53	48	675 ± 35	558 (642) 681
149557	SHS-7-3A	Sheepeater / Upper	Burn surface	FR	57	32	900 ± 35	738 (826) 911
149571	SHS-7-3B	Sheepeater / Upper	Burn surface	FR	57	32	870 ± 35	696 (778) 906
153914	SH5-8-2	Sheepeater / Upper	Debris flow	FR	60	14	4520 ± 90	5039 (5163) 5314
149564	SHS-3-3	Sheepeater/Upper	Debris flow	Scarce	19	13	3481 ± 68	3576 (3756) 3922
149547	SHS-8-5	Sheepeater / Upper	Burn surface below debris flow	FR	30	7	9960 ± 45	11248 (11383) 11611
149561	GHC-1-5	Greyhound / Upper	Sheetflood	FR	14	4	1637 ± 36	1414 (1534) 1615
149559	GHC-2-3	Greyhound / Upper	Overbank	FR	4	2	1462 ± 36	1300 (1350) 1405
149569	GHC-2-5A	Greyhound / Upper	Burn Surface below overbank	FR	4	2	1525 ± 35	1345 (1409) 1518
149556	GHC-2-5B	Greyhound / Upper	Burn surface below overbank	FR	4	2	1485 ± 35	1302 (1368) 1507
AA88198	LC-1-8	Lake / Upper	Charcoal rich sands (flood)	FR	thin	NA	modern	modern
AA88196	LC-1-1	Lake / Upper	Overbank	FR	2	< 1	385 ± 34	318 (450) 509
AA88199	LC-2-5	Lake / Upper	Debris flow	FR	140	27	380 ± 36	316 (442) 508
153904	LC-1B-5A	Lake / Upper	Burn surface below sheetflood	FR	37	7	1880 ± 60	1728 (1828) 1884
153897	LC-1B-5B	Lake / Upper	Burn surface below sheetflood	FR	37	7	1955 ± 60	1827 (1906) 1987
149551	LC-1B-6A	Lake / Upper	Debris flow	FR	23	4	2660 ± 30	2742 (2769) 2844
AA88201	LC-1B-6B	Lake / Upper	Debris flow	FR	23	4	3510 ± 45	3644 (3781) 3899
149566	LC-1B-8A	Lake / Upper	Burn surface	FR	5	1	5785 ± 35	6495 (6587) 6665
AA88197	LC-1B-8B	Lake / Upper	Burn surface	FR	5	1	5850 ± 30	6566 (6672) 6741
153905	LC-1B-7A	Lake / Upper	Burn surface below debris flow	FR	26	5	6325 ± 90	7163 (7256) 7330
153898	LC-1B-7B	Lake / Upper	Burn surface below debris flow	FR	26	5	6280 ± 90	7067 (7212) 7311
149552	LC-1-7	Lake / Upper	Burn surface below overbank	FR	19	4	7347 ± 47	8025 (8154) 8310
149570	LC-1B-11A	Lake / Upper	Debris flow	Scarce	47	9	8040 ± 30	8778 (8942) 9021
149549	LC-1B-11B	Lake / Upper	Debris flow	Scarce	47	9	8780 ± 35	9626 (9792) 10113
149568	OC-4B-2 B	Orelano / Upper	Burn surface below debris flow	FR	11	5	modern	modern
149560	OC-4B-2A	Orelano / Upper	Burn surface below debris flow	FR	11	5	90 ± 30	0 (107) 265
149567	OC-3-6B	Orelano / Upper	Burn surface below debris flow	FR	80	16	875 ± 25	729 (777) 904
AA88203	OC-3-3	Orelano / Upper	Burn surface below debris flow	FR	75	15	955 ± 35	790 (856) 931
AA88195	0C-4-1	Orelano / Upper	Sheetflood	FR	10	2	1195 ± 41	988 (1122) 1201
149575	0C-4-4	Orelano / Upper	Debris flow	FR	120	36	4693 ± 48	5316 (5415) 5526
149546	SC-1-2A	Sunflower / Lower	Burn surface below sheetflood	FR	10 - 197	2 - 39	5110 ± 40	5746 (5823) 5929
AA88204	SC-1-4	Sunflower / Lower	Sheetflood	FR	21	4	5650 ± 35	6318 (6432) 6498
149562	HR-1-6	Hood / Lower	Debris flow	FR	36	24	7720 ± 50	8417 (8499) 8589
149547	JC-1-2	Jack / Lower	Debris flow	Scarce	178	48	11730 ± 130	13315 (13581) 13834
AA88205	RC-3-9	Reservoir / Lower	Burn surface below debris flow	FR	27	8	243 ± 38	0 (289) 429
149576	RC-3B-3	Reservoir / Lower	Sheetflood	FR	5 - 27	2 – 8	2095 ± 30	1994 (2067) 2144
AA88191	RC-1B-8	Reservoir / Lower	Debris flow	Scarce	82	25	2770 ± 45	2767 (2867) 2964
149545	RC-3-4A	Reservoir / Lower	Sheetflood	FR	3	1%	5005 ± 30	5653 (5733) 5889
149548	RC-1B-18	Reservoir / Lower	Sheetflood	FR	2 – 121	1 -36	5585 ± 50	6290 (6366) 6453
149565	RC-3-1	Reservoir / Lower	Sheetflood	FR	14 - 90	4 - 26	5689 ± 64	6318 (6480) 6638
AA88202	BC-1-1	Bernard / Lower	Burn surface below debris flow	FR	22	8	147 ± 38	0 (148) 283
149558	BC-3-3	Bernard / Lower	Burn surface	FR	5	2	95 ± 30	0 (109) 267
149572	BC-3-6B	Bernard / Lower	Debris flow	Scarce	35	14	520 ± 35	505 (536) 630
153909	BC-5-3	Bernard / Lower	Debris flow	Scarce	22	10	365 ± 60	316 (429) 501
149574	BC-3-6A	Bernard / Lower	Reworked charcoal	FR	35	14	925 ± 35	745 (849) 925
AA88210	BC-2-4	Bernard / Lower	Burn surface	FR	2	2	1008 ± 40	795 (928) 1035
153910	BC-5-4	Bernard / Lower	Debris flow	FR	23	11	1830 ± 70	1696 (1769) 1866
153911	BC-5-8	Bernard / Lower	Sheetflood	FR	12 - 55	5-25	2735 ± 90	2756 (2830) 2928
153912	BC-5-9	Bernard / Lower	Overbank	FR	42	19	2975 ± 90	3000 (3158) 3268
153913	BC-5-10	Bernard / Lower	Debris flow	FR	23	11	3405 ± 80	3558 (3656) 3826
AA88208	PC-2-6	Pole / Lower	Sheetflood	FR	10	0.017	modern	modern
AA88206	HR-1-1	Pole / Lower	Burn surface below debris flow	FR	67	19	419 ± 82	299 (449) 557
AA88207	HR-1-2	Pole / Lower	Sheetflood	FR	26	7	135 ± 39	0 (137) 283
149550	PC-8-1A	Pole / Lower	Sheetflood within debris flow	Scarce	2	1	1710 ± 30	1546 (1616) 1697
AA88194	PC-8-1B	Pole / Lower	Sheetflood within debris flow	Scarce	224	79	1620 ± 30	1412 (1505) 1592
149555	PC-8-3A	Pole / Lower	Burn surface below debris flow	FR	31	11	2100 ± 30	1995 (2072) 2146
149563	PC-8-3B	Pole / Lower	Burn surface below debris flow	FR	31	11	2230 ± 35	2152 (2232) 2336
AA88209	NNC-1-1	No name / Lower	Debris flow	FR	158	0.88	modern	modern
AA88200	NNC-1-2	No name / Lower	Overbank	FR	12	7	1060 ± 240	555 (993) 1408

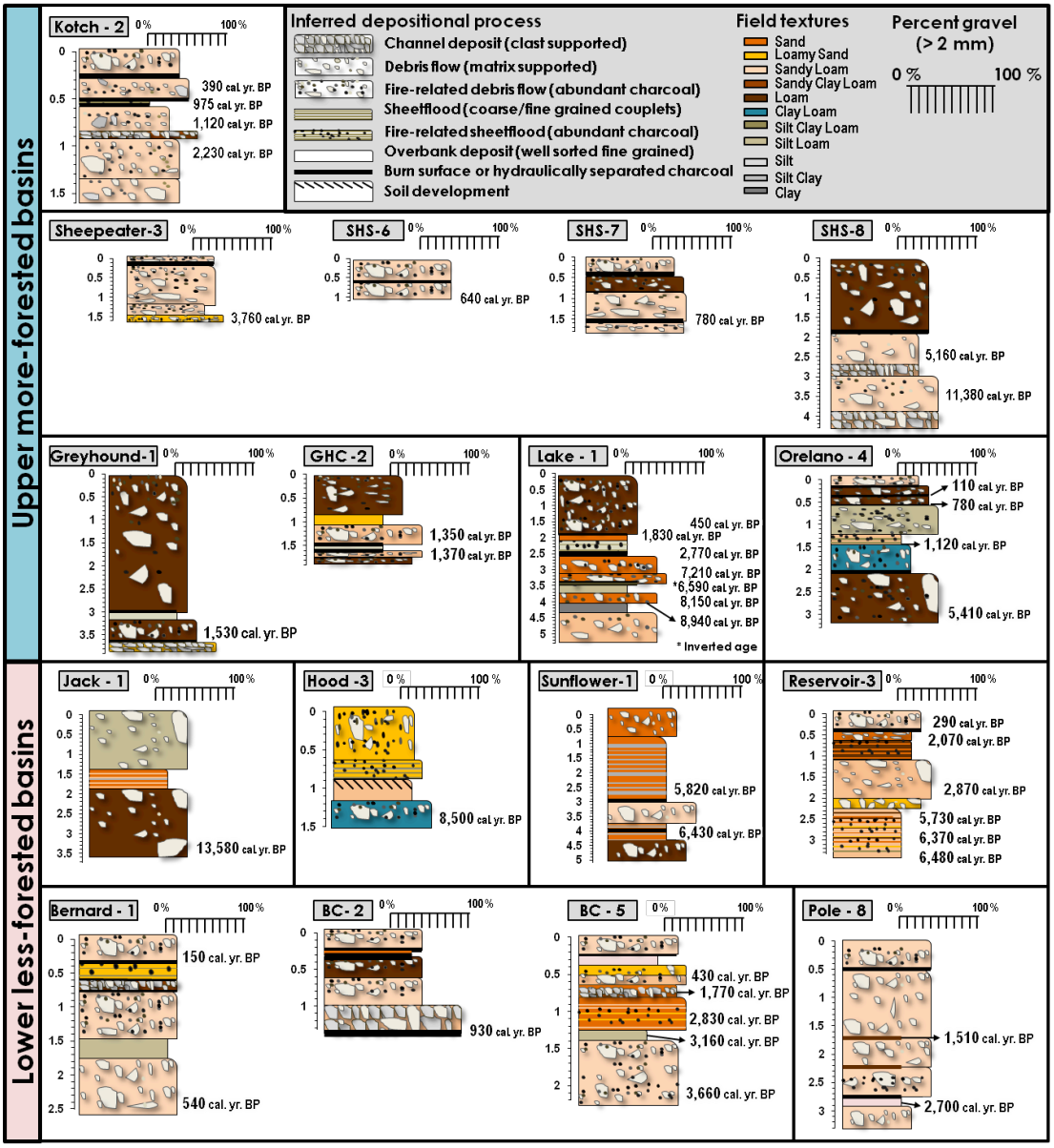

Figure A-1: Illustrations are of radiocarbon dated stratigraphic profiles grouped by alluvial fan study site. Missing profiles include one from Big Creek, outside defined study areas where two fires were dated and one profile from a failure of a high fan surface in Pole Creek where one discrete fire was dated. Three field duplicate dates that showed statistically different ages and therefore represent discrete older fires and erosional events are also missing. In total, 41 discrete fires are shown and six discrete dated fires are not shown in the above illustration. The vertical y-axis scale represents profile depth in meters with zero representing the top of the profile. Note the difference in scale among alluvial fans and similarity in scale within each alluvial fan site.

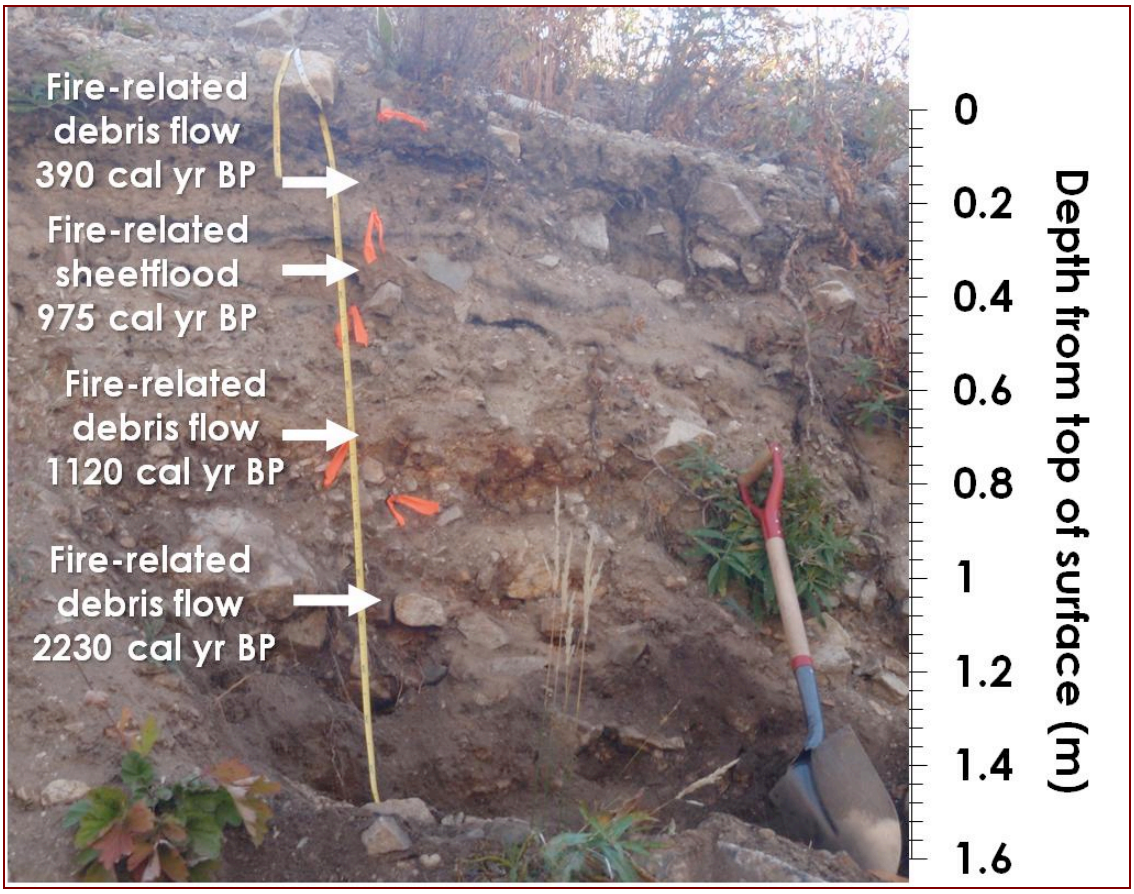

Figure A-2: Kotch Creek (upper basin) stratigraphic profile. The debris flow deposit on the very top of the profile is the most recent (2008) debris flow.

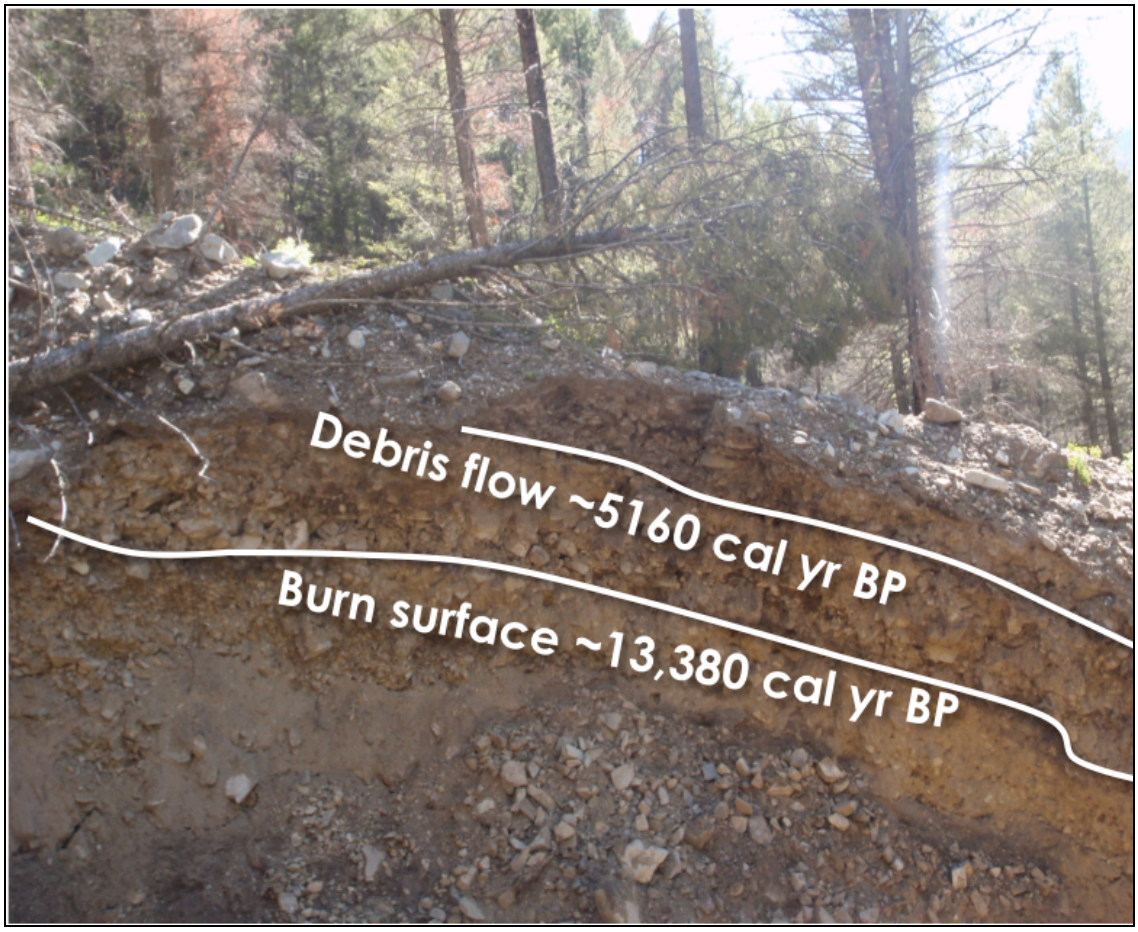

Figure A-3: Stratigraphic profile located at the apex of the perched paleo-fan at Sheepeater study site. The top debris flow deposit is the most recent (2008) debris flow deposition. Fire-related deposits are not labeled.

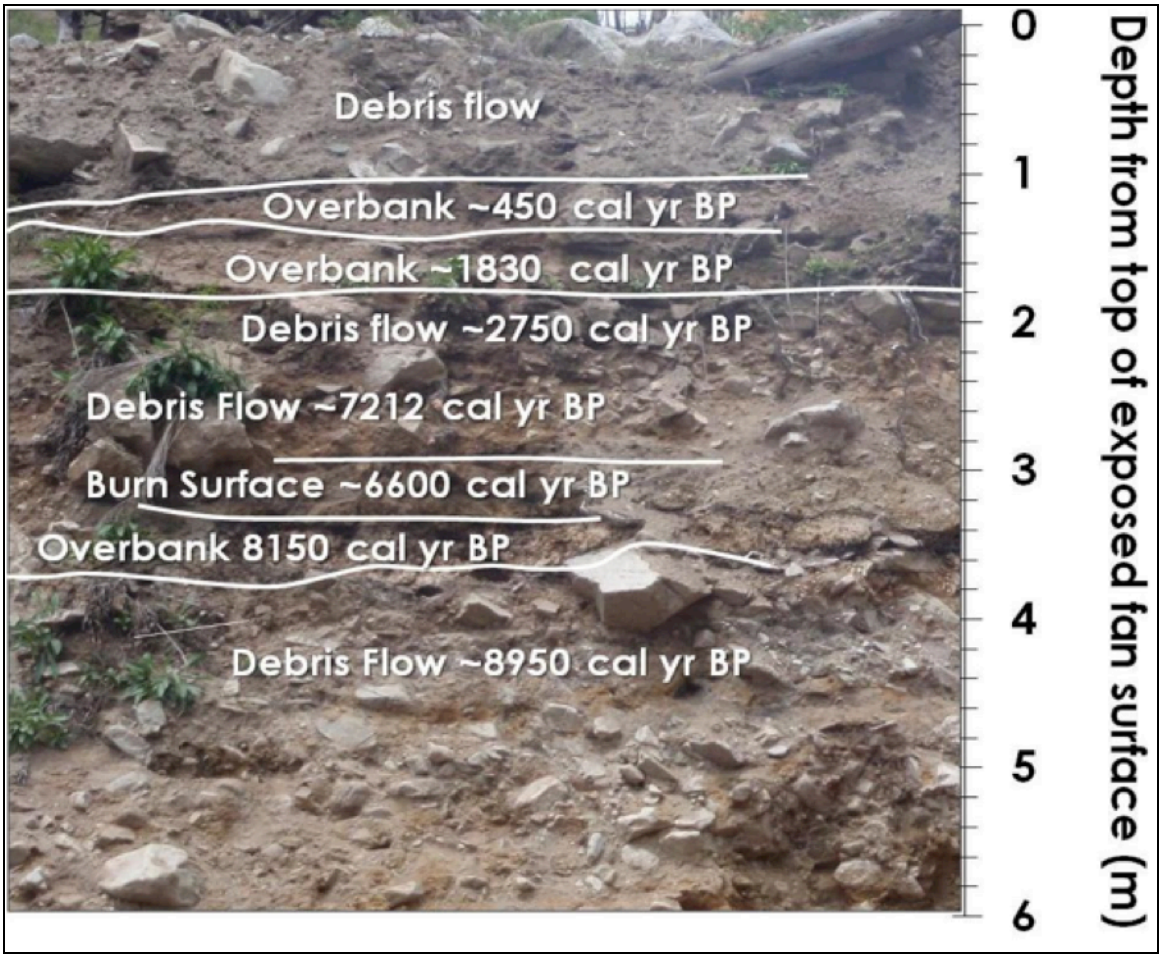

Figure A-4: Stratigraphic profile of Lake Creek. Fire-related deposits are not labeled.

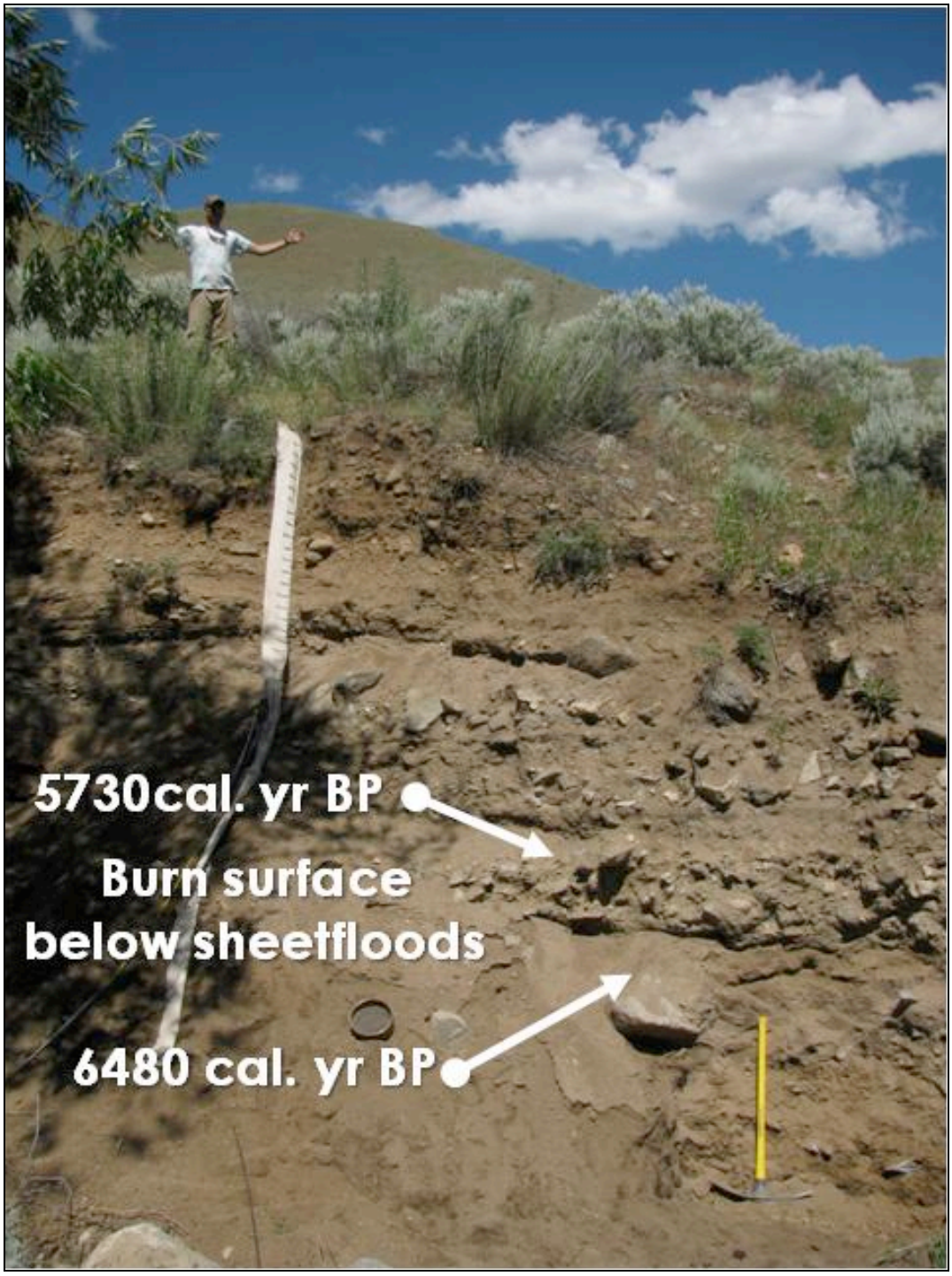

Figure A-5: Stratigraphic profle at Sunflower Creek. Burn surfaces, each below a pachage of sheetfloods was dated.

Figure A-6: Jack Creek stratigraphic profile. The dated deposit is a debris flow which underlies potentially fluvially reworked main-stem sediment.

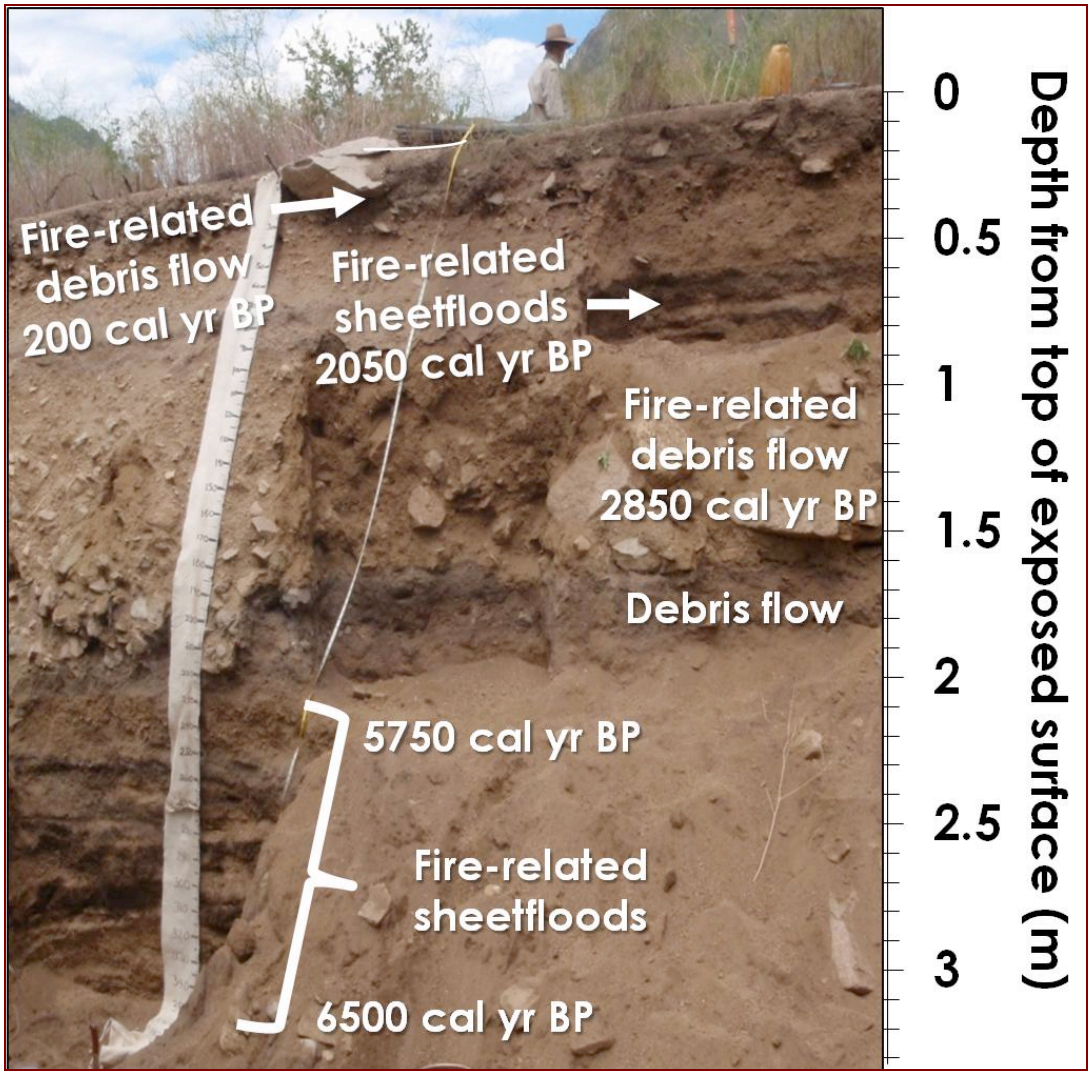

Figure A-7: Stratigraphic profile at Reservoir Creek.

Figure A-8: Stratigraphic profile located in Pole Creek.

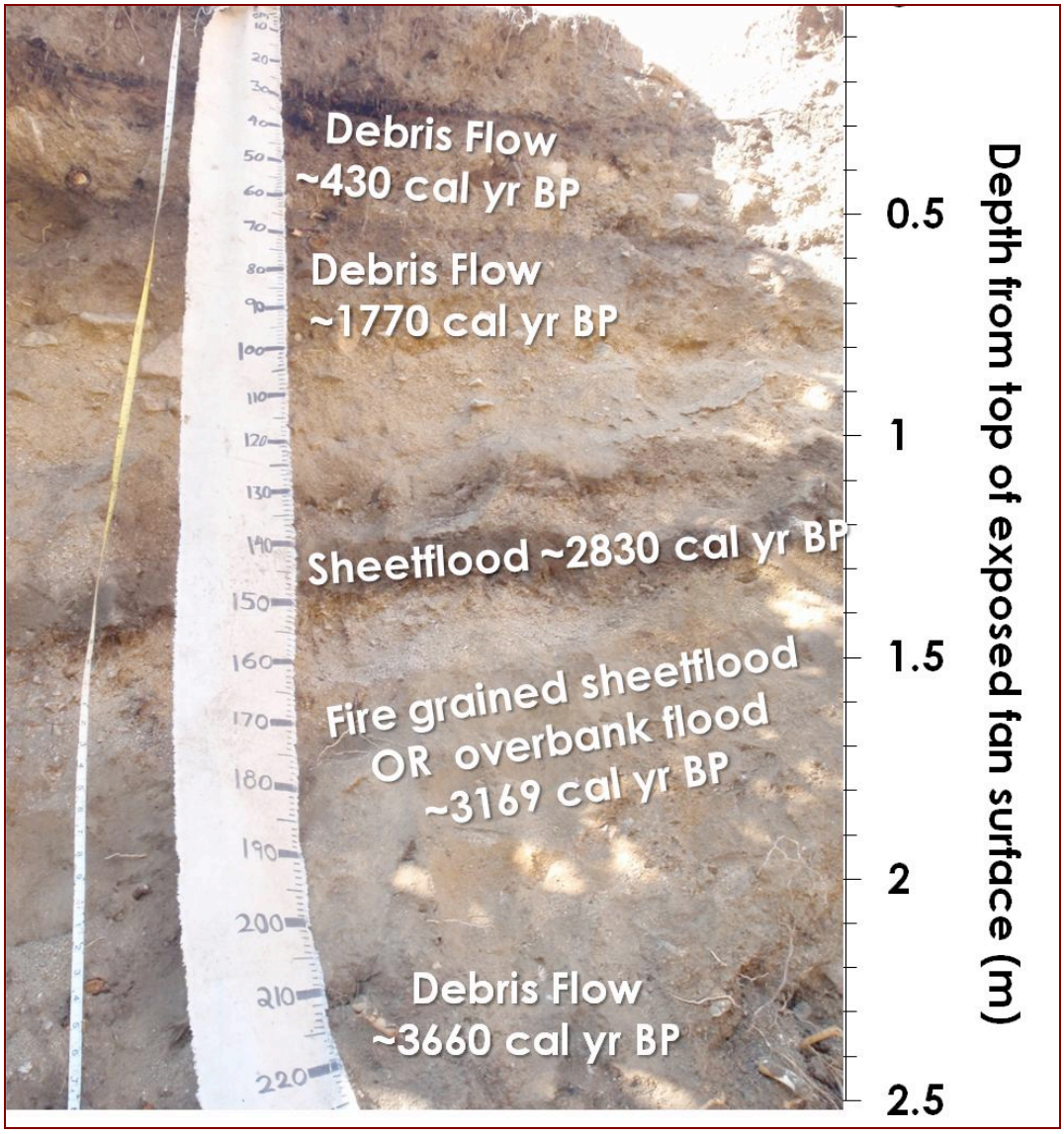

Figure A-9: Stratigraphic profile in Bernard Creek. Fire-related deposits are not labeled.

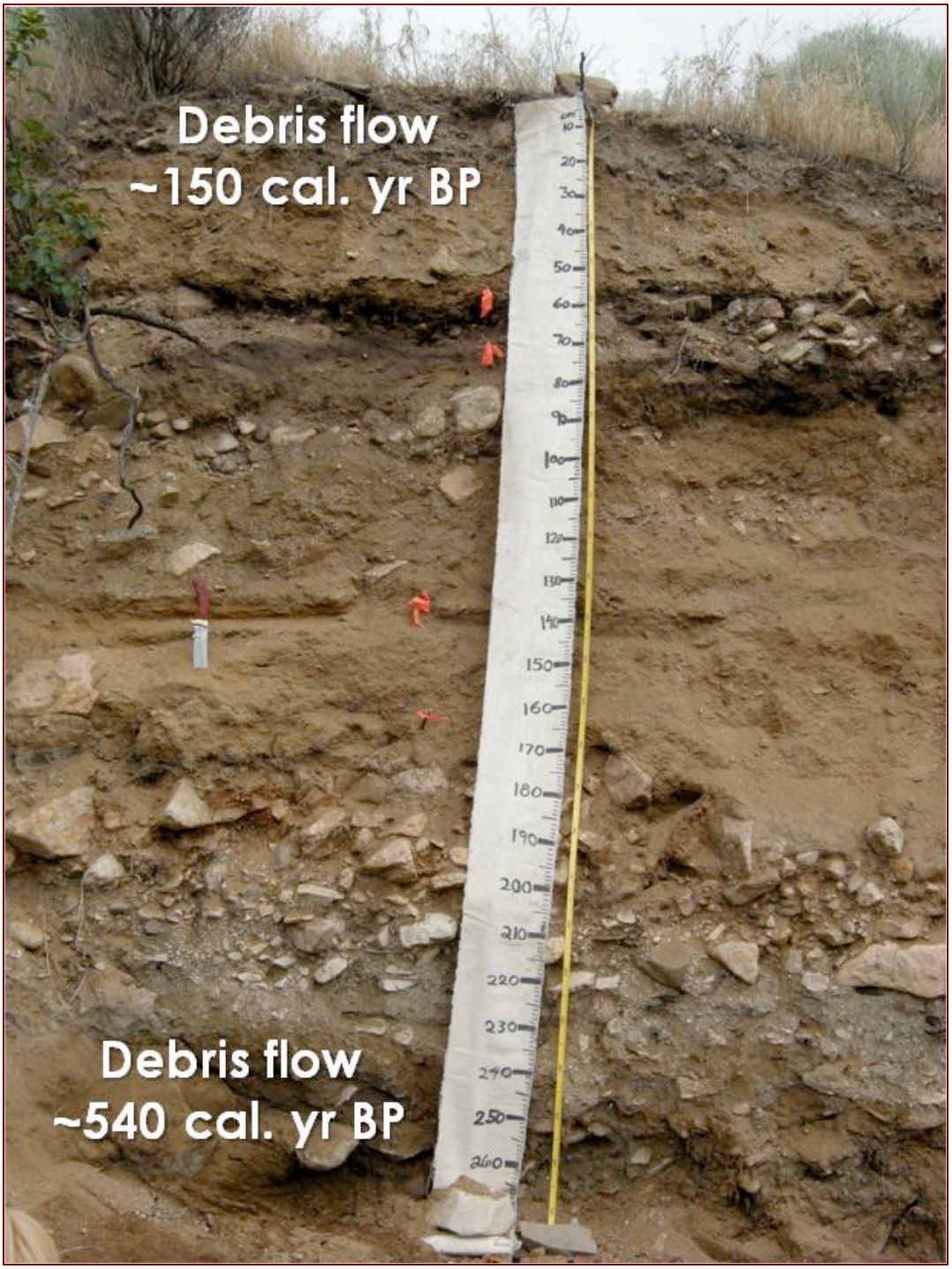

Figure A-10: Stratigraphic profile located at the mouth of Bernard Creek.

Table A-4: Stratigraphic descriptions for ten alluvial fans in the MFSR.

SITE ID	Depth	Depositional Process	% < 2mm	Texture	Sorting	Char. Abund.	Shape	Median dates (cal. yr BP)
KC-1	0-34	debris flow	70	SL	poor	NA	ang	
KC-1	34-212	debris flow	70	LS	poor	NA	ang	
KC-1	212-216	sheetflood	60	LS	moderate	NA	sub-ang	
KC-1	216-233	hyper-concentrated flow	40	LS	poor	NA	ang	
KC-1	233-270	channel deposit	30	LS	poor	na	sub-ang	
KC-2	0-20	debris flow	60	SL	poor	abund	ang	
KC-2	20-30	burn surface	-	-	-	abund	-	
KC-2-1	**30-45**	**debris flow**	**50**	**SL**	**poor**	**abund**	**ang**	**390**
KC-2-2	45-46	burn surface	-	-	-	abund	-	
KC-2-3	46-58	sheetflood	> 98	L	well	abund	ang	
KC-2-4	**58-60**	**burn surface**	**-**	**-**	**-**	**abund**	**-**	**975**
KC-2-5	**60-86**	**debris flow**	**70**	**SL**	**poor**	**abund**	**ang**	**1,116**
KC-2	86-95	channel deposit	50	SCL	poor	rare	ang	
KC-2-6	**95-135**	**debris flow**	**60**	**SL**	**poor**	**moderate**	**ang**	**2,232**
KC-2	135-160	debris flow	60	SL - L	poor	sparse	ang	
KC-3	0-52	debris flow	60	SL	poor	abund	ang	
KC-3	52-53	burn surface	-	-	-	abund	-	
KC-3	53-59	debris flow	70	SL	poor	sparse	ang	
KC-3	59-60	burn surface	-	-	-	abund	-	
KC-3	60-65	debris flow	60	SL	poor	abund	ang	
KC-3	65-66	burn surface	-	-	-	abund	-	
KC-3	66-75	sheetflood	70	SL	moderate	abund	ang	
KC-3	75-170	channel deposit	50	LS	poor	sparse	ang	
SHS-1	0-15	debris flow (recent levee)	70	SL	poor	abund	ang	
SHS-1-1	15-25	burn surface	-	-	-	abund	-	
SHS-1-2	25-96	debris flow	70	SL	poor	abund	ang	
SHS-1-3	96-103	burn surface	-	-	-	abund	-	
SHS-1	103-125	debris flow	60	SL	poor	sparse	ang	
SHS-1	125-210	debris flow	60	SL	poor	sparse	ang	
SHS-2	0-17	debris flow	70	SL	poor	abund	ang	
SHS-2	17-22	burn surface	-	-	-	abund	-	
SHS-2	22-111	debris flow	60	SL	poor	abund	ang	
SHS-2-2	111-113	sandy thin layer b/w charcoal	50	SL	moderate	abund	sub ang	
SHS-2	113-180	debris flow	60	SL	poor	sparse	ang	
SHS-2	180-210	channel deposit	10	SL	poor	sparse	ang	
SHS-3	0-15	debris flow	80	SL	poor	abund	ang	
SHS-3	15-25	buried burn surface	-	-	-	abund	-	
SHS-3-1	25-109	debris flow	75	SL	poor	abund	ang	
SHS-3-2	109-131	debris flow	85	SL	poor	abund	ang	
SHS-3-3	**131-150**	**debris flow (sandy w/ lg clasts)**	**60**	**LS**	**poor**	**abund**	**ang**	**3,756**
SHS-4	0-315	debris flow			poor	abund	ang	
SHS-4-1	315-320	fine grained charcoal layer	100	SiL	well	abund	sub ang	
SHS-4-2	320-362	debris flow			poor	scarce	ang	
SHS-4-3	362-390	sandy deposit with few large clast	95	SL	moderate	scarce	sun ang	
SHS-4-4	**390-415**	**buried burn surface (lots of roots) inset**	**-**	**-**	**-**	**abund**	**-**	**Post bomb**
SHS-4-5	415-480	possible channel deposit inset		SL	poor	scarce	ang	
SHS-6-1	0-40	burn surface with debris flow on top			poor	abund	ang	
SHS-6	40-57	debris flow			poor	abund	ang	
SHS-6-3	**57-110**	**debris flow**			**poor**	**abund**	**ang**	**642**
SHS-7	0-40	debris flow	70	SL	poor	abund	ang	
SHS-7-1	40-41	burn surface (discontinuous, woody)	-	-	-	abund	-	
SHS-7	41-90	debris flow	60	L-SiL	poor	abund	ang	
SHS-7-2	90-91	burn surface (continuous, wood roots)	-	-	-	abund	-	
SHS-7	91-147	debris flow	50	SL	poor	abund	ang	
SHS-7-3	**147-148**	**burn surface**	**-**	**-**	**-**	**abund**	**-**	**826/778**
SHS-7-4	148-180	debris flow	60	SL	poor		ang	
SHS-8	0-180	debris flow	65	L	poor	sparse	ang	
SHS-8-1	180-210	burn surface	-	-	-	abund	-	
SHS-8-2	**210-270**	**debris flow**	**70**	**SL**	**poor**	**sparse**	**ang**	**5,163**
SHS-8	270-300	colluvium	10	S		rare	ang	
SHS-8-4	300-310	debris flow	55	SL	poor	sparse	ang	
SHS-8-3	310-330	burn surface	-	-	-	abund	-	
SHS-8-5	**330-350**	**burn surface**	**-**	**-**	**poor**	**abund**	**-**	**11,383**
SHS-8-4	350-370	debris flow	55	SL	poor	sparse	ang	
SHS-8	370-430	colluvium	10	S	poor	rare	ang	
GHC-1	0-287	debris flow	90	L	poor	abund	ang	
GHC-1-1	287-290	burn surface	-	-	-	abund	-	
GHC-1-2	290-313	connected to above layer	85	L	-	abund	ang	
GHC-1-2	313-315	hydrodynamic separated charcoal	-	-	well	abund	-	
GHC-1-3	313-318	overbank	100	SiL	well	abund	-	
GHC-1-4	318-345	debris flow	75	L	poor	abund	ang	

GHC-1	345-350	sandy layer on top of charcoal	60	LS	moderate	abund	ang	
GHC-1-5	**350-359**	**burn surface**	**-**	**-**	**-**	**abund**	**-**	**1,534**
GHC-1	359-390	channel deposit/debris flow	50	S	poor	sparse	ang	
GHC-2-1	0-80	debris flow	85	L	poor	abund	ang	
GHC-2	80-82	overbank	50	S	well	scarce	sub ang	
GHC-2	82-84	overbank	95	S	well	scarce	sub ang	
GHC-2-2	84-157	debris flow	60	SL	poor	abund	ang	
GHC-2-3	**157-161**	**hydro-dynamically separated**	**-**	**-**	**well**	**abund**	**-**	**1,350**
GHC-2-4	161-163	overbank	100	SiL	well	abund	sub ang	
GHC-2-5	**163-165**	**burn surface**	**-**	**-**	**-**	**abund**	**-**	**1,368/1,409**
GHC-2	165-167	debris flow	40	SL	poor	scarce	ang	
GHC-2-6	167-170	burn surface	-	-	-	abund	-	
GHC-2	170-190	debris flow	60	L	poor	scarce	ang	
LC-1	0-200	debris flow	85	L	poor	abund	ang	
LC-1-1	200-205	burn surface (roots needles)	-	-	-	abund	-	
LC-1-2	205-225	over bank(clustered char)	75	L	well	abund	ang	
LC-1-3	**225-226**	**hydro char – thin, twigs**	95+	**C**	**well**	**abund**	**-**	**450**
LC-1	226-236	over bank	95+	S	well	abund	round	
LC-1	236-240	sheetflood	55	C	well	abund	ang	
LC-1-4	240-268	sheetflood	95+	SiL	well	abund	round	
LC-1-5	**268-277**	**burn surface partially burned**	**60**	**SL**	**-**	**abund**	**round**	**1,828/1,906**
LC-1-6	**277-300**	**debris flow**	**50**	**S**	**poor**	**abund**	**ang**	**2,769/3,781**
LC-1	300-320	hyper-concentrated flow- sandy	40	S	poor	scarce	ang	
LC-1-7	**320-326**	**burn surface**	**-**	**CL**	**-**	**abund**	**-**	**7,212/7,256**
LC-1	326-335	soil development (buried)	85	CL	moderate	scarce	round	
LC-1-8	**335-340**	**burn surface (old/decomposing)**	**-**	**CL**	**-**	**abund**	**-**	**6,587/6,072**
LC-1	340-348	fluvial or soil development	70	CL	moderate	Scarce	sub ang	
LC-1-9	348-355	hard and fine grained	70	CL	Well	abund	sub ang	
LC-1-10	**355-367**	**over bank or ash (roots, orange)**	**95 +**	**SiL**	**Well**	**None**	**sub ang**	**8,154**
LC-1	367-373	fake char -bonding with layer above	-	-	Well	none	-	
LC-1-11	**373-420**	**debris flow red clasts**	**60**	**S**	**Poor**	**scarce**	**ang**	**8,942/9,792**
LC-1-12	420-425	sheetflood (sandy fine grained	90	C	Moderate	scarce	round	
LC-1-13	**425-530**	**debris flow (very sandy) (inset)**	**50**	**SL**	**poor**	**scarce**	**ang**	**Post bomb**
LC-2	0-27	debris flow	60	SL	poor	abund	ang	
LC-2	27-30	buried burn surface	-	-	-	abund	-	
LC-2	30-34	Overbank	98	L	well	scarce	sub ang	
LC-2	34-60	debris flow	65	SL	poor	scarce	ang	
LC-2	60-62		75	L		scarce		
LC-2	62-118	debris flow	65	L	poor	abund	ang	
LC-2-1	118-121	sheet flood/overbank	90	SiL	moderate	abund	sub ang	
LC-2-2	121-155	sheetflood	80	LS	moderate	scarce	sun ang	
LC-2	155-200	channel deposit	50	LS	poor	abund	ang	
LC-2-3	200-210	debris flow/burn surface	90	CL	poor	abund	ang	
LC-2-4	210-350	channel deposit	60	SL	poor	abund	ang	
LC-2-5	**350-470**	**debris flow**	**65**	**LS**	**poor**	abund	**ang**	**442**
OC-3	0-140	debris flow	50	SL	poor	scarce	ang	
OC-3-1	140-180	debris flow	70	L	poor	abund	ang	
OC-3-2	180-235	debris flow	60	LS	poor	abund	ang	
OC-3-3	**235-255**	**buried soil**	**60**	**CL**	**-**	**abund**	**-**	**856**
OC-3-4	255-310	(potentially same soil as above)	65	CL	-	abund	-	
OC-3-5	310-415	debris flow	80	LS	poor	abund	ang	
OC-3-6	**415-495**	**buried burned surface**	**60**	**CL**	**-**	**abund**	**-**	**777**
OC-4	0-14	debris flow	70	SL	poor	abund	ang	
OC-4-1	14-15	burn surface	-	-	-	abund	-	
OC-4	15-25	debris flow	65	L	poor	abund	ang	
OC-4-2	**25-26**	**burn surface**	**-**	**-**	**-**	**abund**	**-**	**107**
OC-4-3	26-39	debris flow	60	L	poor	abund	ang	
OC-4-4	39-40	burn surface	-	-	-	abund	-	
OC-4-5	40-150	debris flow	50/65	SiL/SiCl	poor	abund	ang	
OC-4-6	**150-151**	**overbank**			**well**	**abund**	**ang**	**1,122**
OC-4	151-200	sheetflood	85/30	S/S	moderate	abund	ang	
OC-4-7	**200-201**	**debris flow**	**65**	**L**	**poor**	**abund**	**ang**	**5,412**
HR-1-1	0-65	debris flow	80	S	poor	scarce	ang	
HR-1-2	65-69	sheetflood	75	LS	fair	scarce	ang	
HR-1-3	69-82	sheetflood	65	LS	poor	scarce	ang	
HR-1-4	82-85	sheetflood	70	LS	fair	abund	ang	
HR-1-5	85-86	sheetflood	80	LS	well	scarce	ang	
HR-1	86-111	soil	75/85	SL/SL	poor	scarce	ang	
HR-1-6	**111-147**	**debris flow**	**60**	**CL**	**poor**	**scarce**	**ang**	**8,499**
HR-3-1	0-19	debris flow	75	LS	poor	abund	ang	
HR-3-2	19-36	ash/overbank	>98	Si	well	scarse	small	
HR-3	36-69	sheetflood	60	S	moderate	scarce	ang	
HR-3	69-159	sheetflood	45/60	S	moderate	scarce	ang	
HR-3	159-214	colluvium/soil	65	LS	poorly	scarce	ang	
SC-1	0-119	debris flow	80	S	poor	scarce	mixed	
SC-1-1	119-312	sheetflood (7+ couplets)	85/95	S/SiL	well	scarce	mixed	
SC-1-2	**312-316**	**burn surface**	**-**	**-**	**-**	**abund**	**-**	**5,823**
SC1-3	316-385	debris flow (hard matrix)	65	SL	poor	scarce	ang	
SC-1	385-405	sheetflood	70	S	well	abund	ang	
SC-1-4	**405-406**	**burn surface**	**-**	**-**	**-**	**abund**	**-**	**6,432**
SC-1	406-424	sheetflood	70	S	well	abund	ang	

SC-1	424-509	debris flow	70	L	poor	scarce	ang	
SC-2	0-41	debris flow	75	LS	poor	scarce	ang	
SC-2	41-46	overbank/ash	95	Si	well	scarce	fine	
SC-2	46-51	burn surface	85	SL	poor	scarce	ang	
SC-2	51-66	debris flow			poor	scarce	ang	
SC-2	66-87	?	70	S	poor	scarce	ang	
SC-2-1	87-151	debris flow			poor	abund	ang	
JC-1-1	0-145	debris flow	65	SL	poor	scarce	ang	
JC-1	145-195	sheetflood (>3 couplets)	55/70	SL/S	well	scarce	ang	
JC-1-2	**195-373**	**debris flow (caco3 stage ii)**	**60**	**L**	**poor**	**scarce**	**sub ang**	**13,581**
RC-3-1	0-18	debris flow	70	SL	poor	sparse	ang	
RC-3-2	**18-19**	**burn surface**	**-**	**-**	**organic**	**sparse**	**-**	**289**
RC-3	19-62	channel (imbricated, hard)	75	S	med.	none	mix	
RC-3-3	**62-67**	**sheetflood**	**85**	**L**	**well**	**sparse**	**ang**	**2,067**
RC-3-4	67-71	sheetflood	50	S	well	abund	ang	
RC-3-5	71-75	sheetflood	90	SL	well	abund	ang	
RC-3-6	75-84	sheetflood	40	S	well	abund	ang	
RC-3-7	84-89	sheetflood	95 +	L	well	abund	ang	
RC-3-8	**89-171**	**debris flow**	**60**	**SL**	**poor**	**sparse**	**ang**	**2,867**
RC-3	171-211	debris flow (caco3)	80	LS	poor	none	ang	
RC-3-9	211-236	sheetflood (coarse caco3 present	65	LS	med.	sparse	ang	
RC-3-10	**236-241**	**Sheetflood (fine grained)**	**75**	**SL**	**med.**	**abund**	**ang**	**5,733**
RC-3-11	241-249	sheetflood coarse grained sand lenses	80	S	well	abund	ang	
RC-3-12	249-256	sheetflood fine grained	80	LS	med.	sparse	ang	
RC-3-13	256-262	sheetflood coarse	75	LS	well	abund	ang	
RC-3	262-267	sheetflood fine grained	85	L	med.	scarce	ang	
RC-3-14	267-283	sheetflood coarse grained	60	LS	well	abund	ang	
RC-3-15	283-291	sheetflood fine grained	95 +	SiL	well	abund	ang	
RC-3-16	291-302	sheetflood coarse	80	LS	well	scarce	ang	
RC-3	302-309	sheetflood fine grained	90	LS	well	scarce	ang	
RC-3-17	309-324	sheetflood coarse	70	S	med.	scarce	ang	
RC-3-18	**324-326**	**sheetflood fine grained**	**80**	**SL**	**well**	**scarce**	**ang**	**6,366**
RC-3	**326-332**	**sheetflood coarse**	**70**	**S**	**well**	**none**	**ang**	**6,480**
RC-5	0-25	debris flow	75	SL	poor	abund	ang	
RC-5	25-26	burn surface (organic material)	-	-	-	abund	-	
RC-5	26-53	channel	70	S	Poor	scarce	mix	
RC-5	53-64	sheetflood (fine/coarse/fine)	90/70	L/S	med.	scarce	ang	
RC-5-1	64-136	debris flow	65	SL	Poor	scarce	ang	
RC-5-2	136-171	debris flow - buried soil caco3	70	SL	Poor	scarce	ang	
RC-5	171-175	sheetflood	60	S	Well	abund	ang	
RC-5-3	175-184	sheetflood (potential soil)	90	SL	Well	abund	ang	
RC-5	184-190	sheetflood	75	S	med.	scarce	ang	
RC-5	190-210	sheetflood (potential soil)	70	SL	Poor	abund	ang	
RC-5	210-238	debris flow or hyper-concentrated flow			Poor	scarce	ang	
RC-5-4	238-255	sheetflood	80	S	Well	abund	ang	
RC06	0-27	channel (hyper-concentrated flow)	70	S-LS	imbrication	scarce	mixed	
RC06	27-40	soil	75	SL	moderate	scarce	ang	
RC06	40-93	debris flow	60	SL	Poor	scarce	ang	
RC06	93-103	sheetflood (2-couplets)	80/55	SL/LS	Well	scarce	ang	
RC06	103-154	sheetflood	85	LS	Well	scarce	ang	
RC06	154-157	sheetflood	65	L	Well	abund	ang	
RC06	157-172	sheetflood	50	LS	Well	scarce	sub ang	
RC06	172-178	sheetflood	50	S	Well	scarce	sub ang	
RC06	178-184	sheetflood fine grained	85	SL	Well	abund	sub ang	
RC06	184-189	sheetflood -coarse	60	S	Well	scarce	sub ang	
RC06	189-195	sheetflood fine grained	85	S	Well	abund	sub ang	
RC06	195-198	sheetflood fine/coarse	50	SL	Well	scarce	sub ang	
RC06	198-211	sheetflood coarse	75	S	Well	abund	sub ang	
RC06	211-218	sheetflood fine (soil)	90	SL	moderate	abund	sub ang	
RC06	218-228	sheetflood coarse	85	S-LS	Well	scarce	sub ang	
RC06	228-233	buried soil	70	LS	moderate	abund	sub ang	
RC06	233-261	sheetflood / channel	60	S	moderate	scarce	sub ang	
RC06-01	261-308	debris flow	70	S	Poor	scarce	ang	
BC-1	0-21	debris flow	60		poor		ang	
BC-1	**21-22**	**burn surface**	**-**	**-**	**-**	**abund**	**-**	**150**
BC-1	22-49	sheetflood	60	LS	moderate	abund	ang	
BC-1-1	49-53	burn surface	-	-	-	abund	-	
BC-1	53-63	channel	60	SL	poor	abund	ang	
BC-1-2	63-65	burn surface	-	-	-	abund	-	
BC-1	65-71	soil development	90	SL	moderate	scarce	ang	
BC-1-3	71-76	burn surface	-	-	-	abund	-	
BC-1-4	76-162	debris flow	85	S	poor	scarse	ang	
BC-1-5	162-166	overbank	75	SL	well	abund	sub ang	
BC-1	166-216	channel	60	SL	poor	scarce	ang	
BC-1-6	**216-251**	debris flow	**40**	**SL**	**poor**	**scarce**	ang	**536/848**
BC-2	0-31	debris flow	60	SL	poor	abund	ang	
BC-2-1	31-34	burn surface	-	-	-	abund	-	
BC-2	34-39	sandy layer (sheetflood)	70	LS	moderate	abund	ang	
BC-2-2	39-41	burn surface	-	-	-	abund	-	
BC-2-3	41-58	debris flow	60	L	poor	abund	ang	
BC-2	58-93	channel deposit or debris flow	60	SL	Poor		ang	

BC-2	93-130	channel deposit	30	SL	poor	scarce	ang	
BC-2-4	**130-132**	**burn surface**	**-**	**-**	**-**	**abund**	**-**	**928**
BC-4	0-50	colluviums / debris flow					ang	
BC-4	50-74	overbank / soil	75	LS	well	scarse	sub-ang	
BC-4	74-78	solidified deposit						
BC-4	78-120	debris flow	65	SL	poor	scarse	mixed	
BC-4	120-130	sheetflood	30/80	LS/SL	well	scarse	sub-ang	
BC-4	130-153	debris flow	60	SL	poor	scarse	ang	
BC-4	153-160	overbank	85	LS	well	scarse	ang	
BC-4	160-162	ash or overbank	>98	Si	well	scarse		
BC-4-1	162-177	sheetflood	70/98	LS/SL	well	scarse	ang	
BC-4	177-237	channel			poor	scarse	round	
BC-5	0-26	debris flow	60	SL	poor	scarse	ang	
BC-5-1	26-26.5	burn surface	-	-	-	abund	-	
BC-5	26.5-27.5	overbank	90	SL	well	scarse	sub-ang	
BC-5-2	27.5-28	burn surface	-	-	-	abund	-	
BC-5-3	**28-50**	**debris flow**	**70**	**SL**	**poor**	**scarse**	**ang**	**429**
BC-5-4	**50-73**	**debris flow**	**75**	**LS**	**poor**	**abund**	**ang**	**1,769**
BC-5	73-99	channel	70	S	moderate	scarse	sub-ang	
BC-5-5	99-104	sheetflood	80	S	well	scarse	sub-ang	
BC-5-6	104-115	sheetflood (fine)	85	L	well	abund	sub-ang	
BC-5-7	115-121	sheetflood (coarse)	50	LS	well	abund	sub-ang	
BC-5-8	**121-133**	**sheetflood (fine)**	**95**	**L**	**well**	**abund**	**sub-ang**	**2,830**
BC-5	133-154	sheetflood	70	S	well	scarse	sub-ang	
BC-5-9	**154-196**	**overbank**	**>98**	**SiL**	**well**	**abund**	**small**	**3,158**
BC-5-10	**196-219**	**channel/ debris flow**			**poor**	**abund**	**ang**	**3,656**
BC-6	0-5	burn surface	-	-	-	abund	-	
BC-6	05_17	debris flow	80	LS	poor	scarse	ang	
BC-6-1	17-23	sheetflood (fine)	85	L	poor	abund	ang	
BC-6	23-26	sheetflood	60	LS	well	scarse	ang	
BC-6	26-30	sheetflood	75	SL	well	scarse	sub-ang	
BC-6	30-36	sheetflood	75	LS	poor	scarse	ang	
BC-6-2	36-38	sheetflood (fine)	80	LS	well	scarse	sub-ang	
BC-6	38-70	sheetflood	65	LS	moderate	scarse	ang	
BC-6-3	70-74	sheetflood (fine)	85	LS	well	abund	ang	
BC-6	74-77	sheetflood	60	S	well	abund	ang	
BC-6	77-84	sheetflood (fine)	85	S	well	scarse	ang	
BC-6-4	84-92	sheetflood	40	S	well	abund	ang	
BC-6	92-100	sheetflood	85	LS	well	scarse	ang	
BC-6-5	100-105	sheetflood (fine)	70	L	well	abund	ang	
BC-6-6	105-108	sheetflood (coarse)	60	S	well	abund	sub-ang	
BC-6-7	108-112	sheetflood (fine)	80	SL	well	abund	small	
BC-6	112-116	sheetflood (coarse)	50	S	well	abund	ang	
BC-6-8	116-129	sheetflood (fine)	85	SL	well	abund	ang	
BC-6-9	129-138	sheetflood (coarse)	50	S	well	abund	ang	
BC-6-10	138-159	sheetflood couplets	50/70	S/SL	well	abund	ang	
BC-6-11	159-181	burn surface	85	L	well	scarse	sub-ang	
BC-6-12	181-194	sheetflood (coarse)	50	S	well	abund	ang	
BC-6-13	194-260	?	70	LS	moderate	abund	ang	
BC-6	260-270	sheetflood	70	S	moderate	scarse	mixed	
BC-6-14	270-287	?	75	SL	poor	abund	ang	
BC-6	287-296	?	70	S	poor	abund	ang	
BC-6-15	296-320	sheetflood	70	S	well	abund	ang	
PC-1	0-66	debris flow	70	SL	poor	abund	ang	
PC-1-1	**66-67**	**burn surface**	**-**	**-**	**-**	**abund**	**-**	**449**
PC-1	67-98	debris flow	60	LS	poor	scarce	ang	
PC-1	98-138	sheetfloods	80	S	moderate	scarce	ang	
PC-1	138-158	sheetfloods	90	SL	moderate	scarce	ang	
PC-1	158-270	debris flow	85	SL	poor	scarce	ang	
PC-1-2	**270-296**	**sheetflooding**	**95**	**SL**	**moderate**	**abund**	**Sub ang**	**137**
PC-1	296-360	channel deposit or debris flow			poor	scarce	ang	
PC-5	0-35	debris flow			poor	abund	ang	
PC-5-1	35-38	burn surface	-	-	-	abund	-	
PC-5	38-72	debris flow			poor	scarce	ang	
PC-7	0-45	debris flow	75	SL	poor	abund	ang	
PC-7-1	45-47	burn surface	-	-	-	abund	-	
PC-7	47-150	fine grained over bank/potential soil	95	SiL	med/well	scarce	Sub ang	
PC-8	45-56	debris flow	75	SL	poor	abund	ang	
PC-8	56-64	burn surface	-	-	-	abund	-	
PC-8	64-162	debris flow		L	poor	scarce	ang	
PC-8-1	**162-164**	**sheetflood**	**90**	**L**	**well**	**scarce**	**ang**	**1,505/1,616**
PC-8	164-233	debris flow			poor	scarce	ang	
PC-8-2	233-239	sheetflood	90	SL	well	scarce	ang	
PC-8	239-269	debris flow			poor	scarce	ang	
PC-8-3	**269-270**	**burn surface (caco3 present)**	**95**	**L**	**well**	**abund**	**ang**	**2,072/2,232**
PC-8-4	270-273	overbank	95+	SiL	well	abund	sub ang	
PC-8	273-330	debris flow	90	LS	poor	scarce	ang	

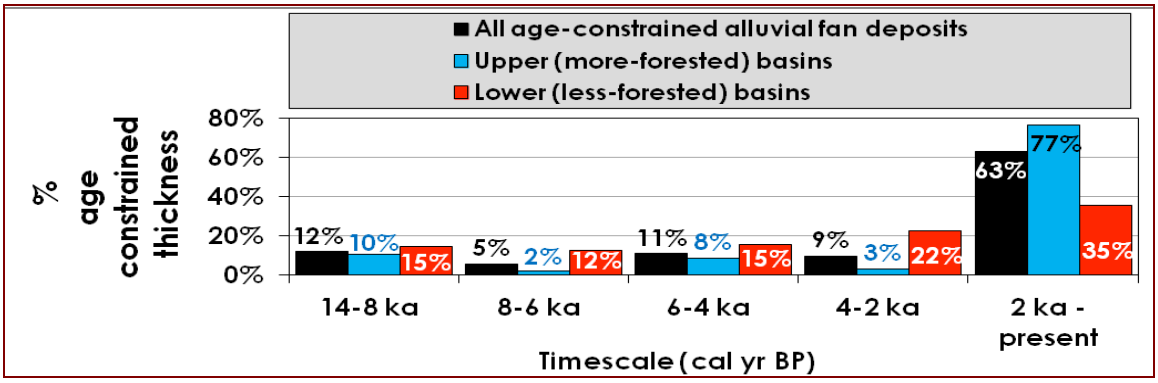

Figure A-11: Data represents deposit thickness trends over 2000 yr increments over the last 14 ka. Data includes all age constrained deposit thicknesses composing alluvial fans. Black bars represent all ten alluvial fans, blue represent five upper basin fans, and red bars represent five lower basin fans. Note the difference in time interval following 8 ka.

APPENDIX B

Fire record correlations not discussed in text

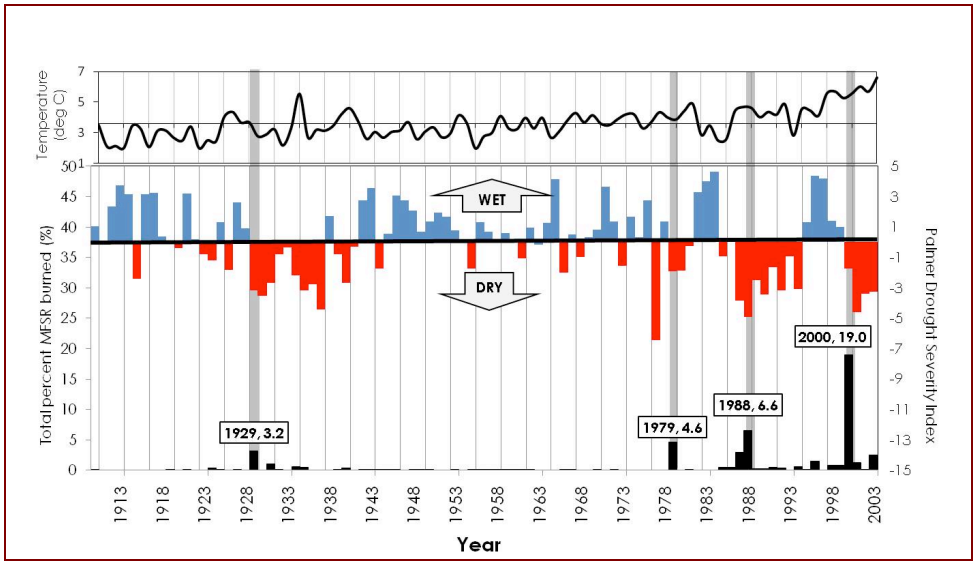

Figure B-1: MFSR 20th century fire record (bottom) compared to the Palmer Drought Severity Index Grid point 69 (Cook, 2004) (middle) and an annual temperature reconstruction by the PRISM climate group, Oregon State University, http://prism.oregonstate.edu, created 1 Dec 2011 for grid point n 44' 73 and w 114' 99. Total percent area burned in the Middle Fork Salmon River was calculated using mapped fire perimeters from the Atlas of Digital Polygon Fire Extents for Idaho and Western Montana (1889-2003), compiled by Gibson and Morgan, 2009

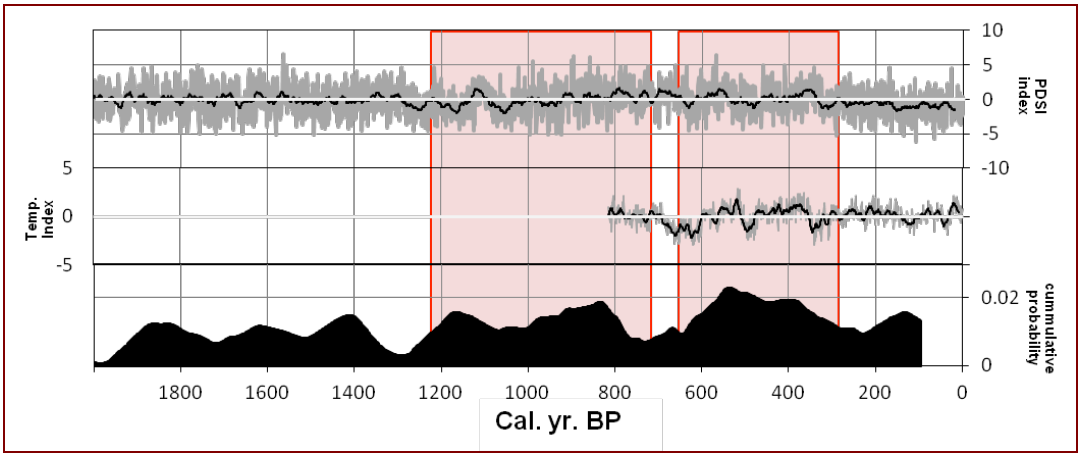

Figure B-2: MFSR fire record for the last 2 ka (bottom) compared to a temperature record reconstructed from dendrochronolgy records in the Salmon-Bitterroot watershed (Biondi et al., 1999) (middle) and the reconstructed Palmer Drought Severity Index Grid point 69 (Cook, 2004) (top).

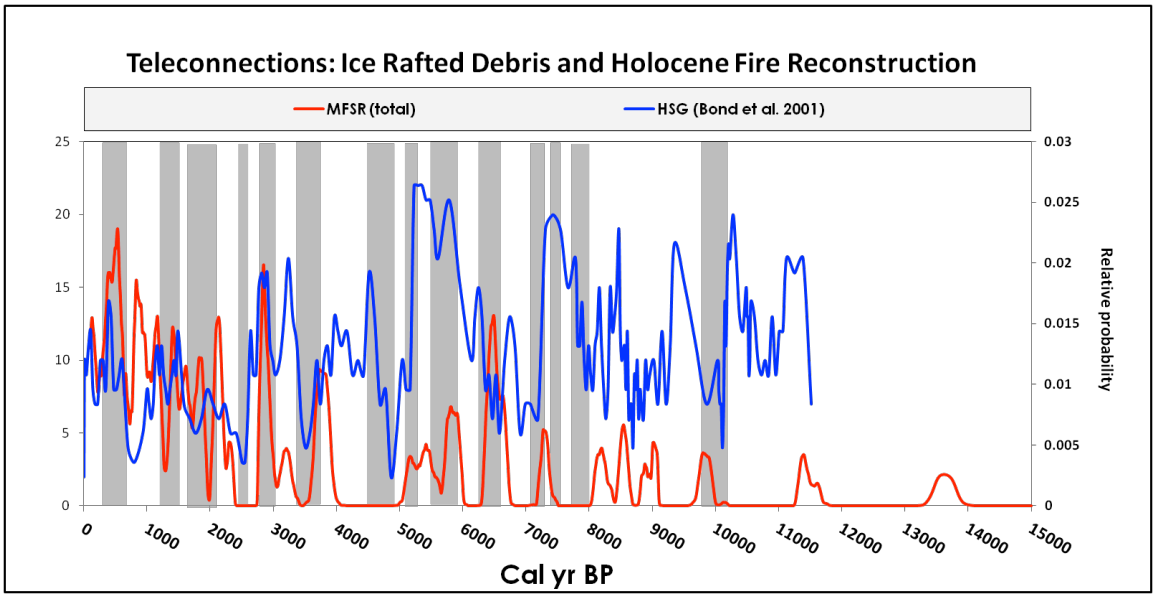

Figure B-3: MFSR fire record compared to ice rafted debris events in the Atlantic recorded by hematite stained grains (Bond et al., 2001).

APPENDIX C

Classified burn severity data

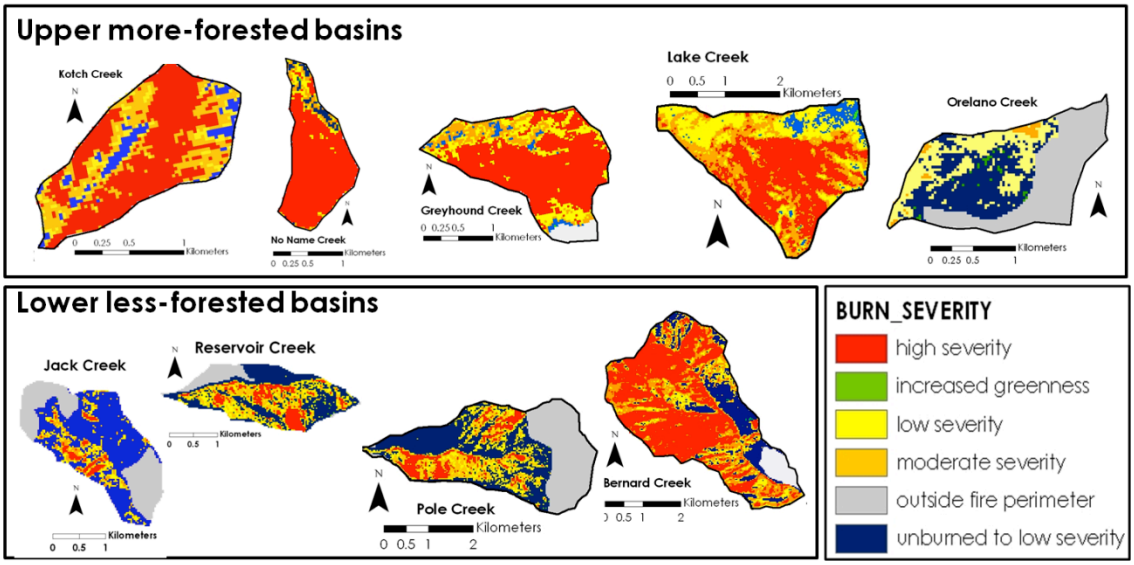

Figure C-1: Classified burn severity data for five upper more forested basins and four lower less-forested basins. Classified burn severity data was obtained from the Monitoring Trends in Burn Severity Project (MTBS, 2010).

APPENDIX D

Power Spectral Analysis

A simple power spectral analysis was done to assess periodicity within the MFSR fire record. A fast Fourier transform was applied to the fire probabilities associated with the final data set. The analysis was done on both normalized data and not normalized smoothed data (100 yr running average). There were no visible differences in the analysis and therefore only the non-normalized smoothed data are presented. Spectral analysis was applied to cumulative probability distributions from upper basins, lower basin, and to all fire probabilities combined. Subsets were analyzed to look for differences in periodicity associated with different ecosystem types.

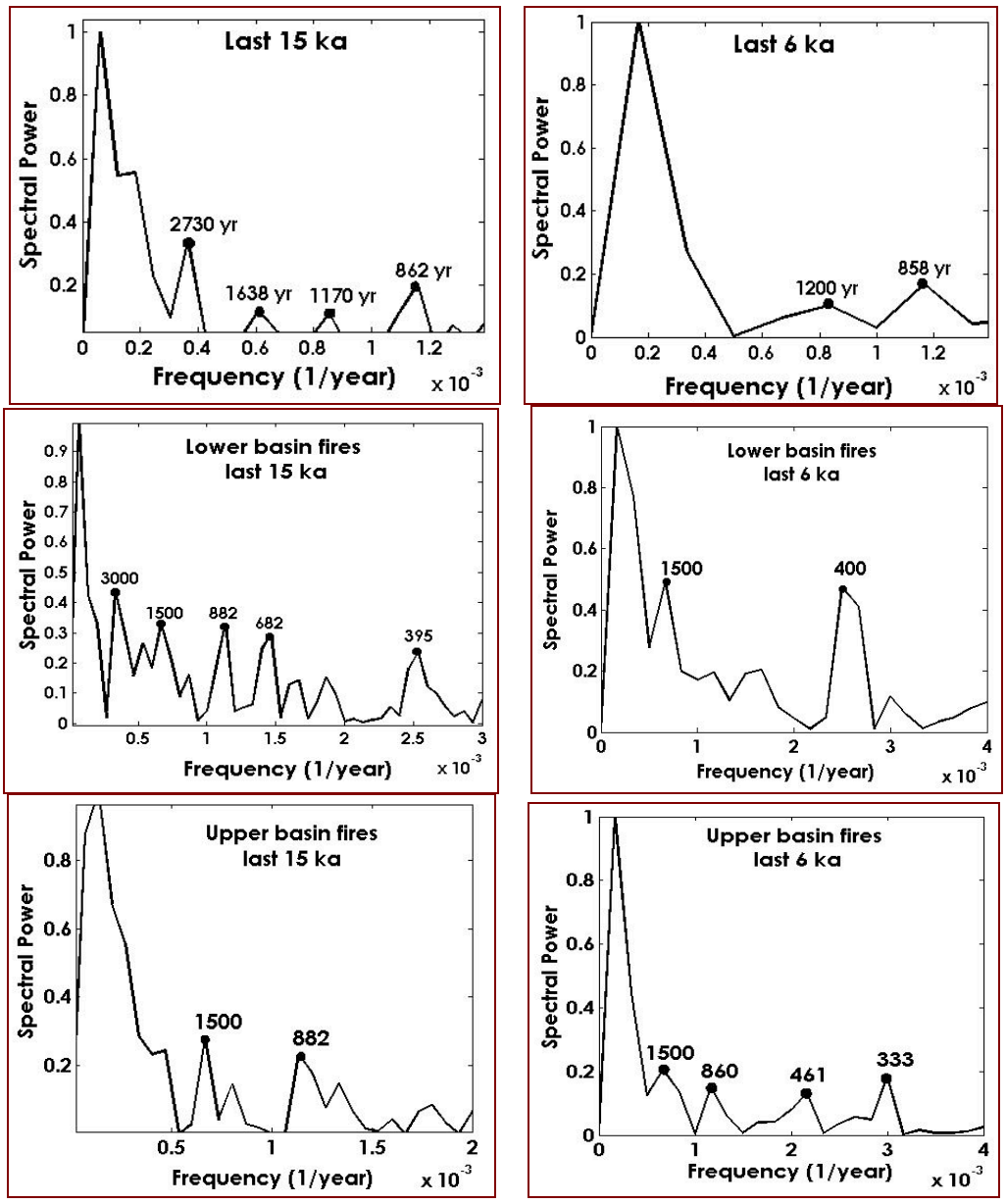

Figure D-1: Spectral analysis of the cumulative fire probability curve from radiocarbon age distributions. The highest amplitude peak in each plot is discarded in the analysis because it approaches the nyquest frequency. The nyquest frequency is half of the number of samples per unit time.

APPENDIX E

Modern (1997-2008) debris flow volume and sediment yield data

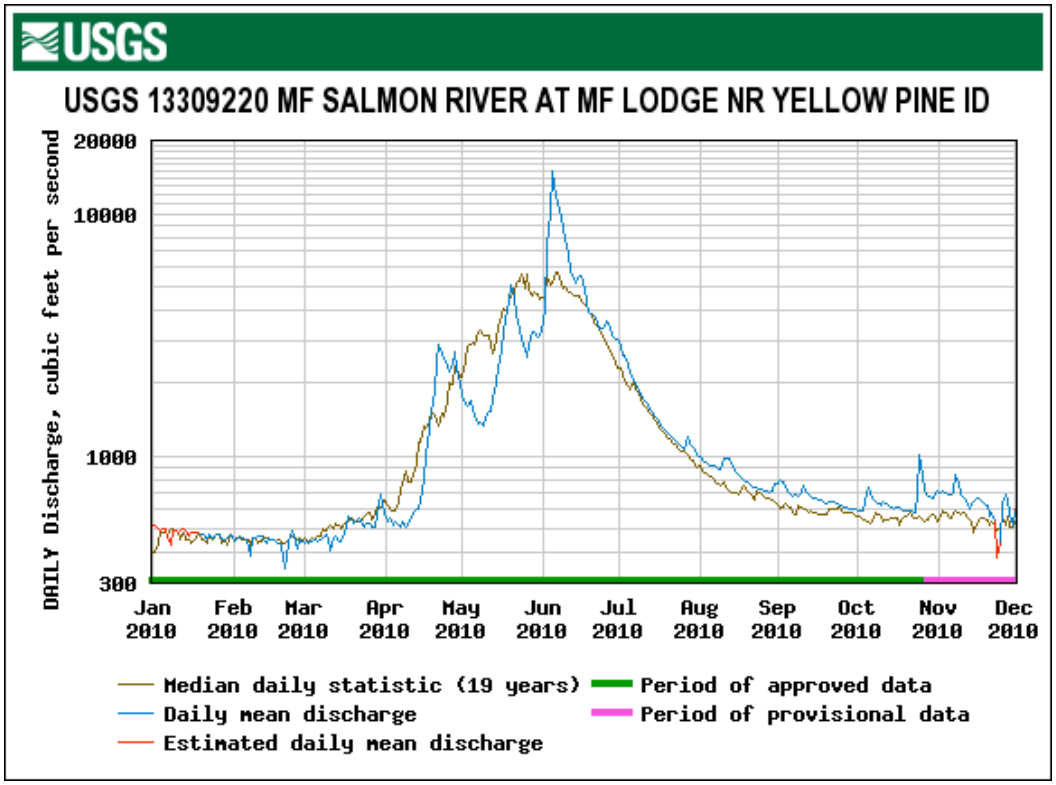

Figure E-1: Hydrograph from Middle Fork Salmon River Lodge recorded in 2010 by the USGS gauging station #13309220. This peak flow caused truncation of 2008 debris flow fans and moved significant amounts of sediment downstream.

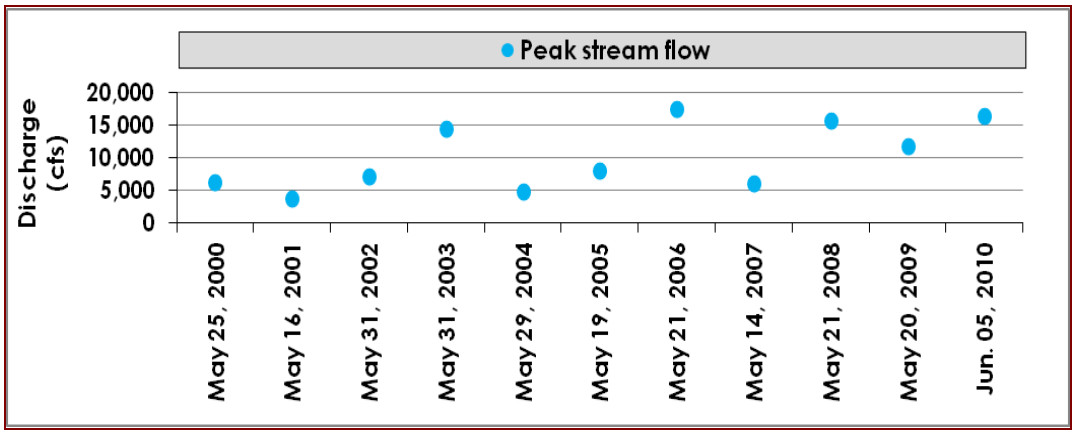

Figure E-2: Peak stream flow data from 2000-2010 recorded at Middle Fork Lodge (USGS gauging station #13309220).

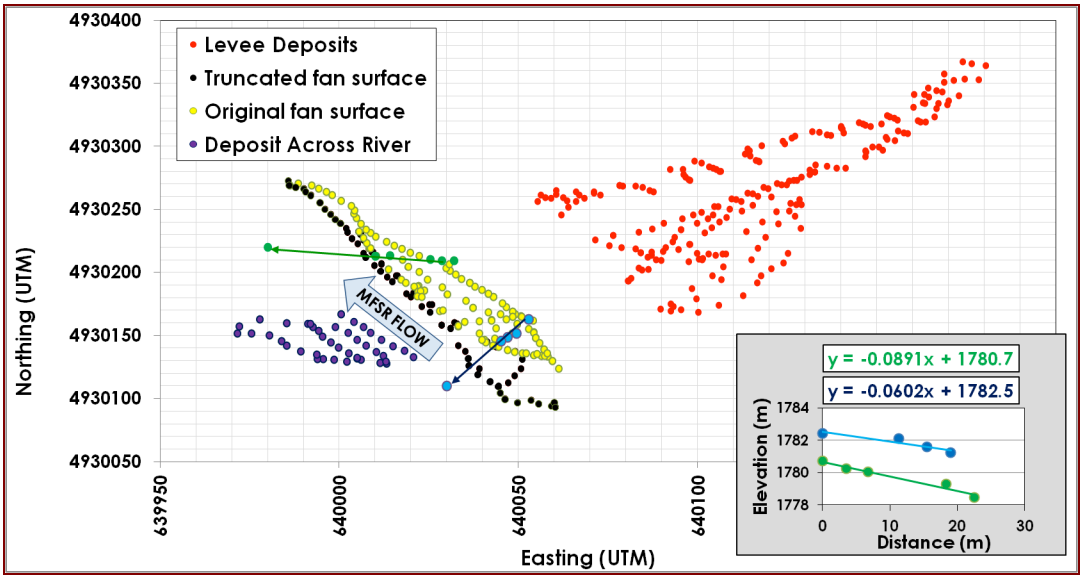

Figure E-3: Colored circles represent the surveyed data points for the 2007 Kotch Creek debris flow deposit. Red circles represent the levee deposits on top of the perched alluvial fan. The yellow circles represent original fan deposit, not yet affected by peak main-stem Middle Fork Salmon flows. The black circles represent the truncated surface, where sediment had been removed by high main-stem flows. The green circles represent debris flow deposit that crossed the main-stem river and deposited sediment on top of the opposite bank. Two fan radial slopes were created and the linear equations used to project fan surface into modern channel. Two extrapolated data points were produced to reconstruct the volume of the original fan surface.

Figure E-4: (left) Ariel photograph from the National Agriculture Imagery Program (NAIP) taken in 2009 of the Kotch Creek debris flow deposit. (right) Profile view of the Kotch Creek debris flow fan taken by Matt Leidecker soon after deposition. Levees are not shown in the right figure because they are on top of the perched fan.

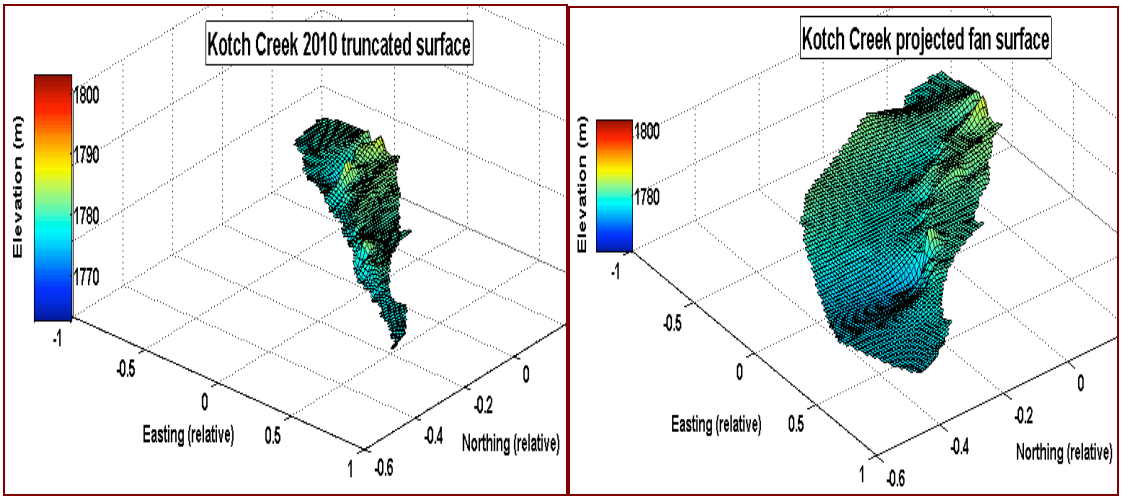

Figure E-5: The above to images are extrapolated survey data points representing the topography of the debris flow deposit fan surface. The surface topography is integrated to a constant base elevation equal to the minimum fan elevation. The Matlab code, to calculate debris flow deposit volume, was written by Grady Wright and Austin Hopkins. The images do not include marginal levees on top of the perched fan and the images do not include deposits across the main stem on top of the terrace. The top figure represents the 2010 surveyed fan deposit that was truncated by high peak flows prior to the survey. The bottom figure is the reconstructed fan surface.

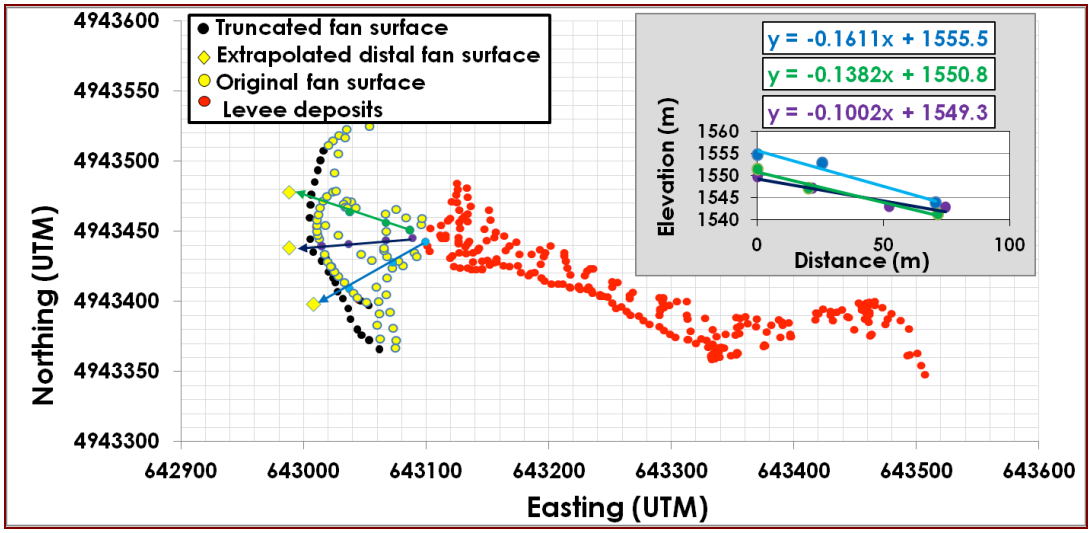

Figure E-6: Colored circles represent the surveyed data points for the 2008 Sheepeater debris flow deposit. Red circles represent the levee deposits on top of the perched alluvial fan. The yellow circles represent original fan deposit not yet affected by peak main-stem Middle Fork Salmon flows. The black circles represent the truncated surface, where sediment had been removed by high main-stem flows. Three fan radial slopes were created and the linear equations used to project fan surface into modern channel. Three extrapolated data points (yellow diamonds) were produced to reconstruct the volume of the original fan surface.

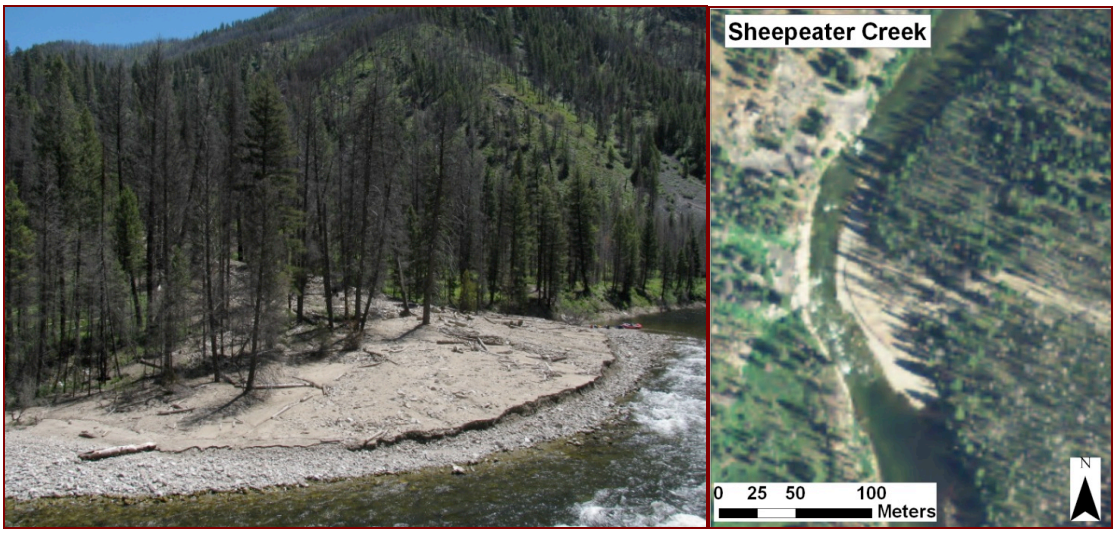

Figure E-7: (left) Photograph taken by Nick Sutfin of Sheepeater fan. (right) NAIP 2009 Ariel photograph of Sheepeater Fan.

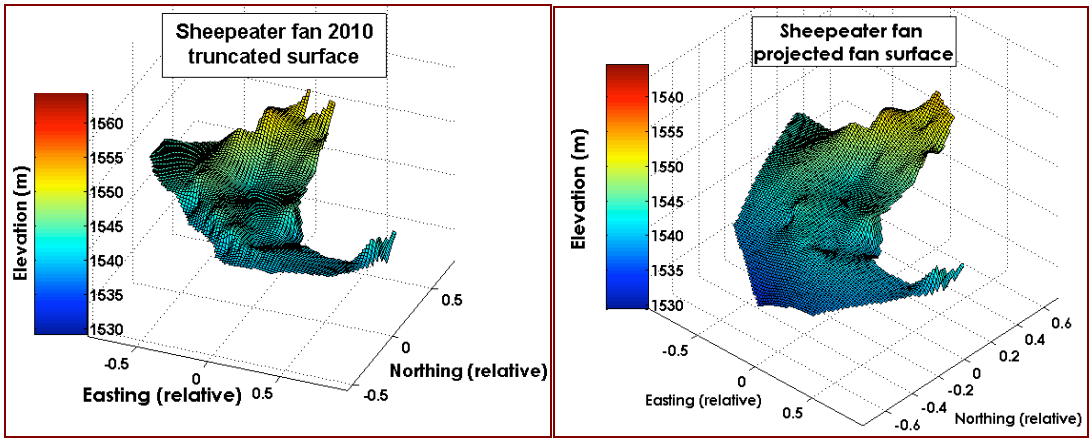

Figure E-8: The above two images are extrapolated survey data points representing the topography of the Sheepeater debris flow deposit fan surface. The images do not include marginal levees on top of the perched fan. The top figure represents the 2010 surveyed fan deposit that was truncated by high peak flows prior to the survey. The bottom figure is the reconstructed fan surface.

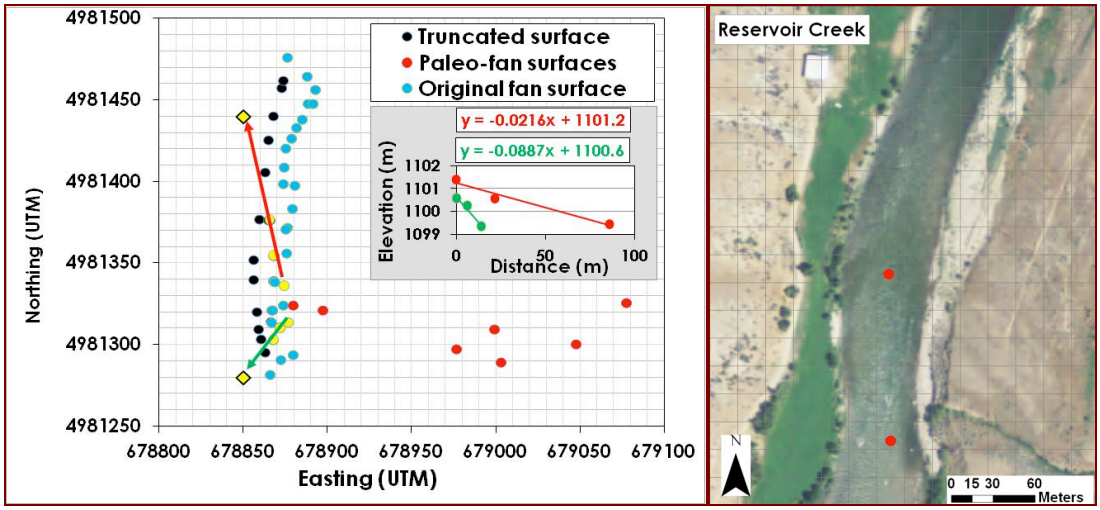

Figure E-9: (Left) Colored circles represent the surveyed data points for the Reservoir Creek debris flow deposit. Red circles represent top surfaces of perched truncated paleo-alluvial fan. The blue circles represent the original fan deposit that was not affected by high main-stem Middle Fork Salmon flows. The black circles represent the truncated surface, where sediment had been removed by high main-stem flows. Two fan radial slopes (yellow circles) were created and the linear equations (green and red lines) used to project fan surface into modern channel. Two extrapolated data points (yellow diamonds) were produced to reconstruct the volume of the original fan surface. (Right) NAIP photograph of Reservoir Creek containing the two extrapolated data points.

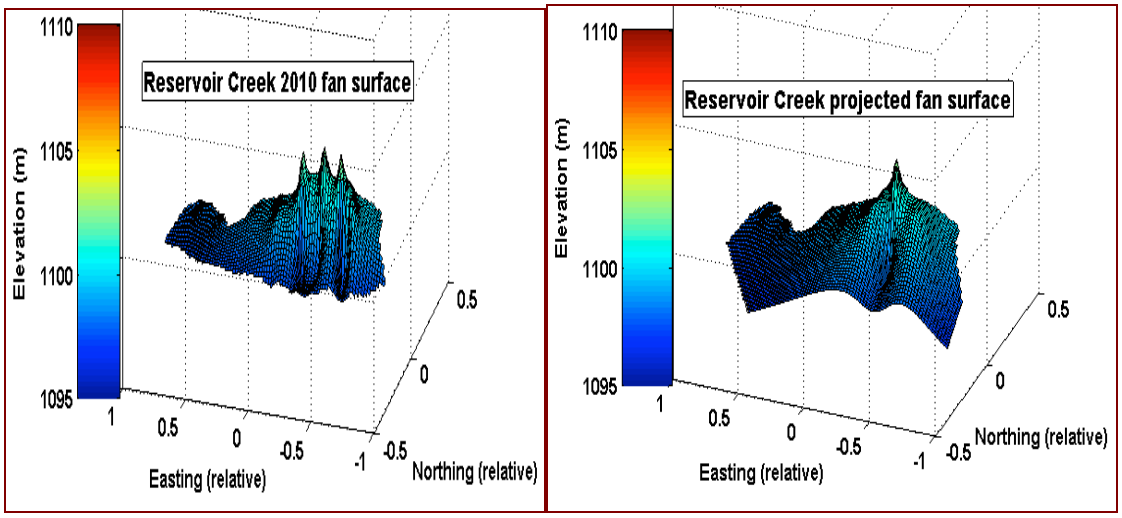

Figure E-10: The above two images are extrapolations of survey data points representing the topography of Reservoir Creek debris flow deposit fan surface. The left figure represents the 2010 surveyed fan deposit that was truncated by high peak flows prior to the survey. The right figure is the reconstructed fan surface.

Figure E-11: A photograph of the remaining deposit from the 1997 debris flow at the tributary (Pole Creek) junction of the main-stem MFSR

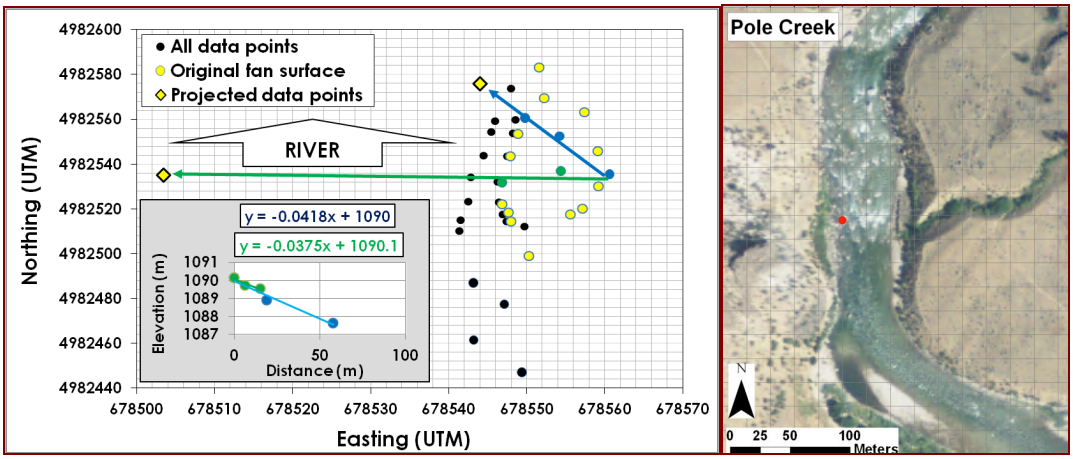

Figure E-12: (Left) Colored circles represent the surveyed data points for the Pole Creek debris flow deposit. The yellow circles represent the original fan deposit that was not affected by high main-stem Middle Fork Salmon flows. The black circles represent the truncated surface, where sediment had been removed by high main-stem flows. Two fan radial slopes (blue and green circles) were created and the linear equations (green and blue lines) used to project fan surface into modern channel. Two extrapolated data points (yellow diamonds) were produced to reconstruct the volume of the original fan surface. (Right) NAIP photograph of Pole Creek containing the one extrapolated data point.

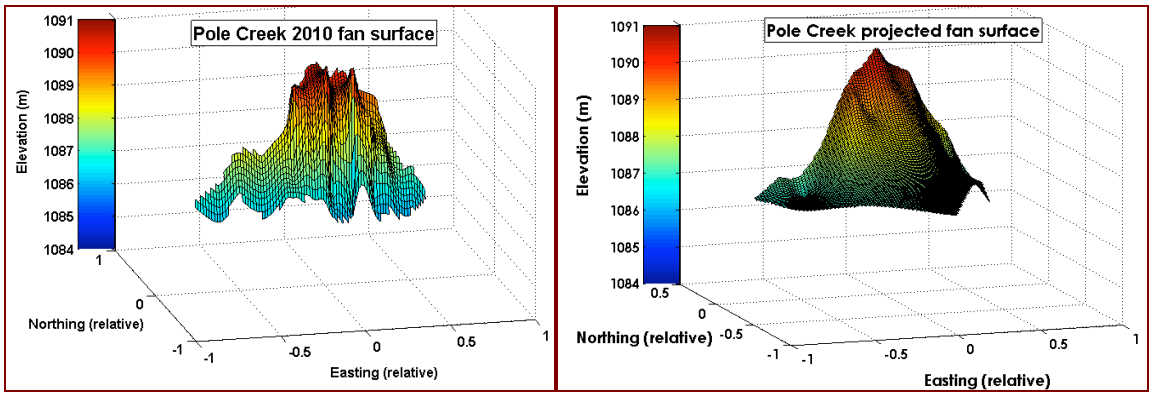

Figure E-13: The above two images are extrapolations of survey data points representing the topography of the debris flow deposit fan surface. The left figure represents the 2010 surveyed fan deposit that was truncated by high peak flows prior to the survey. The right figure is the reconstructed fan surface. Note there is extreme vertical exaggeration.

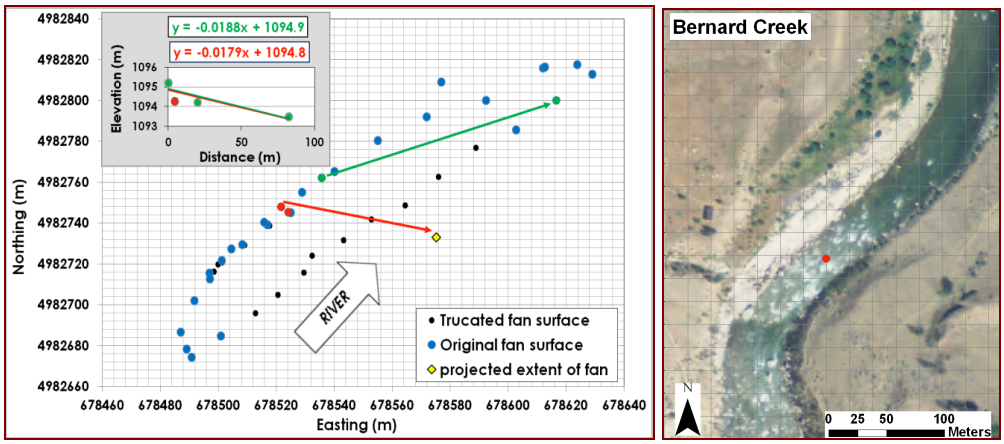

Figure E-14: (Left) Colored circles represent the surveyed data points for the Bernard Creek debris flow deposit. The blue circles represent the original fan deposit not affected by high main-stem Middle Fork Salmon flows. The black circles represent the truncated surface, where sediment had been removed by high main-stem flows. Two fan radial slopes were created and the linear equations used to project fan surface into modern channel. One extrapolated data point (yellow diamond) was produced. (Right) NAIP photograph of Reservoir Creek containing the extrapolated data point.

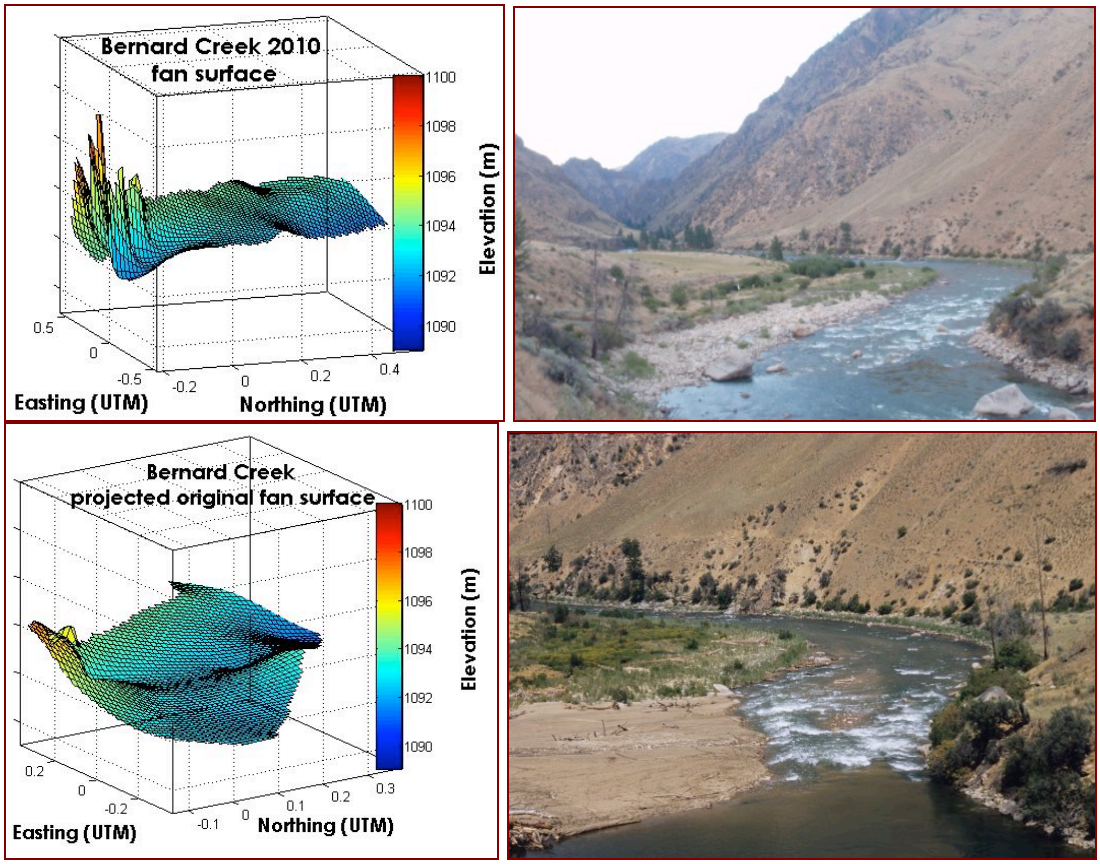

Figure E-15: The above two left images are extrapolations of survey data points representing the topography of the debris flow deposit fan surface. The top figure represents the 2010 surveyed fan deposit that was truncated by high peak flows prior to the survey. The bottom figure is the reconstructed fan surface. The two photographs on the right are pre- (Leidecker, 2008) and post-debris flow images.

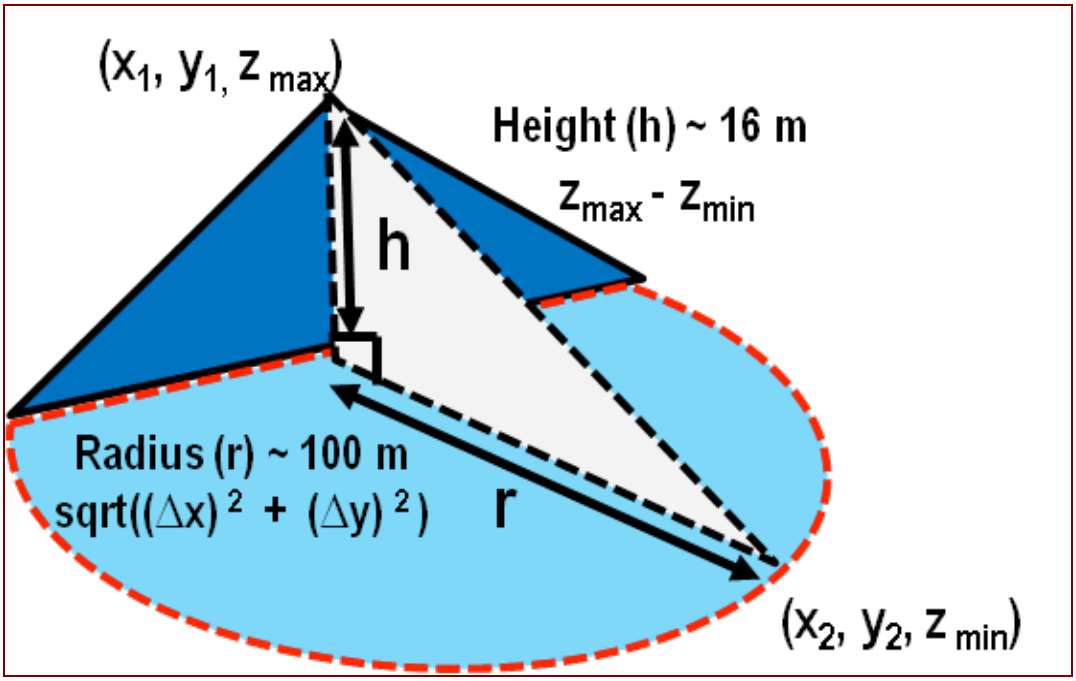

Figure E-16: Sheepeater fan volume calculated using simple half-cone equation is illustrated above.

Table E-1: Half-cone volume calculation for the five alluvial fans surveyed.

Cone Volume = 1/3 * πr^2 * h	Radius (m)	Height (m)	Cone volume (m^3)	Cone volume/2 (m^3)	Extrapolated volume (m^3)
Kotch	58	6.3	22,193	**11,097**	**25,400**
Sheepeater	100	16	167,552	**83,776**	**76,810**
Reservoir	30	5	4,712	**2,356**	**13,500**
Pole	60	4.4	16,588	**8,294**	**9,500**
Bernard	60	6.1	22,996	**11,498**	**13,735**

Debris flow deposit surfaces were digitized using radial basis functions to interpolate across surveyed data points, thus representing the true topography of the debris flow deposit surface. The distmesh2d function (Persson, 2004) was used to delineate the area within the deposit perimeter (user defined perimeter) and then to subdivide the defined area into triangles. The center of mass was calculated for each triangle. Each individual triangle was integrated along its center of mass from an assumed base to the interpolated surface. The Matlab code was written by Austin Hopkins for his undergraduate capstone project, with help from Grady Wright, a professor in the Math Department at Boise State University.

The difference in measured debris flow magnitude between upper and lower basin debris flow deposits could be attributed to the effects of preservation on volume reconstructions. The three lower basin debris flows were older (two events were produced in 1997and one in 2003) compared to two upper basin deposits (both produced in 2008) and therefore less well preserved. There was little original fan surface remaining to extrapolate the original fan surface. An additional confounding factor was the battery life of the RTK system. Sunshine and time available to charge the batteries were limited. The two upper basin debris flow deposits contained many more surveyed data points compared to the three lower basin deposits. However, observed fan sizes of modern debris flow deposits between upper and lower basins support the measured differences. Lower basin fans were consistently smaller and contained gentler slopes.

APPENDIX F

Components of the Cannon et al., 2010 debris flow volume prediction method

The first empirical method (Equation 1) uses basin area with slopes ≥ 30%, burned basin area moderately to severely, and total storm precipitation estimated using summer storm maximum and mean (Cannon et al., 2010). Slopes were classified using a 10 m Digital Elevation Model (DEM), classified burn severity data was obtained from the Monitoring Trends in Burn Severity Project (MTBS, 2010), and precipitation data was obtained from three weather stations within and surrounding the MFRS watershed. A range in total storm precipitation was estimated using the maximum and average total storm depth for the summer (May-Aug) of period of record for the weather stations. Using well-constrained burn severity and slope data, along with a range in total storm depth values from multiple weather stations, we aim to capture the variability in debris flow volumes associated with different total storm depths using the Cannon et al., 2010 method.

Equation 2 $\mathbf{lnV = 7.2 + .6\,(lnA) + .7\,(B)^{1/2} + .2\,(T)^{1/2} + .3}$

A = area with slope ≥ 30% (km^2)
B = area moderately to severely burned (km^2)
T = storm precipitation depth (mm)
V = volume (m^3)

Table F-1: Weather stations used to obtain total storm rainfall depths.

Weather Station	Easting	Northing	Elevation (m)	Summer Storm Precipitation Max. (mm)	Summer Storm Precipitation Ave. (mm)
Middle Fork Lodge	115° 00'59"	44° 43'18"	1,335	15	5
Yellow Pine	115° 30'00"	44° 57'42"	1,419	17	7
Deadwood Reservoir	115° 38'31"	44° 17'31"	1,641	18	6

Table F-2: Cannon et al., 2010 formula measured variables and formula results. Slope data obtained from 10m DEM. Classified burn severity data obtained from the Monitoring Trends in Burn Severity Project (MTBS, 2010). Total storm rainfall data was obtained from weather stations (Table F-1).

Tributary	Area (km^2)	Area with slope >= 30% (km^2)	Area moderate/ severely burnt (km^2)	Total Storm Rainfall (mm)		Volume (m^3)		Sediment Yield (Mg km^{-2} $time^{-1}$)	
				Max.	Ave.	Max.	Min.	Max.	Min.
Kotch	1.66	1.6	1.36	18	6	**12,781**	**8,929**	11,549	8,069
Sheepeater	1.56	1.5	1.35	18	6	**12,152**	**8,490**	11,685	8,163
Greyhound	2.96	2.7	2.11	18	6	**21,283**	**14,869**	10,785	7,535
Lake	6.07	5.3	4.14	18	6	**47,736**	**33,350**	11,796	8,241
Orelano	2.51	2.2	0.06	18	6	**8,047**	**5,622**	4,809	3,360
Reservoir	3.6	3.5	1.09	18	6	**18,477**	**12,909**	7,699	5,379
Pole	7.76	7.4	1.84	18	6	**36,428**	**25,449**	7,041	4,919
Bernard (sub-drainage)	4.6	4.3	3.10	18	6	**34,731**	**24,264**	11,325	7,912

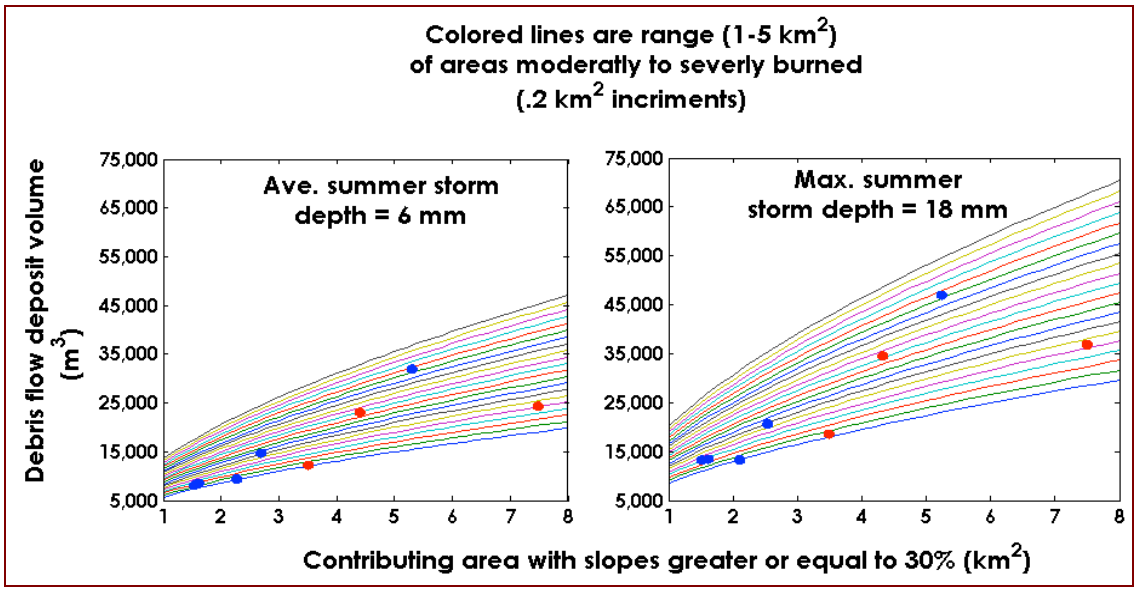

Figure F-1: Sensitivity analysis performed on Cannon et al., 2010 volume prediction equation. The graph on the left used the average storm depth, for the period of instrumental record, measured at three weather stations nearby and within the Middle fork Salmon River. The graph on the right uses the maximum storm depth recorded by the three weather stations. The colored lines vary the size of contributing area moderately to severely burned by increments of .2 km^2 encompassing the range (1-5 km^2) of moderately to severely burned area within the study sub-basins. The x-axis represents the range (1-8 km^2) of study site contributing areas with slopes ≥ 30%. The red dots represent estimated debris flow deposit volumes from lower less forested basins and the blue dots represent debris flow deposit volumes from upper more forested basins.

APPENDIX G

Components of Iverson et al., 1994 debris flow volume prediction method

The second method used to estimate debris flow volume is the super elevation formula applied to debris flows against bends and obstacles (Iverson et. al., 1994). Radius of curvature was calculated using Equation 2. Debris flow velocity was calculated using Equation 3. Flow banking angle around a bend was measured using high marks (marginal levee deposits, mud marks and scars on trees and mud marks on bedrock) on the inside and outside of the bend using an inclinometer. Longitudinal slope was directly measured, for the reach encompassing the channel bend, using a stadia rod, tape measuring, and inclinometer. Discharge was calculated using Equation 4. The cross-sectional area of the boulder snout of the debris flow defined by debris flow high marks was surveyed. To convert volume to sediment yield, we used an assumed sediment bulk density of 1500 kg/m^3 and area of the contributing basin.

Equation 3 **radius of curvature (rc) = C2 / 8M + M/2**

C = chord
M = middle ordinate distance

Equation 4 **velocity (v) = $(g * r_c (\cos\alpha) * (\tan\beta))^{1/2}$**

g = gravity
α = banking angle
β = longitudinal slope

Equation 5 **$Q_{max} = A_{max} * v$**

A_{max} = maximum cross sectional area of debris flow snout
Q_{max} = maximum discharge

Equation 5 **volume = $794.6 * Q_{max}^{0.849}$**

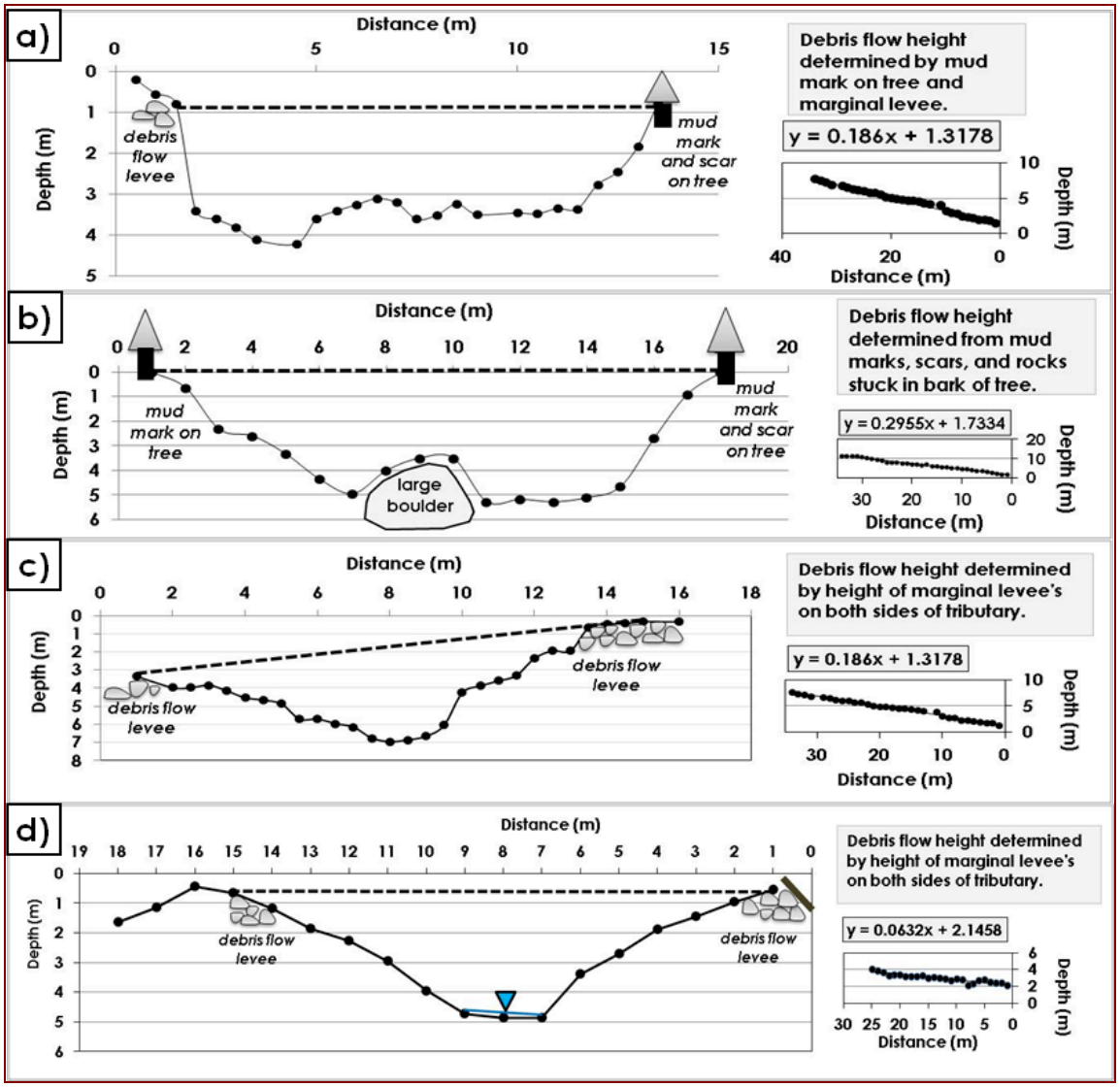

Figure G-1: Graphs show four cross sections of boulder snouts from recent debris flows and longitudinal profiles of four stream reaches encompassing measured cross sections. (a-Kotch, b-Sheepeater, c-Greyhound, and d-Bernard)

Table G-1: Super-elevation formula measured variables

Sub-basin	Flow banking angle (deg)	Middle ordinate distance (m)	Chord (m)	Radius of Curvature (m) (Middle ordinate distance)^2/ (8*Chord)+Chord/2	Longitudinal slope	Cross section area (m^2)	Sub-basin area (km_2)
Kotch	14	8	11.9	6.2	.2955	58.2	1.56
Sheepeater	12	5.75	23.04	14.4	.186	7.54	1.56
Greyhound	24	7.85	21.3	11.1	.0632	29.96	2.96
Bernard	12	5.7	4.2	3.2	.186	26.84	4.6

Table G-2: Super elevation formula results

Equations		Kotch	Sheepeater	Greyhound	Bernard
velocity (m/s)	$(g*R_c(\cos(\text{banking angle}))*\tan(\text{slope})))^{(.5)}$	1.60	2.75	1.71	2.23
Qmax m^3/s	velocity * A_{max}	93.23	20.72	51.34	59.9
Volume(m^3)	$794.6*Q_{max}^{0.849}$	**37,351**	**10,418**	**22,506**	**25,661**
Mass (kg)	Volume * bulk density (1500 kg/m^3)	56,026,576	15,626,417	33,759,007	38,490,496
Sediment Yield (Mg/km^2/event)		**35,900**	**10,000**	**11,400**	**8,370**